NORTHWESTERN UNIVERSITY

# Phosphorylation of a C-terminal RACK1 Loop by Poxviruses Controls Ribosome Translational Capacity

A DISSERTATION

SUBMITTED TO THE GRADUATE SCHOOL

IN PARTIAL FULFILLMENT OF THE REQUIREMENTS

for the degree

DOCTOR OF PHILOSOPHY

Field of Life Sciences

By

Madeline Grace Rollins

EVANSTON, ILLINOIS

December 2021

**Abstract**

Receptor for activated C kinase 1 (RACK1) is a core small (40S) ribosomal subunit protein whose structure is highly conserved among eukaryotes apart from a C-terminal extended loop. We previously showed that a poxvirus kinase phosphorylates this flexible loop in human RACK1, mimicking endogenous negative charge in plant RACK1 to enhance translation of post-replicative poxviral transcripts with unusual polyA tracts in the 5' untranslated region (UTR). However, the broader evolutionary significance of this loop region and the effect of a charged loop on ribosome activity remains unknown. Phylogenetic and bioinformatic analyses reveal that careful spatial organization of negative charge correlates with increased usage of 5' polyA, but only in dicot plants and protists. RACK1 loop mutants and chimeras show that the amino acid composition of the human loop is uncharged and optimized to regulate interactions with eIF6, a eukaryotic initiation factor that controls 60S biogenesis and 80S ribosome assembly. Although in human RACK1 backgrounds both charged and uncharged loop mutants affect eIF6 interactions, only a negatively charged plant – but not uncharged yeast or human loop – enhances translation of mRNAs with adenosine-rich 5′ untranslated regions (UTRs). These data indicate that charge in the loop is the primary driver of the polyA enhancer effect, which modeling suggests operates directly on the 40S subunit. Biochemical and structural studies show that negative charge in the RACK1 loop also remodels the 40S head domain and tRNA binding sites and broadly supports non-canonical modes of translation without impacting ribotoxin-induced stress signaling and ribosome stalling on polyA tracts. Our findings unearth additional layers of translational control enabled by the RACK1 loop and uncover the immense regulatory capabilities endowed by adding a single negative charge to the loop. Collectively, our work provides a rationale for future studies exploring the extent to which specific ribosomal proteins and their corresponding post-translational modifications regulate gene expression and ribosome activity across cell types and in different species as well as the remarkable way in which species-specific functions can be mimicked in human hosts by poxviruses.

## Acknowledgements

"Now unto him that is able to do exceeding abundantly above all that we ask or think according to the power that worketh in us" (Ephesians 3:20)

I would like to thank my advisor, Derek Walsh, for welcoming me into his lab and for your patience, understanding and support throughout my time here. Your guidance has truly helped me grow as scientist; I honestly could not have asked for a better mentor. I would also like to thank my thesis committee members Eva Gottwein, Richard Longnecker and Marc Mendillo for their valuable insight, comments and suggestions.

To my fellow labmates, both past and present: thank you for all the great discussions in the lab and in lab meetings that helped me think more critically about my work. I would especially like to thank two past members, Sujata Jha and Dean Procter, for helping me feel welcome and for always happily answering my questions during my rotation and the first few months in lab. I would also like to thank Mojgan Naghavi for being a second mentor to me and to the current and past members of the Naghavi lab for their generosity and willingness to help whenever possible.

Last but certainly not least, I would like to thank my family for their love, prayers and encouragement that helped me complete my graduate studies. To my sisters, Meaghan and Mallory: thank you for making me laugh, for always being there for me and for always reminding me to have fun. To my mother: thank you for your many sacrifices that helped me get to where I am. Thank you for listening to me, always giving me wise counsel and for helping me put this whole experience in perspective.

## Dedication

For my father – thank you for introducing me to science and I hope that this achievement makes you proud. I wish you were here to celebrate with me.

**Table of Contents**

## List of Figures and Tables

### Figures

**Tables**

# Chapter 1

# Introduction

## Evolutionary origins of Vaccinia virus

Nucleocytoplasmic Large DNA Viruses (NCLDVs) are a monophyletic group of eukaryotic viruses with large, double-stranded DNA genomes that range in size from 100 kilobases to over 2.5 megabases (1, 2). The NCLDV group comprises eight families: Asfarviridae, Ascoviridae, Iridoviridae, Marseilleviridae, Mimiviridae, Phycodnaviridae, Pithoviridae and Poxviridae (Table 1) (2-4). These viruses primarily replicate in cytoplasmic compartments known as viral factories though there are certain families, such as Iridoviridae and Phycodnaviridae, that have nuclear phases in the viral lifecycle (3, 5). Phylogenetic studies suggest that NCLDVs originate from a bacteriophage-like ancestor that built its genome by capturing genes from protist hosts and further remodeled its genome over time through gene deletion and exchange (6, 7). Over time, certain NCLDV group members expanded their host range to include animals or switched from protist to animal hosts. Evolutionary analyses predict that the switch happened on three different occasions. The most recent switch likely occurred in a recent ancestor of asfarviruses and its close relatives, as there are a number of virus species in this cluster that can infect both protists and pigs (8-10). The other two events are ancient and likely occurred in the common ancestors of irido-ascoviruses and poxviruses and enabled the infection of a broad range of animals (11, 12).

Poxviruses infect vertebrates (Chordopoxvirinae subfamily) and insects (Entomopoxvirinae subfamily). Chordopoxvirinae is further subdivided into nine genera, four of which infect humans: orthopoxvirus, parapoxvirus, yatapoxvirus and molluscipoxvirus. Yatapoxviruses and molluscipoxviruses are zoonoses, while parapoxviruses and orthopoxviruses specifically infect humans (13, 14). The orthopoxvirus subfamily includes the infamous human pathogen Variola virus, the causative agent of smallpox which was responsible for an estimated 300 million deaths worldwide during the 20$^{th}$ century alone (15). Other members of the orthopoxvirus genera include cowpox, monkeypox and the peculiar vaccinia virus (VacV), whose exact origins are unknown (16, 17). Many different VacV strains have evolved that can infect a range of mammals including cows, humans and horses, suggesting that the virus is likely a hybrid

| Virus Family/Group | Host Range | Genome Size Range (kb) | Replication site |
|---|---|---|---|
| Ascoviridae | insects (primarily), noctuids | 120-190 | nucleus and cytoplasm |
| Asfarviridae | amoebae, mammals | 170-470 | cytoplasm |
| Iridoviridae | insects, cold-blooded vertebrates | 100-290 | nucleus and cytoplasm |
| Marseilleviridae | acanthamoeba, algae (likely) | 360-380 | nucleus anad cytoplasm |
| Mimiviridae | acanthamoeba, other amoebae (likely); algae, heterokonts (protists) | 280-1570 | cytoplasm |
| Phycodnaviridae | green algae; symbiotic algae of paramecia and hydras; heterokonts; haptophyta | 180-400 | nucleus and cytoplasm |
| Pithoviridae | unknown protists | 460-1470 | cytoplasm |
| Poxviridae | animals: vertebrates, insects | 130-360 | cytoplasm |

**Table 1. Members of the nucleocytoplasmic large DNA virus (NCLDV) family.** Host range, genome size range and replication location of the NCLDV family members. Chart adapted from (1).

of multiple orthopoxviruses including cowpox and smallpox (16, 18). These VacV strains also vary widely in their virulence; for example, the modified vaccinia virus Ankara (MVA) and Lister strains are both highly attenuated, but the Lister strain can replicate in humans and other mammalian hosts whereas the MVA strain cannot (19). By contrast, the Western Reserve strain is the most virulent strain and replicates to high titers in mammals (20-22). Despite its unknown origins or natural host, VacV played a key role in the global vaccination initiative with both the MVA and Lister strains being used as a vaccine during the global smallpox eradication campaign which was completed in 1980 (20, 23). While all three strains are now used as viral vectors for recombinant vaccines and oncolytic therapies, the Western Reserve strain is the laboratory prototype poxvirus to study molecular virology and cell biology (24-27).

**Cascade mechanism of Vaccinia virus gene expression**

VacV compartmentalizes DNA replication, transcription, translation and virion assembly in cytoplasmic compartments known as viral factories (Figure 1) (28, 29). Its 190 kilobase double-stranded DNA genome contains more than 200 open reading frames (ORFs) that encode an assortment of proteins that enable self-sufficiency during viral replication; these include membrane and structural proteins, enzymes, and transcription factors (Figure 2) (30). A cascade mechanism temporally regulates VacV gene expression and is classically divided into three phases: early, intermediate and late (31). Transcription of early genes occurs immediately after infection using transcription machinery produced late in infection and packaged into virions (32, 33). Removal of the viral envelope upon entry, the first stage in a two-step uncoating process, enables early gene expression within the viral core (34, 35). Over 100 early messenger RNAs (mRNAs) are transcribed and then released into the cytoplasm, where they are translated into proteins by host ribosomes (29). Early gene products produce proteins involved in viral DNA replication, nucleotide biosynthesis, intermediate gene transcription and evasion of innate host defenses (36).

The second uncoating step involves breakdown of the viral core wall and release of the genome, which must be replicated before intermediate and late genes can be expressed (34, 37). The temporal definition of intermediate and late gene transcription is poorly defined and the readthrough of neighboring genes further complicates the distinction (38). Therefore, VacV genes are more broadly categorized into pre- and post-replicative classes relative to DNA replication. Pre-replicative genes are the approximately

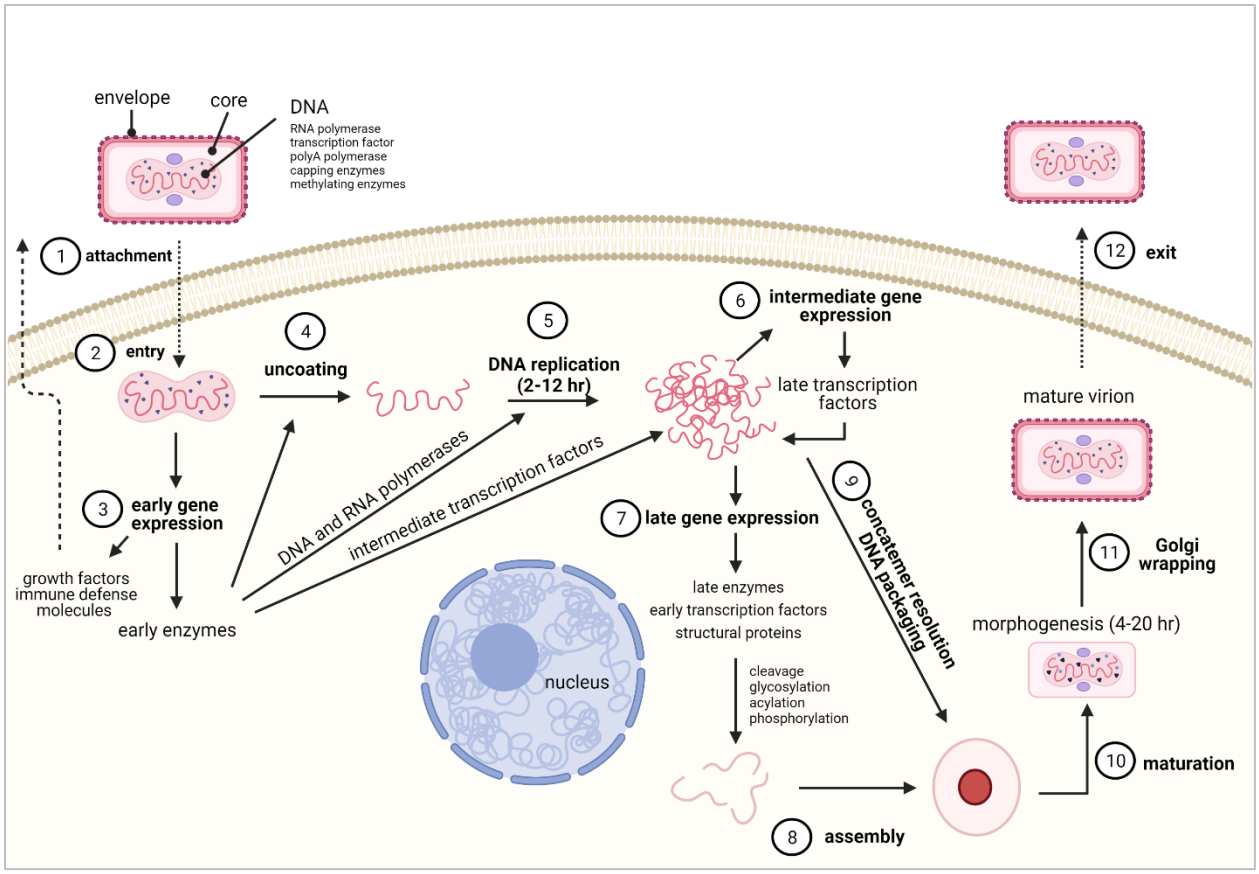


**Figure 1. VacV replication cycle.** Entry of the VacV virion into the host cell, usually by micropinocytosis, releases the viral core into the cytoplasm; this core contains the double-stranded DNA genome as well as pre-packaged early transcription machinery. Activation of the core initiates early gene expression; roughly half of these 100+ early proteins function in host immune response evasion, while the rest mediate the uncoating and replication of the genome. DNA replication, transcription, translation, and virion assembly occur in cytoplasmic viral factories (not shown). Post-replication coincides with the translation of intermediate and late viral transcripts (also known as post-replicative transcripts). Intermediate transcripts encode late transcription factors, DNA binding and packaging proteins as well as other important proteins to be incorporated into the viral core. Late transcripts encode for the early transcription machinery as well as structural and membrane proteins important for virion assembly. Mature virions exit the cell via lysis or exocytosis. Diagram adapted from references (39-41) and created with Biorender.com.

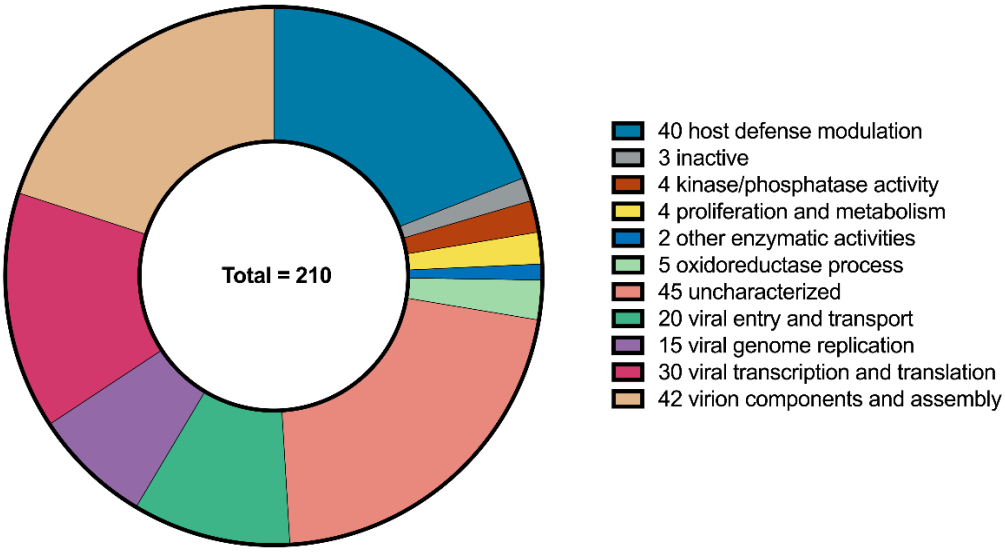


**Figure 2. Broad functional classification of VacV proteins**. Molecular functions of the 210 VacV gene products were determined by the UniProt database for the VacV Western Reserve Strain Proteome and the Poxvirus Gene/Protein database (Virus Pathogen Database and Analysis Resource). Inactive proteins refer to those that are catalytically inactive or truncated and thus missing crucial domains needed for their predicted functions.

117 early genes expressed before DNA replication, while post-replicative genes are the approximately 93 intermediate and late genes expressed after DNA replication (38, 42). Intermediate gene products produce late transcription factors while late transcripts produce structural proteins and transcription complex proteins that are packaged into virions along with the viral genome (30, 43).

The transcription start-sites of post-replicative genes possess a conserved TAAATG motif that is absent in early genes (44, 45). The viral RNA polymerase attempts to initiate on this motif within the A triplet, which corresponds to the T triplet of the template strand, buts slips repeatedly (46, 47). Slippage of the RNA polymerase produces non-templated poly-adenosine (polyA) tracts of heterogeneous length that comprise the majority of the 5' untranslated region (5' UTR) of post-replicative transcripts and overlap with the A residue of the start codon (48, 49). Deep sequencing studies predict these tracts range between 3 to 51 nucleotides (nt) in length, with the majority ranging between 8 and 12 nt (49). However, high-throughput sequencing approaches are biased against homopolymeric tracts, especially polyA, calling into question the accuracy of these estimates (50). For this reason, the 25-35 nt polyA leader length predicted for post-replicative mRNA generated in *in vitro* transcription reactions provides a more conservative estimate (51).

The timed synthesis and broad functional range of viral proteins produced during infection reinforces the high level of self-sufficiency that poxviruses possess. However, similar to all other viruses, VacV displays an absolute dependence on the host protein synthesis machinery and must recruit cellular ribosomes to translate viral transcripts. Therefore, components of the mammalian translational machinery are key regulatory targets during VacV infection.

**Eukaryotic translation machinery and modes of initiation**

*Structure and function of mRNA and ribosomes*

Mature, processed eukaryotic mRNA consists of a coding sequence, which encodes the amino acid sequence of a protein in the form of nucleotide triplets or codons, embedded between terminally modified untranslated regions (UTRs) at both the 5' and 3' end. A 7-methylguanosine cap covalently attached to the first nucleotide of the transcript terminates the 5' end of the transcript, protects the message from degradation by cellular nucleases and facilitates translation initiation (52, 53). At the 3' end, the addition of hundreds of adenines through a process known as polyadenylation forms a polyA tail that

mediates transcript processing and transport and promotes transcript stability and translation (54, 55). Like many other viruses, VacV also modifies its transcripts with a methylguanosine cap and polyA tail using its own guanylyltransferase, methyltransferase and polyA polymerase (56-58). These shared structural features increase competition between viral and host transcripts for ribosomes.

Ribosomes are large ribonucleoprotein complexes that synthesize proteins using mRNA as the template and amino acids as the building blocks. The 80S eukaryotic ribosome consists of a small (40S) and a large (60S) subunit, each with distinct functions in protein synthesis (Figure 3) (59). The human 40S subunit consists of a single 18S ribosomal RNA (rRNA) and 33 ribosomal proteins (RPs). The 40S or “small” subunit also contains the decoding center, where mRNA codons are read and inspected for complementarity with the anticodon of transfer RNA (tRNA) carrying the amino acids to be incorporated into the growing polypeptide chain. The human 60S subunit consists of three rRNA (28S, 5S and 5.8S) and 47 RPs and is the site of the peptidyl transferase center, which catalyzes peptide bond formation between the polypeptide chain and the incoming amino acid (60, 61). The 60S or “large” subunit rRNA also forms a peptide exit tunnel through which the nascent chain is extruded (62, 63). The core functions of the large and small subunits are conserved in ribosomes across all kingdoms of life. The basic mechanism of translation is also universally divided into four cyclical steps: initiation, elongation, termination and recycling. A primary focus for study is translation initiation as eukaryotes have evolved a complex and highly regulated translation initiation step that adds layers of control over protein synthesis (64).

*Canonical Translation*

In contrast to bacteria where base pairing of the small subunit rRNA and the 5’ end of mRNA, or the Shine Dalgarno interaction, is used to align the ribosome with the start codon, eukaryotes primarily use a scanning mechanism to initiate translation (summarized in Figure 4) (64). During scanning, the initiation machinery inspects the 5’ untranslated region (UTR) or leader for a start codon, which is usually AUG (65). The process begins with the formation of the ternary complex (TC) comprised of the initiator methionyl-tRNA (Met-tRNA$_i$); a GTPase, eukaryotic initiation factor 2 (eIF2); and GTP, which is bound to eIF2. The initiation factors eIF1, eIF1A and eIF3 stimulate TC binding to the 40S subunit, thus forming the 43S pre-initiation complex (PIC). Once formed, the 43S PIC binds the methylguanosine cap at the 5’ end of the

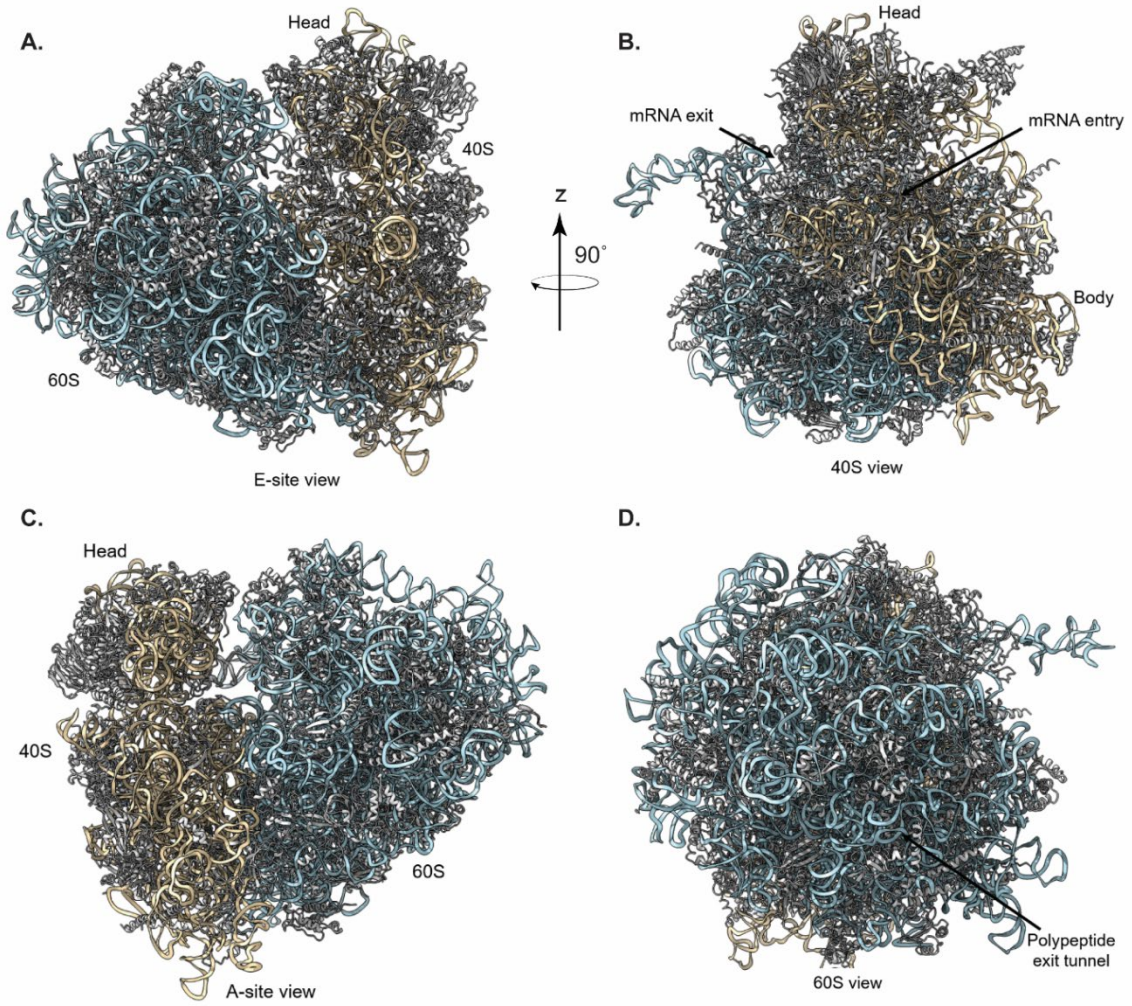


**Figure 3. Cryo-EM structure of the human (*H. sapiens*) 80S ribosome.** (**A-D**) E-site, 40S (small subunit), A-site and 60S (large subunit) views of the ribosome, respectively. Panels B-D have been rotated 90°, 180° and 270° degrees about the z-axis with respect to panel A and labeled as done in reference (66). Large subunit rRNA (28S, 5.8S, 5S) ribbon diagrams are colored blue and small subunit rRNA (18S) ribbon diagram is colored tan. Ribosomal protein ribbon diagrams colored gray. PDB: 6QZP.

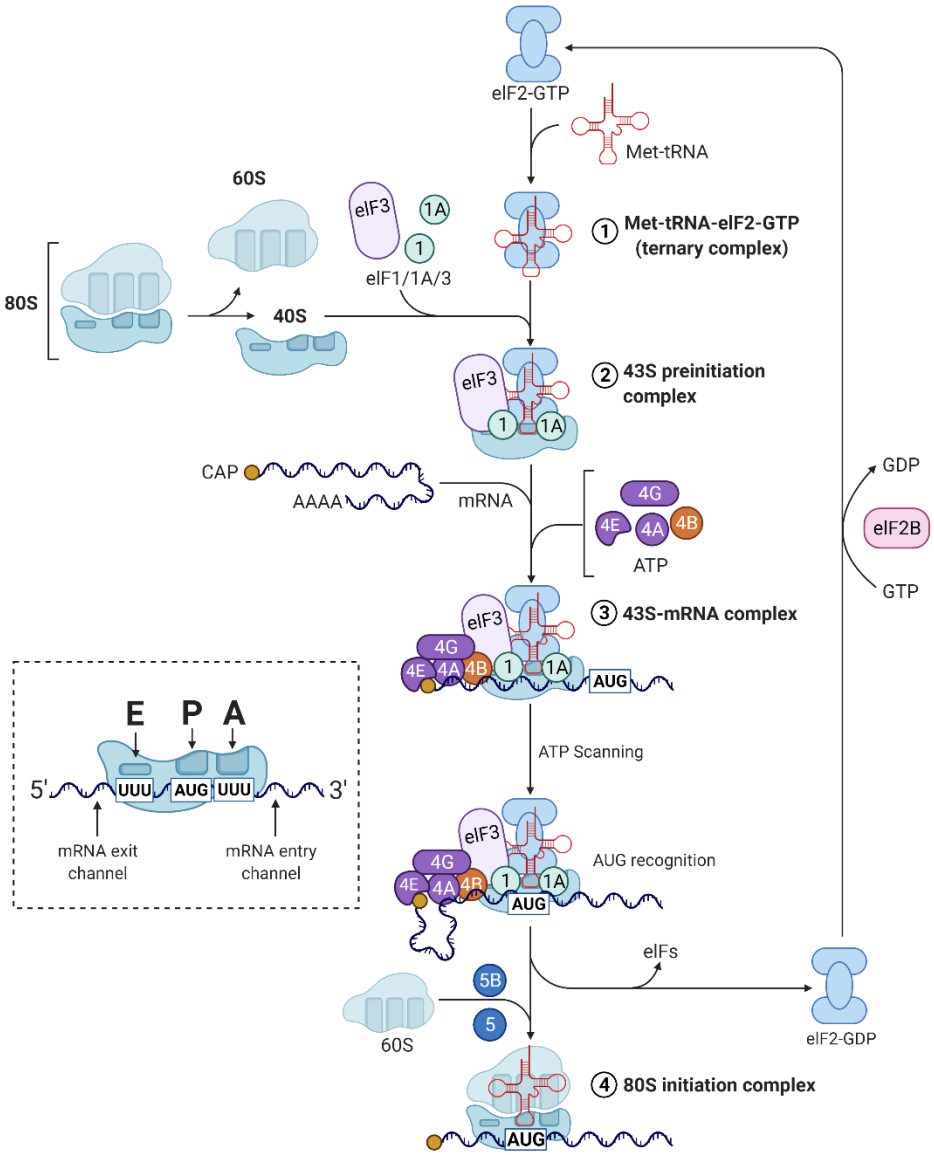


**Figure 4. Overview of eukaryotic cap-dependent translation initiation.** The first step of initiation is the formation of the ternary complex (TC) comprised of methionyl tRNA (Met-tRNA) and GTP-bound eukaryotic initiation factor 2 (eIF2). eIF1, 1A, and 3 recycle 80S ribosomes that have terminated translation and generate individual subunits. They also facilitate the recruitment of the ternary complex to a free 40S subunit to form the 43S preinitiation complex (PIC). Messenger RNA (mRNA) is activated by binding of the eIF4F complex (comprised of eIF4E, eIF4G and eIF4A) to the cap at the 5' end of the mRNA. Activated mRNA is recruited to the 43S PIC which scans the 5' untranslated region (UTR) or leader for the AUG start codon. During scanning, ATP-dependent helicase activity of eIF4A unwinds secondary structure in the leader to enable inspection of nucleotide triplets or codons. AUG recognition halts scanning and activates the release of initiation factors. eIF5B catalyzes 60S joining to form a translationally competent 80S complex primed for elongation. Reprinted with permission from "Protein Translation Cascade," by Biorender.com (2021). Retrieved from https://app.biorender.com/biorender-templates.

mRNA (67, 68). Initiation from most eukaryotic transcripts requires cap binding and scanning; therefore, this cap-dependent mode of initiation is often considered the “canonical” mode of translation initiation.

The eIF4F complex mediates 43S PIC attachment to the cap. eIF4F consists of the cap-binding protein eIF4E, the scaffold protein eIF4G and the RNA helicase eIF4A. eIF4G possesses N-terminal binding domains for eIF4E and poly(A) binding protein (PABP) and C-terminal binding sites for eIF4A and the 13-subunit eIF3 complex (67). As it was mentioned earlier, eIF3 helps recruit the 43S PIC and stimulates its attachment to mRNA. The poly(A) binding proteins (PABPs) are an important class of regulatory proteins that bind to the poly(A) tail at the 3’ end of transcripts and shield it from degradation (69). Simultaneous engagement of PABP with the 3’ poly(A) tail and the eIF4G complex at the cap circularizes the mRNA and forms a highly stable closed-loop structure hypothesized to optimize translation on mature and properly-processed transcripts (70).

Once bound, the 43S PIC scans the 5’ UTR in search of an initiation codon within the proper sequence context, known as the Kozak sequence. In mammals, the Kozak motif is directly upstream of the initiator AUG and is guanine- and cytosine-rich with a consensus sequence of CGCC(A/G)CC<u>AUG</u>G (initiator AUG is underlined) (71). During scanning, RNA helicases, such as eIF4A and other DEAD box helicases bound to the PIC, unwind secondary structure in the 5’ leader to produce a single stranded region in the mRNA so each triplet codon can be inspected (72, 73). Complementarity of the initiator tRNA anticodon and a context-appropriate AUG start codon induces conformational changes by eIF1, eIF2, eIF1A and eIF5 that signify start codon recognition and halt scanning (74). Release of eIF1, hydrolysis of the GTP bound to eIF2 by the GTPase-activating protein (GAP) eIF5B, release of the inorganic phosphate and dissociation of eIF2-GDP forms a new complex, known as the 48S PIC (75, 76). Additional conformational changes allow eIF5B to bind to the 40S subunit and catalyze its joining to the large 60S subunit (77, 78). The final product is a competent 80S initiation complex primed for elongation.

During elongation, the ribosome undergoes large scale intersubunit rotation or “ratcheting” and more localized swiveling of the small subunit head domain – both of which coordinate movement, or translocation, of the tRNA and mRNA through the ribosome (79-82). The mRNA threads through a 12 nucleotide (nt)-long entry channel on the back of the 40S subunit that is formed by 18S rRNA and framed

by the small subunit ribosomal proteins S2 (RPS2) and RPS3 (67, 83). This mRNA entry channel precedes the three decoding sites formed at the subunit interface that hold the tRNA as they move through the ribosome. The A (aminoacyl) site receives the incoming aminoacyl-tRNA carrying the amino acid to be incorporated; the P (peptidyl) site holds the tRNA conjugated to the growing peptide chain; and the E (exit) site holds the deacylated tRNA before it exits the ribosome. As the mRNA is decoded, it leaves through a 12 nt-long exit channel that also opens on the back of the 40S subunit and is surrounded by RPS5, RPS26 and RPS28 (67, 84). Termination of translation occurs upon recognition of a stop codon at the 3' end of the mRNA coding sequence. Once translation is terminated, the nascent chain is released and the ribosome can be recycled and bind to new mRNA or reinitiate on the same transcript (85).

*Alternative translation*

Non-canonical translation mechanisms provide alternative ways to directly assemble the ribosome at or near the start codon, often without cap-binding and/or scanning. These mechanisms are often activated under conditions where cap-dependent translation is impaired, as occurs during cell stress, proliferation and differentiation (86-88). A minority of viral and cellular transcripts use cap-dependent discontinuous scanning, also known as ribosome shunting, to initiate translation. In this mechanism, the PIC attaches to the cap and scans for a short distance before bypassing or "jumping" regions of the 5' UTR en route to the initiation site. This mechanism is often employed under conditions that restrict eIF4F complex formation or activity (89-91). More frequently, RNA virus transcripts and a subset of cellular transcripts adopt highly structured 5' UTR elements, known as internal ribosome entry sites (IRESs), that recruit the ribosome independent of cap binding (86, 92, 93). Cellular IRESs are often embedded in long leader elements and tend to rely more heavily on the eIF4F helicase activity to melt complex secondary structures, while the different classes of viral IRESs vary widely in their length, structure and requirement for eIFs (94, 95). Class I and II IRES elements use almost the full complement of eIFs for ribosome assembly except for the cap-binding protein eIF4E. While class I IRESs still scan the leader element in search of the start codon, class II IRES elements recruit the ribosome directly to the initiation site. Class III IRES elements are more structured compared to classes I and II and only require a subset of eIFs (eIF2,

eIF3 and eIF5) to recruit the ribosome to the start codon. Class IV IRESs are the most structurally complex and directly engage the ribosome independent of eIFs (96).

**Vaccinia virus exploitation of host protein synthesis machinery**

VacV transcripts utilize canonical cap-dependent initiation and compete with host transcripts for access to eIFs and ribosomes (95, 97). To favor viral protein synthesis, VacV degrades the translational repressor protein 4E-binding protein (4E-BP). Under normal cellular conditions, 4E-BP sequesters the cap binding protein eIF4E to regulate its association with eIF4G and the assembly of the eIF4F complex as part of an important checkpoint in translational control (98). VacV-mediated reduction of cellular 4E-BP levels increases the proportion of free eIF4E and stimulates eIF4F assembly and translation initiation (99). VacV also stimulates signaling pathways that activate the eIF4G-associated kinase Mnk1 which phosphorylates eIF4E; this modification enhances viral replication and protein synthesis (99). Another tactic VacV utilizes is to spatially redistribute and sequester core initiation factors like eIF4E and eIF4G within viral factories where viral transcription and translation occur (28, 99-101).

VacV infection also relocates PABP to viral factories which is expected to facilitate formation of closed loop mRNA in initiation complexes and stimulate translation (99). However, virus-produced small non-coding polyadeylated RNAs (POLADs) complicate our understanding of the precise function of VacV-induced PABP redistribution (102). POLADs are produced when the VacV polyA polymerase, VP55, non-specifically polyadenylates the 3’ end of fragments from tRNAs, small nuclear RNAs and the 5’ ends of viral or host mRNAs (103). The polyadenylated tails of these RNA fragments reportedly sequester PABP and impair both viral and host translation, which can be reversed by adding PABP back to the system (104-106). Intriguingly, VacV mRNA are more resistant to POLAD-mediated inhibition of translation compared to host mRNA, with post-replicative transcripts being more resistant than early transcripts which suggests that the polyA leaders of post-replicative transcripts may dampen the inhibitory effect of POLADs (107, 108).

Degradation of cellular mRNA is another common approach used to decrease competition for the translational machinery and suppress the production of host defense proteins (109, 110). VacV produces its own decapping enzymes, D9 and D10, that catalyze cap removal which destabilizes both viral and host transcripts and primes them for degradation by cellular nucleases; degradation of viral transcripts facilitates

the temporal transitions required for cascade gene expression. D9 is expressed before DNA replication and is only expressed by vertebrate poxviruses whereas D10 is expressed post-replication and is expressed by all poxviruses (111, 112). Both enzymes are redundant yet essential to infection; the timing of D10 expression, however, better correlates with global impairment or “shut-off” of host gene expression that occurs towards the later stages of infection (109, 113-115).

During host shut-off, VacV blocks formation of the 43S PIC (116, 117) and utilizes alternative initiation strategies with reduced requirement for canonical initiation factors such as eIF4F (118, 119). Indeed, VacV western reserve (WR) strain expresses a protein encoded by the early gene VACVWR 169 that modulates host protein synthesis by broadly inhibiting both cap-dependent and cap-independent modes of translation initiation. These changes result in an accumulation of non-translating monosomes and a reduction in the number actively translating polysomes in infected cells (120). However, beyond this discovery, how VacV directly targets the ribosome to regulate translation awaits further investigation. The pervasive perception of the ribosome as a passive molecular machine with little to no intrinsic regulatory capabilities partially explains the lack of ribosome-centric studies of translational control (121, 122). However, growing evidence from the fields of developmental biology and virology suggests that the ribosome is highly dynamic and can diversify its composition to enhance its functionality.

**Functional heterogeneity of eukaryotic ribosomes**

“Functional heterogeneity” is used to describe ribosomes that vary in the composition of their rRNA or subunit proteins or in the post-transcriptional and post-translational modifications to either of these components. These diverse ribosomes enable selective regulation of translation through interactions with specific 5’ UTR mRNA elements or motifs (123-126). Examples of compositionally heterogeneous ribosomes are ubiquitous in organism development, with well-studied examples found in the slime mold *Dictyostelium discoideum* and the plants *Zea mays* and *Arabidopsis thaliana* (127-130). In humans, ribosome heterogeneity caused by loss of function mutations in RP genes produces distinct clinical phenotypes known as ribosomopathies, such as Diamond-Blackfan anemia (DBA), that manifest as developmental defects (131, 132). Humans and fruit flies both display testis-specific expression of ribosomal protein paralogs or paralog-switching during gonad development (133), and there is growing

evidence in support of intracellular heterogeneity in ribosome subunit composition that enables differential selectivity for subsets of transcripts (134).

There are many examples where specific subunit proteins enable the ribosome to assemble on and initiate from structured leader elements in both cellular and viral transcripts. For example, Drosophila C virus (DCV) and poliovirus both require the small subunit proteins S6 (RPS6) and S19 (RPS19) for the IRES-dependent translation of their viral transcripts while RPS25 mediates 40S binding to IRES elements present in Cricket paralysis virus (CrPV) and Hepatitis C virus (HCV) transcripts (135, 136). The large subunit protein L40 (RPL40) enables ribosomes to initiate from IRESs in vesicular stomatitis virus (VSV) transcripts but is also required to translate a subset of cellular stress response transcripts (137). Perhaps one of the more well-studied examples arises during vertebrate development where expression of RPL38 is required to translate the Homeobox (Hox) mRNAs which function in axial skeletal patterning during animal development. RPL38 mediates 80S assembly on IRES-like regulatory elements present in the 5' UTR of Hox mRNA (138, 139), though the structural basis for this interaction remains unknown and recent evidence suggests the involvement of other ribosome structures, such as rRNA expansion segments (140). Post-translational modifications to RPs are another important source of functional heterogeneity that alter mRNA selectivity (141-144). For example, phosphorylation of ribosomal protein S6 (RPS6) purportedly regulates the selective translation of cellular 5' terminal oligopyrimidine (TOP) motif-containing mRNA, though these claims remain disputed (145, 146).

Functional heterogeneity manifests in other ribosome activities besides mRNA selectivity, including changes in translational fidelity, non-AUG codon initiation and alternative stop codon usage (123, 144). For example, ribosome quality control (RQC) and related mRNA surveillance pathways are influenced by changes in ribosome composition or post-translational modifications. The non-stop decay (NSD) and no-go decay (NGD) pathways target aberrant mRNAs; these include transcripts where the stop codon is missing or out of frame and transcripts with stall sequences, such as inhibitory codons or long polyA tracts (147-150). Collision of trailing ribosomes with the stalled or "leading" ribosome activates stress signals and triggers dissociation of the ribosome along with degradation of both the defective transcript and the incomplete nascent peptide (151-154). Monoubiquitination of specific small subunit RPs at the interface of

the two collided ribosomes by the ubiquitin E3 ligase zinc finger protein 598 (ZNF598) introduces heterogeneity in the ribosome pools and marks the ribosomes for subunit dissociation and recycling (147, 155-161). The small subunit protein receptor for activated C kinase 1 (RACK1, Asc1 in yeast) facilitates mRNA degradation during RQC and ribosomes depleted of RACK1 display defects in mRNA surveillance pathway activation (162).

**RACK1 as a hub for cellular signaling and translational control**

Beyond its role in RQC, RACK1 functions more broadly in translation. RACK1 is a eukaryote-specific, evolutionarily conserved member of the family of Trp-Asp (WD) repeat proteins with significant homology to the G protein beta subunit, a key participant in GPCR signaling pathways. WD repeat proteins typically form a seven- or eight-bladed β-propeller structure; these blades act as a scaffold for protein binding (163, 164). RACK1 is located on the head domain of the 40S subunit near the mRNA exit channel with much of its surface being solvent exposed (Figure 5) (165, 166). The cytosol-facing blades serve as docking sites for eIFs as well as stress and mitogenic kinases which helps integrate cellular signaling with translational output (167-169). There is strong evidence that in many cell types and like other RPs, extra-ribosomal RACK1 is degraded to restrict its signaling and other activities to the ribosome (169-173). Although RACK1 depletion is embryonic lethal in mice (174), RACK1 is not required for ribosome integrity or global protein synthesis in many cellular contexts, though its ribosome association reportedly stimulates overall rates of protein synthesis (169, 170). RACK1 also controls the translation of specific subsets of cellular transcripts (175, 176) and viral IRESs (93, 177, 178).

Until recently, the regulatory capacity of other structural domains besides the RACK1 blades were not known. RACK1 possesses a short loop connecting blades six and seven whose amino acid sequence varies across species, and which is not required for ribosome binding (165, 166). The human loop sequence consists of uncharged amino acids, but we found that during VacV infection, the viral B1 kinase introduces negative charge into the tip of the loop through single-site phosphorylation at Serine 278 ($S^{278}$). This post-translational modification uniquely occurs in VacV, and not in uninfected cells or cells infected with other DNA viruses, such as herpes simplex virus 1 (HSV-1) or RNA viruses such as vesicular stomatitis virus (VSV) and encephalomyocarditis virus (EMCV) (179). We unexpectedly discovered that phosphorylation at

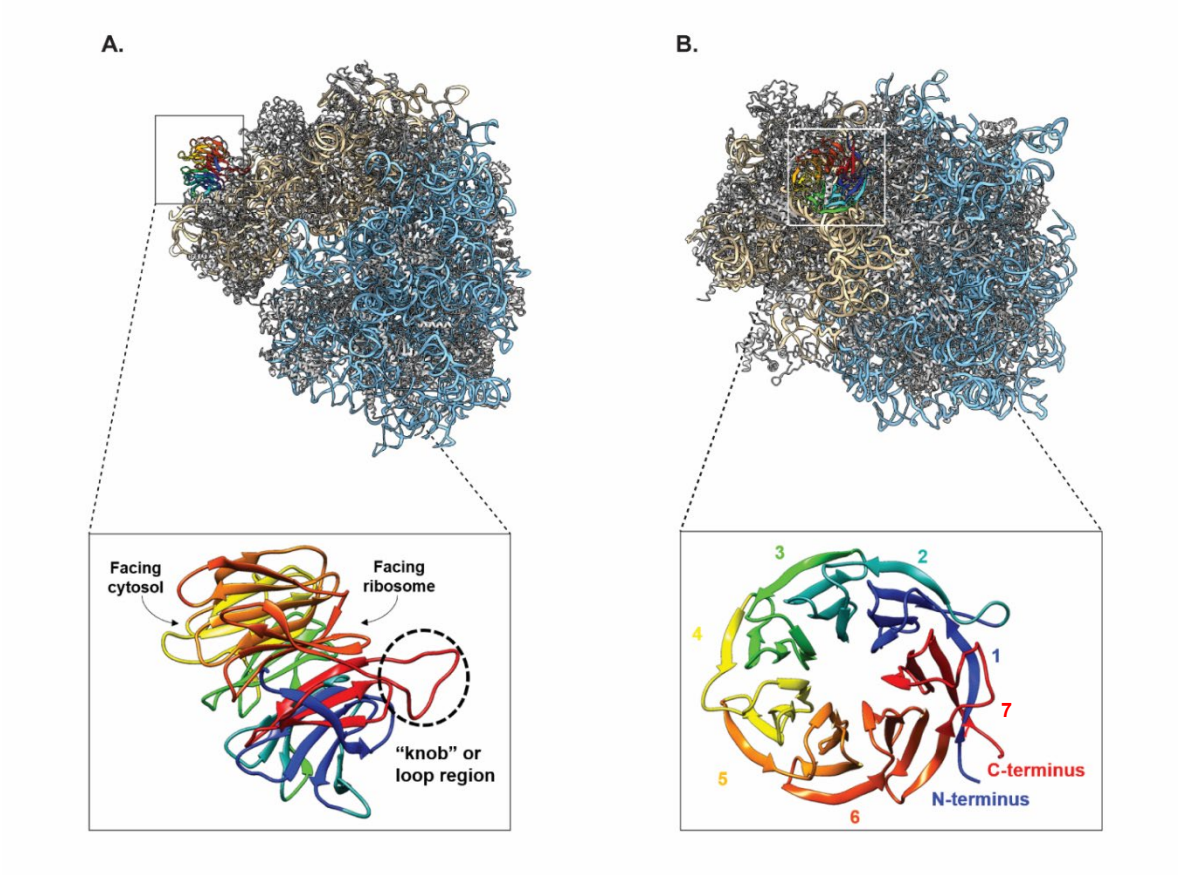


**Figure 5. Positioning of RACK1 on the ribosome**. (**A-B**) Ribbon diagram of RACK1 bound to the 40S subunit of the 80S ribosome. Rainbow coloring of RACK1 is based on WD repeats. 18S rRNA of 40S subunit (tan) and 5S, 5.8S and 28S rRNA of the 60S subunit (light blue) are also shown. In the inset for B, RACK1 is rotated 180° about the y-axis with respect to the main figure to help visualize the extended C-terminal loop between blades 6 and 7. PDB: 5T2C.

Serine 278 ($S^{278}$) enhances the translation of post-replicative viral transcripts with 5' polyA leaders. Prior to this finding, the function of 5' polyA leaders in a mammalian translational system remained an unexplained anomaly in poxvirus research. As described earlier, homopolymeric stretches of adenosines are well-known stall sequences that are rarely found outside of the 3' polyA tail of human transcripts, as tracts longer than 11nt causes ribosomes to undergo bi-directional "phaseless wandering" or sliding (160, 180, 181). Decoding of polyA present in the coding sequence or 3' polyA tail generates lysine repeats that alerts the ribosome quality control (RQC) machinery of aberrant translation events that stall ribosomes. When present in a non-coding 5' UTR sequence, however, sliding of initiating ribosomes on polyA tracts only inhibits processivity and slows the rate of initiation (180). This finding unearthed a role for poxvirus polyA leaders as translational enhancers and identified a novel regulatory function for the RACK1 loop region in translational control.

Adenosine-rich leader elements are well-documented enhancers in the transcripts of certain plants, such as *Arabidopsis thaliana* (182, 183), and plant viruses such as the omega leaders of tobacco mosaic virus which infects cultivated tobacco plants (*Nicotiana tabacum*) (184-186). Phylogenetic analysis revealed RACK1 from the plants *Nicotiana tabacum* and *Arabidopsis thaliana* encodes negatively charged residues in the loop region, suggesting that poxvirus mimics the use of negative charge in plant RACK1 by phosphorylation of the human loop to enable polyA enhancer activity. Expression of RACK1 in which we replaced $S^{278}$ with a glutamic acid ($S^{278}E$), which mimics poxvirus phosphorylation of human RACK1, or expression of a chimeric human RACK1 with the negatively charged *Arabidopsis thaliana* loop is sufficient to enhance translation of mRNAs with adenosine-rich 5' UTRs (179). Taken together, our preliminary investigations defined a role for negative charge in the RACK1 loop in VacV protein synthesis. But beyond this, the evolutionary and functional importance of RACK1 loop variability and the broader effects of a negatively charged loop on ribosome structure and translational output remains unknown. Using phylogenetic and biochemical approaches, we show that the RACK1 loop displays broad sequence plasticity across eukaryotes and is a species-specific regulator of the eukaryotic initiation factor eIF6, which controls 60S biogenesis and 80S assembly. Cryo-EM structure analysis shows that negative charge in the loop restructures the ribosome at tRNA binding sites which correlates with increased resistance to several

elongation inhibitors that bind in these regions. Charge in the loop also alters 40S head swivel motion to mimic the effect of several viral IRESs and support non-canonical, eIF4A-independent translation. These discoveries provide mechanistic insight into how the RACK1 loop region controls distinct aspects of translation and show how a single post-translational modification to an RP drastically impacts ribosome behavior and translational output.

# Chapter 2

## Materials and Methods

### Cell culture and viruses

Validated and certified human dermal fibroblasts from neonatal foreskin (NHDF-Neo) were purchased from Lonza Walkersville, Inc. (CC-2509). BSC40 and 293T cells used to generate viruses were obtained from Dr. Ian Mohr (NYU School of Medicine) and Dr. Mojgan Naghavi (Northwestern University), respectively. Phoenix-Ampho HEK 293 cells used to produce retrovirus were purchased from ATCC (CRL-3213). NHDF, BSC40, 293T and Phoenix-Ampho 293 cells were cultured in Dulbecco's Modified Eagle's Medium (DMEM; Fisher Scientific, MT15013CV) supplemented with 2 mM L-glutamine and 5% fetal bovine serum (FBS) and 1x penicillin-streptomycin. HAP1 cells (Horizon, C859) were grown in Iscove's Modified Dulbecco's medium with 4 mM L-glutamine and HEPES (IMDM; Fisher Scientific, SH3022801) that was supplemented 5% FBS and 1x penicillin-streptomycin. All cell cultures were maintained at 37°C with 5% $CO_2$ and confirmed negative for mycoplasma by DNA staining and imaging as well as biochemical testing using the MycoAlert TM PLUS Mycoplasma Detection Kit (Lonza Biosciences).

Vaccinia virus Western Reserve strain (VACV-WR) was grown in BSC40 cells infected at a multiplicity of infection (MOI) of 0.001 in DMEM with 2 mM L-glutamine and 1% FBS. Once the cytopathic effect was visible in 90% of the culture (48-72 h post-infection), the plates were scraped into the medium and collected in a 50 ml falcon tube. Cell free-lysates were prepared by three freeze-thaw cycles followed by centrifugation at 4,000rpm for 5 minutes at 4°C. Small (i.e., 1 mL) aliquots were stored at -80°C and virus stock titer was quantified by plaque assay of BSC40 cells.

To produce lentivirus, plasmids encoding gag-pol (p8.91) and env (pVSV-G) proteins were co-transfected into 293T cells along with the transducing plasmid. To produce other retroviruses, only the transducing plasmid was transfected into Phoenix-Ampho 293 packaging cells. Supernatants containing virus were collected 48 h post-transfection, filtered using a 0.45μm filter and used to transduce NHDFs or HAP1 cells and generate cell lines stably expressing the protein of interest (described below in more detail).

### Cloning of RACK1-eGFP constructs and generation of stable NHDF lines

Human receptor for activated C kinase 1 (RACK1) with a C-terminal eGFP tag was purchased from Addgene (pEGFPN1-RACK1; plasmid 41088). RACK1–eGFP cDNA was amplified using a forward primer with SpeI site: 5′-AAAAAACTAGTCTCAAGCTTATGACTGAGCAGATG-3′; and a reverse primer with NotI site: 5′-AAAAAGCGGCCGCTTACTTGTACAG-3′. PCR-amplified cDNA expressing human or wild-type (WT) RACK1 with a C-terminal eGFP was digested with SpeI and NotI (NEB Biolabs) and ligated into pLVX-IRES-Hygromycin plasmid (Takara Bio USA, Inc.) using standard cloning procedures. PCR and gel extraction kits used were from Qiagen, restriction enzymes and T4 DNA ligase were from NEB Biolabs, and subcloning efficiency DH5α competent cells were from Thermo Fisher Scientific. Site-directed mutagenesis of RACK1 was performed with two separate pairs of primers using QuickChange II XL Site-Directed Mutagenesis Kit (Agilent Technologies) or Q5 HighFidelity DNA polymerase reaction followed by Dpn1 treatment (NEB Biolabs). Primers used for site directed mutagenesis were:

(1) <u>S278E phosphomimetic mutant</u>: forward 5′-GTTATCAGTACCGAAAGCAAGGCAG-3′, reverse 5′-GTTATCAGTACCGAAAGCAAGGCAG-3′.

(2) <u>S276E/T277E/S278E/S279E phosphomimetic (STSS-EEEE)</u>: forward 5′-CAAGAAGTTATCGAAGAGGAAGAAAAGGCAGAACCAC-3′, reverse 5′-GTGGTTCTGCCTTTTCTTCCTCTTCGATAACTTCTTG-3′.

(3) <u>TS277-278DE phosphomimetic (TS-DE)</u>: forward 5′-GAAGTTATCAGTGATGAAAGCAAGGCAG-3′, reverse 5′-CTGCCTTGCTTTCATCACTGATAACTTC-3′.

The *Arabidopsis thaliana* loop chimera (plant), STSS deletion (ΔSTSS), STSS-AAAA mutant and *Saccharomyces cerevisiae* loop chimera (yeast) mutants were created by Gibson cloning using Gibson assembly master mix (NEB Biolabs) and a gBlock DNA fragment (Integrated DNA Technologies). gBLOCK DNA fragments were digested with BamHI and ligated into BamHI-digested peGFP-N1-RACK1 (Addgene, plasmid #41088). Insertions were confirmed by sequencing and used as templates for PCR amplification and subcloning into pLVX-IRES-Hygromycin, using the following primers and SpeI and NotI digestion: RACK1 Fwd SpeI 5′-AAAAAACTAGTCTCAAGCTTATGACTGAGCAGATG-3′, RACK1 Rev NotI 5′-AAAAAGCGGCCGCTTACTTGTACAG-3′. The gBLOCK sequences for the mutants and chimeras are provided below. Uppercase letters within the gBLOCK represent the mutations made to the STSS motif.

The uppercase letters at the 3′ end of the gBLOCK represent the introduction of a BamHI restriction site (GGATCC) and the inclusion of an 18 nt overhang for cloning. Lowercase letters indicate the original human RACK1 sequence:

*Arabidopsis thaliana* loop chimera (VISTSS> LKAEAEKADNSGPAAT): 5'-

gtgactgtctctccagatggatccctctgtgcttctggaggcaaggatggccaggccatgttatgggatctcaacgaaggcaaacacctttacacgct

agatggtggggacatcatcaacgccctgtgcttcagccctaaccgctactggctgtgtgctgcTacaggccccagcatcaagatctgggatttagag

ggaaagatcattgtagatgaactgaagcaagaaCTCAAGGCTGAGGCTGAAAAGGCTGACAACAGTGGTCCTGCT

GCCACCaaggcagaaccaccccagtgcacctccctggcctggtctgctgatggccagactctgtttgctggctacacggacaacctggtgcga

gtgtggcaggtgaccattggcacacgcGGGGTACCGCGGGCCCGGGATCCACCGGTCGCCACCatggt-3'.

ΔSTSS: 5′-

gtgactgtctctccagatggatccctctgtgcttctggaggcaaggatggccaggccatgttatgggatctcaacgaaggcaaacacctttacacgct

agatggtggggacatcatcaacgccctgtgcttcagccctaaccgctactggctgtgtgctgctacaggccccagcatcaagatctgggatttagag

ggaaagatcattgtagatgaactgaagcaagaagttatcaaggcagaaccaccccagtgcacctccctggcctggtctgctgatggccagactctg

tttgctggctacacggacaacctggtgcgagtgtggcaggtgaccattggcacacgcGGGGTACCGCGGGCCCGGGATCCACC

GGTCGCCACCatggt-3′

STSS-AAAA:

5′-

gtgactgtctctccagatggatccctctgtgcttctggaggcaaggatggccaggccatgttatgggatctcaacgaaggcaaacacctttacacgct

agatggtggggacatcatcaacgccctgtgcttcagccctaaccgctactggctgtgtgctgctacaggccccagcatcaagatctgggatttagag

ggaaagatcattgtagatgaactgaagcaagaagttatcGCTGCCGCTGCCaaggcagaaccaccccagtgcacctccctggcctggtct

gctgatggccagactctgtttgctggctacacggacaacctggtgcgagtgtggcaggtgaccattggcacacgcGGGGTACCGCGGGC

CCGGGATCCACCGGTCGCCACCatggt-3′.

*S. cerevisiae* loop chimera (VISTSS>FAGYS):

5′-

gtgactgtctctccagatggatccctctgtgcttctggaggcaaggatggccaggccatgttatgggatctcaacgaaggcaaacacctttacacgct

agatggtggggacatcatcaacgccctgtgcttcagccctaaccgctactggctgtgtgctgcTacaggccccagcatcaagatctgggatttagag

ggaaagatcattgtagatgaactgaagcaagaaTTCGCCGGCTACAGCaaggcagaaccaccccagtgcacctccctggcctggtct

gctgatggccagactctgtttgctggctacacggacaacctggtgcgagtgtggcaggtgaccattggcacacgcGGGGTACCGCGGGC CCGGGATCCACCGGTCGCCACCatggt-3′.

All constructs were verified by sequencing at the NUSeq Core Facility, Northwestern University or at ATGC, Inc. Original GFP-tagged RACK1 constructs were generated by Sujata Jha (Northwestern University).

To generate NHDF RACK1-eGFP lines, lentivirus carrying the RACK1-eGFP forms was produced as described in the “Cell culture and viruses” section of the methods using the RACK1-eGFP constructs described above as the transducing plasmid. NHDFs were transduced with the RACK1-eGFP lentiviruses and then selected with 100 µg/ml hygromycin B to generate pools of NHDFs stably expressing RACK1-eGFP forms in a background of endogenous RACK1. For “high transduction” lines (see Chapter 3), polybrene was used. For “moderate transduction” lines (see Chapter 3), polybrene was not used. NHDF RACK1-eGFP lines were maintained in DMEM supplemented with 20 µg/ml hygromycin B; however, the antibiotic was removed from the media for all experiments performed.

**CRISPR-Cas9 knockout of RACK1 in HAP1 cells**

To produce RACK1-knockout HAP1 cells, DNA oligonucleotides (GNB2L1 exon 2, 5′-CACCGATTCCACAGCGTGCTCTGCG-3′ and 5′-AAACCGCAGAGCACGCTGTGGAATC-3′, and GNB2L1 exon 3, 5′-CACCGACCACCACGAGGCGATTTGT-3′ and 5′-AAACACAAATCGCCTCGTGGTGGTC-3′) representing single-guide RNA sequences targeting exons 2 and 3 were annealed and cloned into pSpCas9(BB)-2A-GFP (pX458, Addgene Plasmid #48138), which expresses Cas9. The pX458 plasmids encoding these exon-targeting guide RNAs were then transfected into parental HAP1 cells using lipofectamine 2000 (Life technologies) using the manufacturer’s protocol. 48 h after transfection, GFP+ cells were FACS sorted, subcloned and clonal cell lines were screened by immunoblotting with RACK1 antibody. Potential CRISPR-knockout cell lines were then genotyped using the primers 5′-CCAGTGTGTTAAACGGGCTGC-3′ and 5′-GGAAGAGATCCTTGGAGATGG-3′ for amplification and sequencing. RACK1-knockout cells were generated by Gabriele Fuchs (SUNY Albany).

**Cloning of RACK1-Flag constructs and generation of HAP1 rescue lines**

To generate C-terminally Flag-tagged RACK1 constructs, RACK1 was amplified from our original pLVX constructs with either eGFP-tagged WT or $S^{278}E$ phosphomimetic RACK1 using the following primers:

(1) forward primer with SpeI site (RACK1 coding sequence regions underlined):

5'- AAAAAACTAGTCTCAAGCTTATGACTGAGCAGATG-3'

(2) reverse primer that introduced a Flag tag and a NotI restriction site: 5'-

ACCGAGCGGCCGCCTACTTGTCGTCATCGTCTTTGTAGTCGCCGCTGCCGCGTGTGCCAATGGT-3'.

Amplicons were digested with NotI and SpeI and subcloned into the empty pLVX-IRES-Hygromycin vector using standard cloning procedures. Both plasmid inserts were verified by sequencing at ATGC, Inc. To produce HAP1 RACK1 rescue lines, lentivirus carrying WT or $S^{278}E$ RACK1-Flag forms was produced as described in the "Cell culture and viruses" section of the methods with the RACK1-Flag constructs used as the transducing plasmid. HAP1 RACK1 knockout cells were transduced with the RACK1-Flag lentiviruses and then selected with 1 mg/ml hygromycin B to generate pools of HAP1 RACK1 knockout cells rescued with either WT or $S^{278}E$ RACK1-Flag. Polybrene was used to maximize transduction efficiency. HAP1 RACK1-Flag rescue lines were maintained in IMDM supplemented with 200 µg/ml hygromycin B; however, the antibiotic was removed from the media for all experiments performed.

**Cloning of Firefly Luciferase reporters**

The Firefly luciferase (FLuc) reporter plasmid was produced by first modifying the vector, pQCXIN (Clontech) to replace the linker sequence between the transcription start site (TSS) and FLuc open reading frame (ORF) with a shortened leader. We first digested pQCXIN with XbaI and EcoRI (NEBiolabs) to remove the linker between the CMV promoter/TSS and major cloning site, and replaced it with the following sequence in the form of a gBlock (the TSS and AgeI site used to insert reporters are underlined): 5′-

agatctgggggatcgatcctctagagtccgttacataacttacggtaaatggcccgcctggctgaccgcccaacgacccccgcccattgacgtcaat

aatgacgtatgttcccatagtaacgccaatagggactttccattgacgtcaatgggtggagtatttacggtaaactgcccacttggcagtacatcaagt

gtatcatatgccaagtacgccccctattgacgtcaatgacggtaaatggcccgcctggcattatgcccagtacatgaccttatgggactttcctacttgg

cagtacatctacgtattagtcatcgctattaccatggtgatgcggttttggcagtacatcaatgggcgtgaatagcggtttgactcacggggatttccaag

tctccaccccattgacgtcaatgggagtttgttttggcaccaaaatcaacgggactttccaaaatgtcgtaacaactccgccccattgacgcaaatgg

gcggtaggcgtgtacggtgggaggtctatataagcagagctcgtttagtgaaccgtcagatgcggccgcaccggtaggcctcgtacgcttaattaac ggatcggaattc-3′.

To generate firefly luciferase with a 30 nt polyA leader directly upstream, we PCR amplified the luciferase gene using the following primers:

(1) PolyA leader luciferase forward

5 ′- AAAACCGGTAAAAAA AAAAAAAAAAAAAAAAAAAAAAAACATATGGAAGACGCCAAAAAC-3′,

(2) PolyA leader luciferase reverse

5′-AAAAAGGATCCTTACAATTTGGACTTTCCGCCC-3′.

The PCR product was originally ligated into the retroviral vector pBABE-puro using AgeI and BamHI restriction enzymes and T4 ligation (NEB Biolabs). However, we sub-cloned the 30nt poly(A) leader and the FLuc ORF into the modified pQCXIN vector. This resulted in the following leader ahead of the FLuc ORF, with the TSS and ATG start sites underlined:

5′-tcagatgcggccgcaccggtAAAAAAAAAAAAAAAAAAAAAAAAAAAAAAcatatg-3′.

The sequence of the modified 5' UTR, polyA leader and FLuc ORF was verified by sequencing at ACGT, Inc.

**Sucrose gradient analysis (Polysome assay)**

For polysome analysis, cells were treated for 10 minutes with 100 µg/ml cycloheximide (in 70% ethanol) to freeze ribosomes, washed with ice-cold PBS containing cycloheximide and then scraped into ice-cold 1X lysis buffer (1% Triton X-100, 100 U/ml RiboLock RNase Inhibitor, Pierce™ complete mini EDTA-free protease inhibitor tablet [Roche], 20 mM Tris pH 7.5, 10 mM $MgCl_2$, 100 mM KCl, 5 mM DTT, 100 µg/ml cycloheximide). Cells were lysed for 20 min with gentle rocking. Lysates were clarified by spinning at 10,000xg for 10 minutes before layering on top of 10ml of 5-50% sucrose gradient made in 1X polysome buffer (20mM Tris-Cl pH 7.5, 10 mM $MgCl_2$, 100 mM KCl, 1 mM DTT, 100 µg/ml cycloheximide) and centrifuged in a SW 41-Ti rotor (Beckman Coulter, Inc.) at 36,000 rpm, 4 °C for 2 h. Lysates were loaded based on equal amounts of RNA (500 µg; RNA levels were also found to be equal by cell number). Following centrifugation, sucrose gradients were fractionated using an automated Density Gradient Fractionation System (Brandel Biomedical Research & Development Laboratories, Inc.) with continuous

monitoring at 254 nm using an UA-6 absorbance detector and recorded using PeakChart Software. For western blot analysis, fractions were trichloroacetic acid (TCA)-precipitated as follows: samples were incubated at 4°C overnight in TCA at a final concentration of 10%. Samples were then spun down at 10,000xg for 15 minutes. Pellets were washed twice in a 1:4 solution of 1X polysome buffer:acetone followed by centrifugation at 10,000xg for 15 minutes. Supernatants were removed and protein pellets were air dried, suspended in 1X Laemmli buffer (62.5 mM Tris-HCl at pH 6.8, 2% SDS, 10% glycerol, 0.7 M β -mercaptoethanol) and boiled for 3 min. Polysome total lysate samples used for SDS-PAGE were not TCA precipitated.

**Isolation of eGFP-tagged RACK1 complexes**

RACK1–eGFP complexes were isolated from soluble cell lysates as follows: NHDFs stably expressing wildtype, phosphomimetic or mutant RACK1–eGFP forms were seeded onto 6 cm or 10 cm dishes. Confluent cells were then washed with ice-cold PBS and scraped into 1X NP-40 lysis buffer (50 mM HEPES pH 7.4, 150 mM NaCl, 1.5 mM MgCl2, 2 mM EDTA, 1.6 mM $Na_3VO_4$, 25 mM glycerophosphate 1.5% NP-40 and Pierce™ complete mini EDTA-free protease inhibitor cocktail [Roche]). After incubation at 4 °C with continuous rocking for 40 min, lysates were clarified by centrifugation and incubated for at least 4h with GFP-Trap Agarose beads (Chromotek). Samples were then extensively washed before boil-elution in 1X Laemmli buffer. To rescue binding of the STSS-EEEE mutant, the same isolation assay was performed using 1X polysome lysis buffer (see “Sucrose gradient analysis” methods section). To detect eIF6 in RACK1-eGFP complexes, immunoprecipitation lysis buffer with 50 mM NaCl was used and cells were lysed with continuous rocking for 40-80 min.

**Western blotting**

Whole-cell lysates were prepared in 1X Laemmli followed by boiling for 3 min. Samples were resolved using 10% Tris-glycine SDS-PAGE performed under reducing conditions. Proteins resolved by gel electrophoresis were transferred to a 0.2 µm pore-size nitrocellulose membrane (GE Healthcare Life Sciences) using a wet electroblotting system (Mini Trans-Blot, Bio-Rad Laboratories, Inc.) at 57 V for 70 min. After transfer, the membrane was blocked in 5% non-fat dry milk in 1X TBS + 0.1% Tween (1X TBS-T) for 1 h at room temperature. Blocking buffer was then removed and membranes were rinsed in 1X TBS-

T before incubation with primary antibody (diluted in 3% BSA in 1X TBS-T) overnight at 4°C. The next day, membranes were washed with 1X TBS-T before incubation with HRP-conjugated secondary antibody (GE Healthcare Life Sciences) diluted 1:3000 in 5% non-fat dry milk, 0.1% tween in TBS for 1 h at room temperature, followed by washing. For detection, the membrane was incubated with Pierce ECL Western Blotting Substrate (Thermo Fisher Scientific) for 2 min before exposure to X-ray film. If standard ECL produced low level protein detection, membranes were incubated with Pierce SuperSignal West Femto Maximum Sensitivity substrate for 2 min. Western blots were quantified using densitometry. All antibodies used are listed in Table 2.

**Luciferase assays and qRT-PCR analysis**

For luciferase assays or RNA analysis, 10cm dishes of NHDFs stably expressing the RACK1-eGFP forms were electroporated with 2 µg pQCXIN reporter plasmid. For Luciferase assays, immediately following electroporation the cell suspension was seeded onto 12-well plates. 24 h post transfection, cultures were washed with PBS and lysed with 200 µl Luciferase Cell Culture Lysis Reagent (Promega). Lysates were clarified by centrifugation at 10,000xg for 2 min. 20 µl supernatant was added to 96-well plates and luminescence was measured using either a Spectramax (Molecular Devices) or a CLARIOstar microplate reader (BMG Labtech). For qRT-PCR analysis, cells were seeded onto 6-well plates immediately following electroporation. 24 h post transfection, cells were harvested and total RNA was isolated using Trizol (Thermo Fisher Scientific). 10 µl of total RNA was reverse transcribed using Transcriptor First cDNA synthesis kits (Roche Life Science) or RevertAid First Strand cDNA Synthesis kits (Thermo Fisher Scientific). The following primers were used for qRT-PCR: luciferase forward primer 5′-TCAAAGAGGCGAACTGTGTG-3′, luciferase reverse primer 5′-TTTTCCGTCATCGTCTTTCC-3′. Quantitative Real-Time PCR (qRT-PCR) was performed using PowerUp SYBR Green Master Mix (Applied Biosystems) on a 96-well plate using 7500 Fast Real-Time PCR System (Applied Biosystems). Absolute quantification of firefly luciferase reporter RNA was performed using the standard curve method. The pQCXIN polyA reporter plasmid linearized using XhoI (NEBiolabs) was used as the template for the standard curve. 115 ng of sample cDNA was used as the template for the reactions.

| Primary Antibodies (1°) | | | | | |
|---|---|---|---|---|---|
| **Antibody** | **Manufacturer/Source** | **Catalog Number** | **Host Species** | **Dilution** | **Application** |
| RACK1 | Cell Signaling Technologies | 5432 | rabbit | 1:1000 | WB |
| RPL11 | Cell Signaling Technologies | 14382 | rabbit | 1:1000 | WB |
| RPL13a | Cell Signaling Technologies | 2765 | rabbit | 1:1000 | WB |
| eIF3A | Cell Signaling Technologies | 3411 | rabbit | 1:1000 | WB |
| eIF3C | Cell Signaling Technologies | 2068 | rabbit | 1:1000 | WB |
| β-actin | Cell Signaling Technologies | 3700 | mouse | 1:10,000 | WB |
| eIF6 | Cell Signaling Technologies | D16E9 | rabbit | 1:1000 | WB |
| RPS10 | abcam | ab151550 | rabbit | 1:500 | WB |
| RPS3a | abcam | ab174894 | rabbit | 1:500 | WB |
| α-tubulin | Sigma Aldrich | T6199 | mouse | 1:4000 | WB |
| GAPDH | Santa Cruz Biotechnology | sc-47724 | mouse | 1:1000 | WB |
| eIF4E | BD Transduction Laboratories | 610270 | mouse | 1:1000 | WB |
| eIF4G | (Walsh & Mohr, 2006) | non-commercial | rabbit | 1:5000 | WB |
| PABP | (Walsh & Mohr, 2006) | non-commercial | rabbit | 1:5000 | WB |
| HSP90 | Cell Signaling Technologies | 4877 | rabbit | 1:1000 | WB |
| HSP40 | Cell Signaling Technologies | 4868 | rabbit | 1:1000 | WB |
| p-SAPK/JNK (Thr183/Tyr185) | Cell Signaling Technologies | 4668 | rabbit | 1:1000 | WB |
| p-p38 (Thr180/Tyr182) | Cell Signaling Technologies | 9211 | rabbit | 1:1000 | WB |
| eEF2 | Bethyl Laboratories | A301-688A | rabbit | 1:1000 | WB |
| SERBP1 | Bethyl Laboratories | A303-938A | rabbit | 1:1000 | WB |
| Ebp1 | Bethyl Laboratories | A303-084A | rabbit | 1:1000 | WB |
| RPS2 | GeneTex | GTX114734 | rabbit | 1:1000 | WB |
| GFP | Cell Signaling Technologies | 2956 | rabbit | 1:1000 | WB |
| RFP | ChromoTek | 6g6-100 | mouse | 1:1000 | WB |
| Raptor | Cell Signaling Technologies | 2280 | rabbit | 1:1000 | WB |
| FLAG M2 | Sigma Aldrich | A220 | mouse | 1:1000 | WB |
| **Secondary Antibodies (2°)** | | | | | |
| Antibody | Manufacturer/Source | Catalog Number | Host Species | Dilution | Application |
| HRP-linked anti-Rabbit IgG | Cytiva | NA934-1ML | donkey | 1:3000 | WB |
| HRP-linked anti-Mouse IgG | Cytiva | NA931-1ML | sheep | 1:3000 | WB |

**Table 2. Primary and Secondary Antibodies used for western blotting.**

**$^{35}$S-Methionine/Cysteine labeling and liquid scintillation counting**

Metabolic labeling was performed by incubating cells in methionine/cysteine (Met/Cys)-free DMEM (Corning, 17-204-CL) supplemented with 40 mM HEPES, 2 mM L-glutamine and a $^{35}$S-L-methionine and $^{35}$S-L-cysteine mix (PerkinElmer, NEG072007MC) for 30 min prior to cell lysis. For each ml of labeling media prepared, 0.035 mCi of the $^{35}$S Met/Cys mix was added. After in-well lysis in Laemmli buffer, samples were resolved by SDS-PAGE and gels were then fixed in 10% acetic acid/25% methanol solution for 30 min. The fixed gels were then dried at 80°C for 2 h using a Model 583 Gel Dryer (Biorad) and exposed to audioradiography film.

To quantify the activity of $^{35}$S present in the samples, 20 µl of radiolabeled sample was incubated with 10 µl of 10 mg/ml BSA and 1 ml of ice-cold 10% TCA solution for 30 min on ice. Precipitated proteins were vacuum filtered using a 1225 Sampling Manifold (Millipore Sigma) onto glass microfiber filters (GE Life Sciences, 1822-025), and washed twice each with ice-cold 10% TCA solution and 95% ethanol. Filter counting was performed by immersing the filters into 3 ml of Complete Counting Cocktail 3a70B (Research Products International Corp., 111154). The number of counts registered per minute (CPM) was measured using a Beckman LS 6500 liquid scintillation counter with a counting time of 5 min.

**Phylogenetic analysis and structure modeling of the RACK1 loop region**

The UniProt Basic Local Alignment Search Tool (BLAST) was used to search the UniProtKB database and identify known or expected RACK1 homologues. *H. sapiens*, *D. melanogaster*, *S. cerevisiae*, *A. thaliana*, *Phytophthora parasitica* and *Dictyostelium discoideum* RACK1 sequences were used as templates to retrieve sequences for vertebrate and invertebrate animals, yeast, plants, stramenopiles and amoeboids, respectively. For the search parameters, the E-threshold was set at 10. The search results were manually filtered for non-RACK1 sequences and duplicates, such that there would only be one sequence per species. In the cases that there were multiple sequences returned for a single species, only the longest and/or most recently updated sequence was retained. After filtering, the remaining 979 sequences were aligned using Clustal Omega and further analyzed using ESPript 3.0 (http://espript.ibcp.fr/ESPript/ESPript/index.php). All conserved residues are highlighted in black and similar residues in bold. Loop regions were manually inspected for the presence of negative charge and specific

charge organizations. The NCBI common tree generator was used to produce the cladogram, which was further processed and annotated using Evolview (https://www.evolgenius.info/evolview/#login).

All structures analyzed were obtained from the Protein Data Bank (PDB) and visualized using UCSF Chimera (https://www.cgl.ucsf.edu/chimera/). For the structures generated in Figure 5, unstructured regions of human RACK1 (PDB: 4AOW) were built with the standard loop modeling protocol with the UCSF Chimera interface to MODELLER (https://salilab.org/modeller/) using the default settings. One model was generated for display and propeller blades were color coded by WD repeat regions. Clash modeling of the RACK1 charged mutants (Figure 19A) was performed with the comparative modeling tool of the MODELLER interface in UCSF Chimera, using the default settings. RACK1 present in the cryo-EM structure of the 80S human ribosome (PDB: 5T2C) was used as the template. The target sequences modeled included the single site ($S^{278}E$) and quadruple-site (STSS-EEEE) phosphomimetics, and the *A. thaliana* plant loop (VISTSS>LKAEAEKADNSGPAAT) chimera. Of the five models generated, the structure that contacted the 18S rRNA phosphate backbone was selected for display. Interatomic clashes between loop motifs and the 18S rRNA were calculated with the FindClashes/Contacts tool in UCSF Chimera, using the default settings.

**RNAi treatment**

Pre-designed siRNAs were acquired from Thermo Fisher Scientific: control non-targeting siRNA (Cat No. AM4635), SERBP1 siRNA #1 (Cat No. 4392420, ID: s25142), SERBP1 siRNA #2 (Cat No. 4392420, ID: s25143). When at approximately 60% confluency, cells were transfected with siRNA (100 pmol/ml) using Lipofectamine RNAiMAX reagent (Thermo Fisher Scientific). Complete IMDM was added to the 500 µl OptiMEM used for RNAi approximately 4 h post-transfection. At 48 h post-transfection, cells were trypsinized and re-suspended in IMDM to minimize clumping. At 72 h post-transfection, cells were metabolically labeled and harvested.

**Inhibitor treatment**

Inhibitor stocks were prepared as follows with the appropriate vehicle noted in parentheses: 10 mM anisomycin (DMSO), 100 mg/ml cycloheximide (70% ethanol), 10 mM emetine ($dIH_2O$), 100 µM hippuristanol (DMSO), 100 µM silvestrol (DMSO), and 20 mg/ml puromycin (PBS). For the experiments

where inhibitor-treated cells were metabolically labeled, cells were pre-treated with the inhibitors for either 30 min (anisomycin, cycloheximide, emetine and puromycin) or 2h (hippuristanol and silvestrol) and, in all cases, inhibitors remained present during labeling. The final concentrations of the inhibitors used for treatment are indicated in the figures.

**Dual fluorescence translation stall assay**

HAP1 cells were seeded onto 12-well plates with or without coverslips, depending on downstream analysis. The control dual fluorescence reporter plasmid (pmGFP-P2A-$K_0$-P2A-RFP; Addgene #105686) or polyA dual fluorescence reporter plasmid (pmGFP-P2A-K$(AAA)_{20}$-P2A-RFP, Addgene #105688) were purchased from Addgene. Dual fluorescence reporter plasmids (1 µg) were transfected into cells using Lipofectamine 3000 (Thermo Fisher) according to the manufacturer's protocol. For transfection experiments where cells were treated with either 300 nM hippuristanol or DMSO solvent control, the vehicle or inhibitor were added 12 h post-transfection. 48 h post-transfection, cells seeded onto plates without coverslips were harvested for Western blotting and densitometry was used to measure GFP and RFP levels, as previously described. Cells seeded onto plates with coverslips were used to measure cellular GFP and RFP fluorescence and perform single-cell fluorescence analysis.

**Fluorescence microscopy and single-cell fluorescence analysis**

HAP1 cells expressing the WT or $S^{278}E$ RACK1-Flag constructs and transfected with the dual fluorescence stall reporters were seeded on glass coverslips and fixed 24 h later in 4% formaldehyde in PBS (Affymetrix) for 20 min at room temperature. Coverslips were then blocked in PBS containing 10% FBS and 0.25% saponin for 30 min at 37°C and then washed three times in PBS containing 0.025% saponin. After the washes, the coverslips were stained with Hoechst 33342 and mounted onto glass slides using FluorSave Reagent (Calbiochem) for direct imaging of GFP and RFP. Cells were imaged using a Leica DMI6000 wide-field microscope using a 100× objective (HC PL APO 100× /1.44 NA oil), ORCA FLASH 4.0 cMOS camera and Metamorph software. The Metamorph multi-dimensional acquisition function ensured that all sample sets were imaged using the same acquisition settings and that all images within a given dataset were processed equivalently. Image analysis was completed using Metamorph and compiled using the Fiji distribution of ImageJ.

For single cell RFP and GFP intensity measurements, randomized images were entered into the CellProfiler pipeline and resized to 256x256 pixels. The pipeline was used to identify target objects using the images in the RFP channel. Locations were marked based on RFP intensity relative to the background. Once the target object locations were identified, CellProfiler measured the RFP and GFP frequency at the location of each object. The mean intensity measurements of the object locations were used to generate violin plots and single-cell scatter plots.

**Ribosome purification for Cryo-EM**

HAP1 WT RACK1 or $S^{278}E$ RACK1 rescue cells were cultured in IMDM supplemented with 10% (v/v) FBS and 1X penicillin-streptomycin. Cells were grown to 80% confluency in 6 x 15cm dishes before discarding media by aspiration and washed with ice cold PBS thereafter. After aspiration, the residual PBS was used to scrape the cells from the dishes and the collected cells were pelleted by centrifugation at 2500xg for 5 min. Freshly harvested cells were resuspended in IP buffer (100 mM KOAc, 10 mM $MgCl_2$, 25 mM HEPES-KOH pH 7.4, 5% glycerol, 0.2% Igepal CA-630, 1 mM DTT, and a protease inhibitor cocktail comprising 0.5 µg/mL leupeptin, 0.5 µg/mL aprotinin, 0.7 µg/mL pepstatin, and 16.67 µg/mL PMSF) in a 4:1 (w/v) ratio and supplemented with benzonase (2.5 U/mL). Cells were lysed using a Dounce homogenizer submerged in ice with ~60 continuous strokes. Lysates were clarified by centrifugation, and the supernatant was incubated with anti-FLAG M2 affinity resin (Sigma) for 1 h at 4°C. Resin was washed thoroughly with IP buffer followed by several washes using the same buffer without detergent and glycerol. Ribosome complexes were recovered from the resin by competitive elution with synthetic 3x Flag peptide (APExBIO) for 1 h at 4°C with mild agitation. Eluted samples were immediately used for cryo-EM grid preparation.

**Electron cryo-microscopy**

UltrAuFoil R1.2/1.3 Au300 mesh grids (Quantifoil) were glow discharged using a Pelco easiGlow (Ted Pella, Inc.) for 25 s at 25 mA. 3.5 µL of sample were applied to the glow discharged grid, and grids were vitrified using a Mk. II Vitrobot (Thermo Fisher Scientific) operating at ~85% relative humidity, 4°C, and 2.5 seconds blot time, and then plunge frozen into liquid ethane.

A total of 3,842 cryo-EM movies of $S^{278}E$ RACK1 samples were recorded using a 300kV Titan Krios G3 (Thermo Fisher Scientific) equipped with a K2 Summit direct detector (Gatan, Inc.) at a nominal magnification of 105K x, corresponding to 1.348 Å pixel size. Movies were recorded using SerialEM with a defocus range of -1.0 to -3.0 µm and at a dose rate of 1.0 $e^-/Å^2$/frame with a total exposure of 40 frames and each movie recording time was 8 sec.

For WT RACK1 samples, a total of 2,141 movies were recorded on a 300kV Titan Krios G3 equipped with a K3 direct detector (Gatan) at a nominal magnification of 81,000x corresponding to 1.058 Å pixel size. Data were collected in super-resolution mode using SerialEM with a defocus range of from -0.8 to -1.8 µm and at a dose rate of 1.1 $e^-/Å^2$/frame with a total exposure of 40 frames and each movie recorded for 2.53 sec.

**Cryo-EM image processing**

Cryo-EM movie frames were dose weighted, motion corrected and summed using MotionCor2. All downstream steps were performed in cryoSPARC, including CTF estimation, particle selection, 2D class averaging, 3D classification, and 3D refinement. Micrographs with poor CTF estimates or crystalline ice were discarded. For RACK1 $S^{278}E$ images, a total of 191,242 particles were selected from 3,522 micrographs. A total of 103,133 particles were sorted into well-defined classes after two rounds of 2D classification (K=50) and used for ab-initio 3D reconstruction (K=5). Resulting classes revealed the separation of 80S particles in 40S rotated and nonrotated states (52,603 and 14,878 particles, respectively), a 40S class (16,758 particles), and two junk classes. The 80S and 40S classes were processed separately using non-uniform refinement followed by local resolution estimation and local filtering. Final resolution estimates were 3.1 Å for the 80S rotated state, 4.0 Å for the 80S nonrotated state, and 5.2 Å for the 40S particle.

For processing of WT RACK1 dataset, a total of 1,985 dose weighted, motion corrected, and summed movie frames (generated using MotionCor2) were used after discarding poor micrographs based on CTF estimation and ice quality. A total of 30,650 particles were resolved into clear 2D classes after two rounds of 2D classification from an initial number of 73,284 boxed particles. Particles were subject to ab-initio 3D reconstruction (K=3). Resulting classes revealed the separation of 80S particles in 40S head

rotated and nonrotated states (10,413 and 15,813 particles, respectively) and one junk class. No 40S classes were recovered. The 80S classes were refined separately using non-uniform refinement, as described above. Final resolution estimates were 4.2 Å for the 80S rotated state and 5.0 Å for the nonrotated state. Visualization and segmentation of density maps for both datasets were carried out in UCSF Chimera. All models were fitted with published ribosome structures using rigid body fitting in UCSF Chimera.

**Bioinformatic analyses**

5'UTR sequences were downloaded for each organism from the following Ensembl BioMart servers:

(1) Vertebrates: http://mart.ensembl.org/biomart/martview/

(2) Fungi: http://fungi.ensembl.org/biomart/martview/

(3) Plants: http://ensembl.gramene.org/biomart/martview/

The Saccharomyces cerevisiae 5'UTR sequences were downloaded from the SGD download pages accessible at https://downloads.yeastgenome.org/sequence/S288C_reference/. In cases in which a gene in a particular organism was represented by multiple transcripts, the transcript with the longest 5'UTR was chosen to represent the gene. Custom perl and R scripts were developed with the help of Dr. Elizabeth Bartom to process the 5'UTR sequences, report their nucleotide frequencies, identify the longest homopolymer tract for each nucleotide in each sequence, and visualize the results.

**Quantification and statistical analysis**

No statistical methods were used to pre-determine sample size. Investigators were neither blinded to sample treatment allocation during experiments nor outcome assessment. GraphPad Prism version 7 or 8 software was used for all statistical analyses. Results are displayed as the mean ± standard error of the mean (SEM) unless otherwise noted. Unpaired t-tests or analysis of variance (ANOVA) were performed to determine statistical significance (ns, $P>0.05$; *$P\leq0.05$; **$P\leq0.01$; ***$P\leq0.001$ and ****$P\leq0.0001$). ANOVA was followed by either Dunnett's or Sidak's multiple comparison post-hoc test. Additional statistical details can be found in the figure legends.

# Chapter 3

## A flexible RACK1 loop acts as a multifunctional species-specific regulator of ribosome assembly and polyA leader activity

*Parts of this chapter appeared as the published article "RACK1 evolved species-specific multifunctionality in translational control through sequence plasticity within a loop domain."*

### INTRODUCTION

Beyond transcriptional responses, regulated translation of individual mRNAs enables cells to rapidly adjust the levels of specific proteins during a wide range of processes. Although this regulation occurs at all stages of translation, much of it occurs during initiation when the 40S ribosomal subunit is first loaded onto and scans the 5′ untranslated region (UTR) of an mRNA (187). Once the 40S subunit identifies a start codon it is joined by a 60S subunit to form a translationally competent 80S ribosome that can begin decoding the mRNA open reading frame (ORF). Although each step is regulated by several eukaryotic initiation factors (eIFs) to control translation efficiency, ribosomes themselves are emerging as central players that can regulate the translation rates of individual mRNAs (188, 189). This concept of "ribosome specification" posits that ribosomes are not homogenous and indiscriminate machines but, instead, vary in composition to selectively control translation through the activity of individual ribosomal protein (RP) subunits that operate on specific 5′ UTR elements. However, we have a limited understanding of how and when ribosome diversification arises.

Receptor of activated protein C kinase 1 (RACK1) has recently emerged as a particularly intriguing small ribosomal protein (RPS) that functions in several aspects of translation. Containing seven Trp-Asp (WD) repeats and adopting a seven-bladed β-propeller structure, RACK1 is a highly conserved eukaryotic protein that is positioned on the head of the 40S subunit in the vicinity of the mRNA exit channel (165, 168). Although RACK1 has both ribosomal and extra-ribosomal functions in some transformed cell lines, it is now clear that it in several cell types and many normal cells RACK1 predominantly functions on the ribosome (168, 169). In doing so, RACK1 serves as a hub for host signaling to the protein synthesis machinery and directly controls translation (168-170). A number of its cytosol-facing β-propeller domains enable RACK1 to interact with eIF3c (190), one of several subunits of the eIF3 complex that interacts with various RPSs to bridge the 40S subunit to the 5′-end of mRNAs (187). Similarly oriented propeller domains also mediate

interactions with kinases, such as PKCβII, to transmit signals to ribosome-associated initiation factors (171, 172, 191). RACK1 is generally not required for the efficient synthesis of most proteins but, instead, facilitates translation of certain viral transcripts that contain either internal ribosome entry sites (IRESs) or polyA tracts, as well as small subsets of mRNAs in mammals and yeast (170, 175, 179, 192-198). Indeed, RACK1 can directly regulate ribosome activity and controls for example, frameshifting and ribosome quality-control responses induced by certain mRNA 'stall sequences' (156-158, 162, 199-203). Yet, beyond its β-propeller domains that facilitate several of its protein–protein interactions, how RACK1 regulates translation remains poorly understood.

We recently found that the poxvirus family member vaccinia virus (VacV) phosphorylates an STSS motif in a short variable loop that lies between the 6$^{th}$ and 7$^{th}$ β-propeller blade and extends from RACK1 toward the ribosome (179). Intriguingly, phosphorylation of this motif does not appear to occur outside the context of VacV infection, being driven by a unique viral kinase, and functions to promote translation of poxvirus mRNAs that contain unusual 5′ polyA leaders (97, 179). Moreover, the introduction of phosphate by VacV mimics the presence of negatively charged amino acids that are present in the RACK1 loop of the plants *Nicotiana tabacum* and *Arabidopsis thaliana* but are absent in human, mouse, worm and yeast loops (179). However, although these findings revealed a role for the RACK1 loop in VacV mRNA translation, the mechanistic basis by which the loop region functions and its broader importance beyond infection remain unknown. Here, we show that the RACK1 loop exhibits broad sequence plasticity across species and controls two distinct aspects of translation. First, independent of its charge status, RACK1 loop sequences are differently optimized in species to regulate interactions with the eukaryotic initiation factor eIF6, which controls 60S biogenesis and 80S assembly pathways. Second, phylogenetics reveals that specific groups known to utilize mRNAs with 5′ polyA leaders also encode RACK1 loop regions that harbor negatively charged residues. Functional testing reveals that distinct from regulating eIF6 interactions, only a negatively charged plant RACK1 loop enhances translation of mRNAs with 5′ polyA leaders. Moreover, modeling and biochemical testing suggests that the RACK1 loop charge generates electrostatic forces that are carefully controlled through spatial organization, and possibly remodel the mRNA exit channel to accommodate the

unusual structures adopted by polyA leaders. Overall, our findings suggest that sequence plasticity in its loop region enables RACK1 to control distinct aspects of translation in different species.

## RESULTS

### Evolutionary divergence of RACK1 loop sequence and charge usage

RACK1 displays high sequence homology among distantly related eukaryotes (204-207). However, the C-terminal loop between blades six and seven varies widely in amino acid usage, especially as it concerns the number and organization of negatively charged residues (Figure 6). The loop is uncharged in mammals and fungi but in certain plants, the loop is extended and possesses non-consecutive negatively charged amino acids (166, 179). Prompted by this observation, we performed a more extensive sequence analysis to check for broader variability in loop sequence across eukaryotes. We first assembled a phylogenetic tree from a BLAST search of available and predicted RACK1 protein sequences in the UniProtKB Protein database (Figure 7). Once duplicates and non-RACK1 sequences were removed, we analyzed approximately 979 species variants of RACK1. This included 31 protists, 332 animals, 485 fungi and 131 plants. This approach provided broad coverage of kingdoms, despite the more limited sequence availability of protists and plants. We discovered that most plants and animals have short loops that primarily consist of uncharged amino acids that display broader variations in size and polarity. Most metazoan (i.e., vertebrate and invertebrate) species' loops have polar residues with a S[T/P][S/N]S consensus sequence, similar to the STSS motif found in *Homo sapiens* (human) RACK1 that is targeted by VacV (Figure 8). The worm *C. elegans*, has a slightly altered SSGSS motif (Figure 8). Notably, 46.2% of yeast loops harbor negatively charged amino acids (i.e., aspartic acid and glutamic acid residues) (Figure 7 and Table 3). The remaining 53.8% of yeast loops that we analyzed primarily utilize uncharged, non-polar aliphatic or aromatic residues (Figure 7 and Table 3). For example, the VISTSS sequence in the human loop is replaced by an FAGYS motif in the yeast *Saccharomyces cerevisiae* (Figure 8).

Distinct from these other species, protists and dicot plants are unique in that most species analyzed possessed negative charge in the RACK1 loop (Figure 7). For example, 93.6% of all protist loops include at least one negatively charged residue (Figure 7 and Table 3). Of these, 34.5% encode a single negatively charged residue while the remaining 65.5% contain multiple charged residues, either in a consecutive,

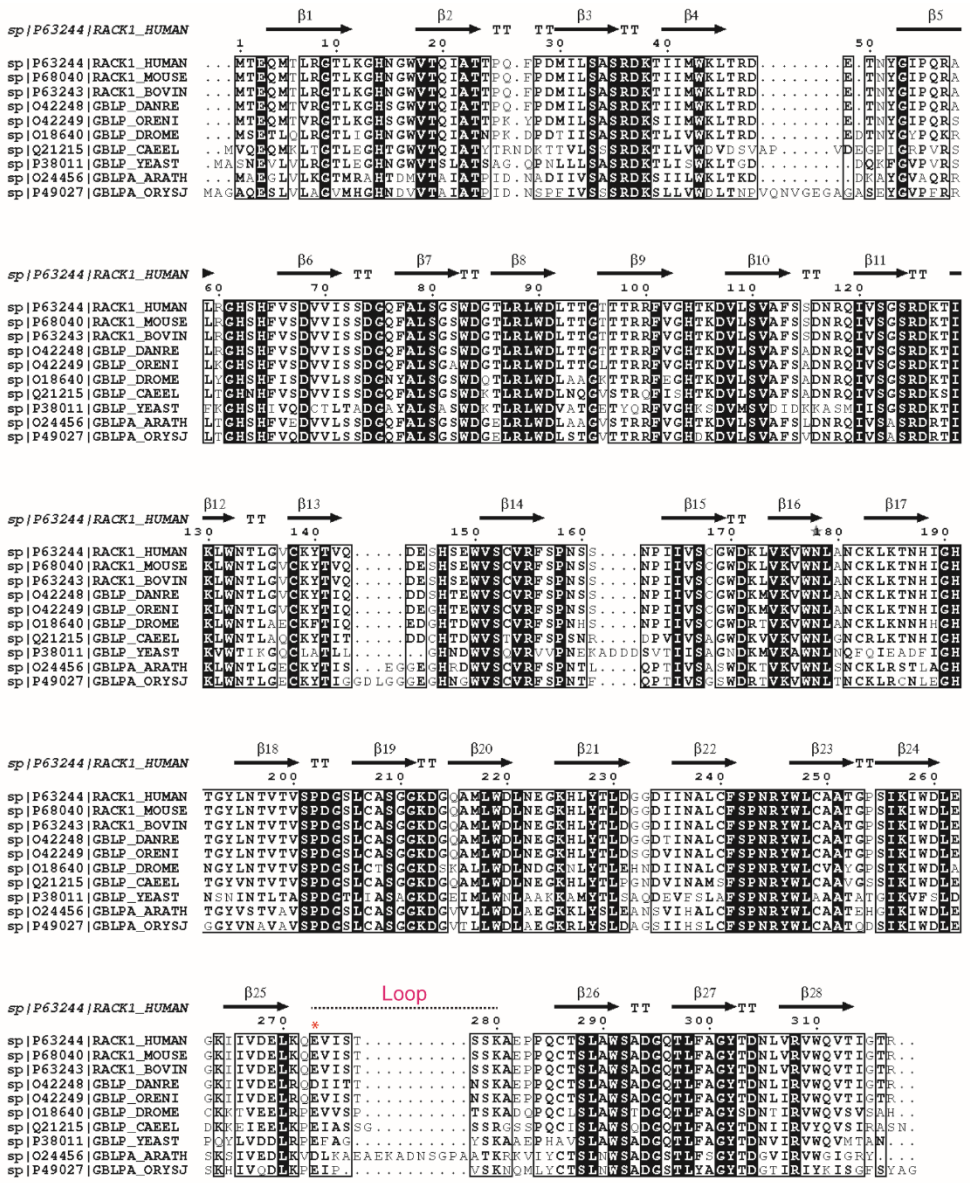


**Figure 6. Complete alignment of representative eukaryotic RACK1 sequences.** Sequences used in alignment were retrieved from UniProt, aligned in Clustal Omega and visualized using the black and white color scheme in ESPript. Black boxes with white letters depict strict sequence identity and bolded black letters show similarity. Human RACK1 (PDB: 4AOW) was used to generate the secondary structure elements and sequence numbering shown at the top of the alignment. β, β-strands; TT, strict β-turns. The red asterisk highlights a negatively charged residue at the border of the β-propeller/loop connection that is conserved across species.

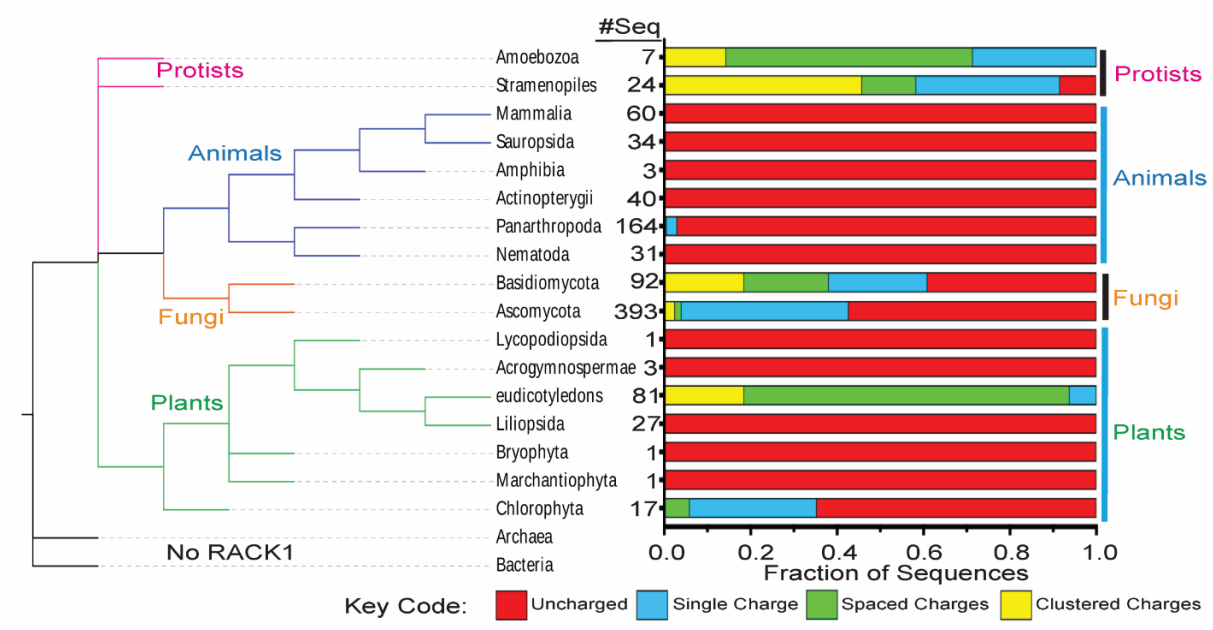


**Figure 7. Negative charge usage in RACK1 loop sequences across a phylogenetic tree.** Horizontal bar chart shows fractions of loop sequences from each group that have no (red), single (blue), multiple spaced (green) or clustered (yellow) negatively charged amino acids. The number of sequences for each group is indicated (also see Table 3). Branch lengths of phylogenetic tree do not indicate evolutionary time

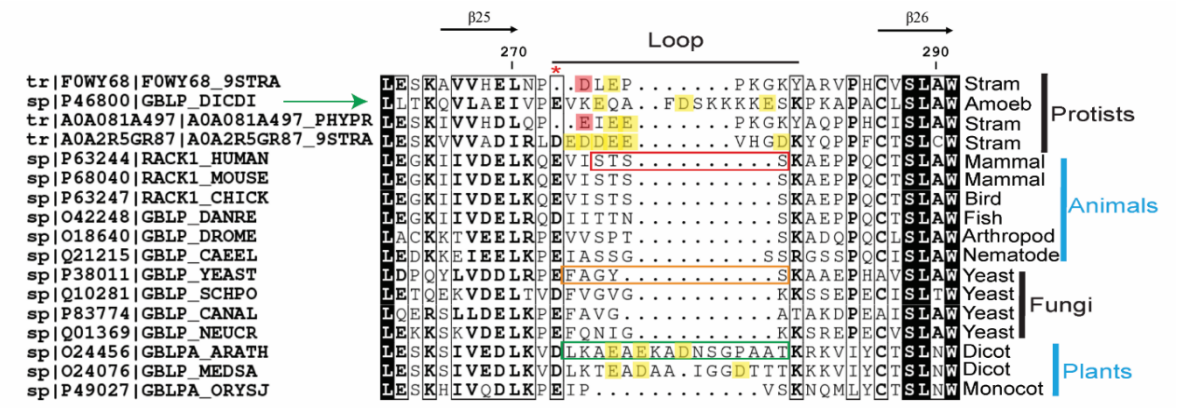


**Figure 8. Multiple sequence alignment of representative RACK1 loop sequences.** Human RACK1 (PDB: 4AOW) was used to generate the secondary structure and sequence numbering, which was manually annotated at the top of the alignment. Red asterisk highlights a negatively charged residue at the border of the β-propeller/loop connection that is conserved across species (red shaded boxes highlight this residue when shifted by the alignment program). Loops are longer in protists and plants, where yellow shaded boxes highlight negatively charged residues. Examples of single and multiple spaced or clustered charge organizations in protists are provided. The green arrow indicates the *D. discoideum* loop with spaced charge organization. Sequences used to generate loop chimeras in a human RACK1 background are shown in colored boxes.

| Number of RACK1 loop sequences analysed per group and their negative charge organization | | | | | | | |
|---|---|---|---|---|---|---|---|
| **Kingdom** | **Subkingdom or Superphylum** | **Phylum or Class** | **Uncharged** | **Single Charge** | **Spaced Charge** | **Clustered Charge** | **Total** |
| Protista | Stramenopile | | 2 | 8 | 3 | 11 | 24 |
| Protista | Amoebozoa | | 0 | 2 | 4 | 1 | 7 |
| Fungi | Dikarya | Ascomycota | 225 | 152 | 6 | 10 | 393 |
| Fungi | Dikarya | Basidiomycota | 36 | 21 | 18 | 17 | 92 |
| Animalia | Chordates | sauropsida (birds and reptiles) | 34 | 0 | 0 | 0 | 34 |
| Animalia | Chordates | mammals | 60 | 0 | 0 | 0 | 60 |
| Animalia | Chordates | amphibians | 3 | 0 | 0 | 0 | 3 |
| Animalia | Chordates | bony fish | 40 | 0 | 0 | 0 | 40 |
| Animalia | Ecdysozoa | panarthropoda | 159 | 4 | 1 | 0 | 164 |
| Animalia | Ecdysozoa | nematodes | 31 | 0 | 0 | 0 | 31 |
| Viridiplantae | Anthophyta | monocots | 27 | 0 | 0 | 0 | 27 |
| Viridiplantae | Anthophyta | dicots | 0 | 5 | 61 | 15 | 81 |
| Viridiplantae | Chlorophyta | green algae | 11 | 5 | 1 | 0 | 17 |
| Viridiplantae | other | | 6 | 0 | 0 | 0 | 6 |
| Total Number of Sequences | | | 634 | 197 | 94 | 54 | 979 |

| RACK1 loop sequences by negative charge organization - Protist Breakdown with Percentages | | | | | | | |
|---|---|---|---|---|---|---|---|
| **Kingdom** | **Subkingdom or Superphylum** | **Phylum or Class** | **Uncharged** | **Single Charge** | **Spaced Charge** | **Clustered Charge** | **Total** |
| Protista | Stramenopile | | 2 | 8 | 3 | 11 | 24 |
| Protista | Amoebozoa | | 0 | 2 | 4 | 1 | 7 |
| Total Number | | | 2 | 10 | 7 | 12 | 31 |
| Percent of Protists | | | 6.5 | 32.3 | 22.6 | 38.7 | 100.0 |

| RACK1 loop sequences by negative charge organization - Plant Numbers as Percentages | | | | | | | |
|---|---|---|---|---|---|---|---|
| **Kingdom** | **Subkingdom or Superphylum** | **Phylum or Class** | **Uncharged** | **Single Charge** | **Spaced Charge** | **Clustered Charge** | **Total** |
| Viridiplantae | Anthophyta | monocots | 100.0 | 0.0 | 0.0 | 0.0 | 100 |
| Viridiplantae | Anthophyta | dicots | 0.0 | 6.2 | 75.3 | 18.5 | 100 |
| Viridiplantae | Chlorophyta | green algae | 64.7 | 29.4 | 5.9 | 0.0 | 100 |
| Viridiplantae | other | | 100.0 | 0.0 | 0.0 | 0.0 | 100 |

**Table 3. Breakdown analysis of RACK1 loop charge usage by group.** The number of RACK1 loop sequences analyzed per group is provided along with a breakdown of the numbers based on charge status and organization. Additional tables show specific breakdowns referenced in the main text.

"clustered" organization or a non-consecutive, "spaced" charge organization (Figure 7 and Table 3). The latter classification notably includes the single-celled amoeba *Dictyostelium discoideum*, which we will discuss later. Strikingly, 100% of eudicotyledons or dicot plants, which includes *A. thaliana*, encode negatively charged residues in the RACK1 loop (Figure 7 and Table 3). While some species organize the negatively charged residues in a cluster, 75.3% of RACK1 loop sequences among dicot plants contain multiple, spatially separated aspartates and/or glutamates (Figure 7 and Table 3).

**Species that encode a negatively charged RACK1 loop utilize long polyA leaders**

We next tested whether these differences in RACK1 loop amino acid sequence correlate with differences in homopolymer usage in mRNA 5' UTRs. To do this, we performed genome-wide bioinformatic analyses of long (≥ 13 nt) adenosine (A), cytosine (C), guanosine (G) or thymidine/uracil (T/U) tracts in the 5' UTRs of a subset of species for which databases were available. Most higher organisms select against polyA in both 5' UTRs and coding regions (160, 181, 208, 209). This is due, at least in part, to the fact that polyA stretches ≥11 nt cause both initiating 40S subunits in PICs and elongating 80S ribosomes to slide which impairs their forward processivity (160, 180, 181). Functional studies of polyA leaders report that these elements are generally absent and lack translational enhancer activity in human cells or yeast (119, 179, 209). In line with these findings, most animals, fungi and plants with uncharged RACK1 loops possess a small fraction of transcripts with polyA tracts ≥13 nt in length (Figure 9).

The six dicot plants with negatively charged loops had the largest fraction of genes with ≥13 nt 5' polyA tracts compared to the other species we analyzed (Figure 9); the increased frequency of long polyA tracts in dicot plants was not observed for other nucleotide homopolymers (Figure 10). Among the other species, only two bony fishes possessed a fraction of genes with long polyA tracts that was comparable to dicot plants, despite fish having an uncharged loop like other vertebrates (Figure 10). Given that there are no reports of polyA-mediated enhancer activity in fish or other vertebrates, these two species are likely rare outliers. It is also possible that these species may use strategies that are unrelated to RACK1 loop charge to exploit the regulatory potential of polyA-rich leader elements.

In addition, the few polyA tracts that were identified in species with an uncharged loop such as humans and budding yeast, increased in length and frequency as a function of overall UTR length (Figure

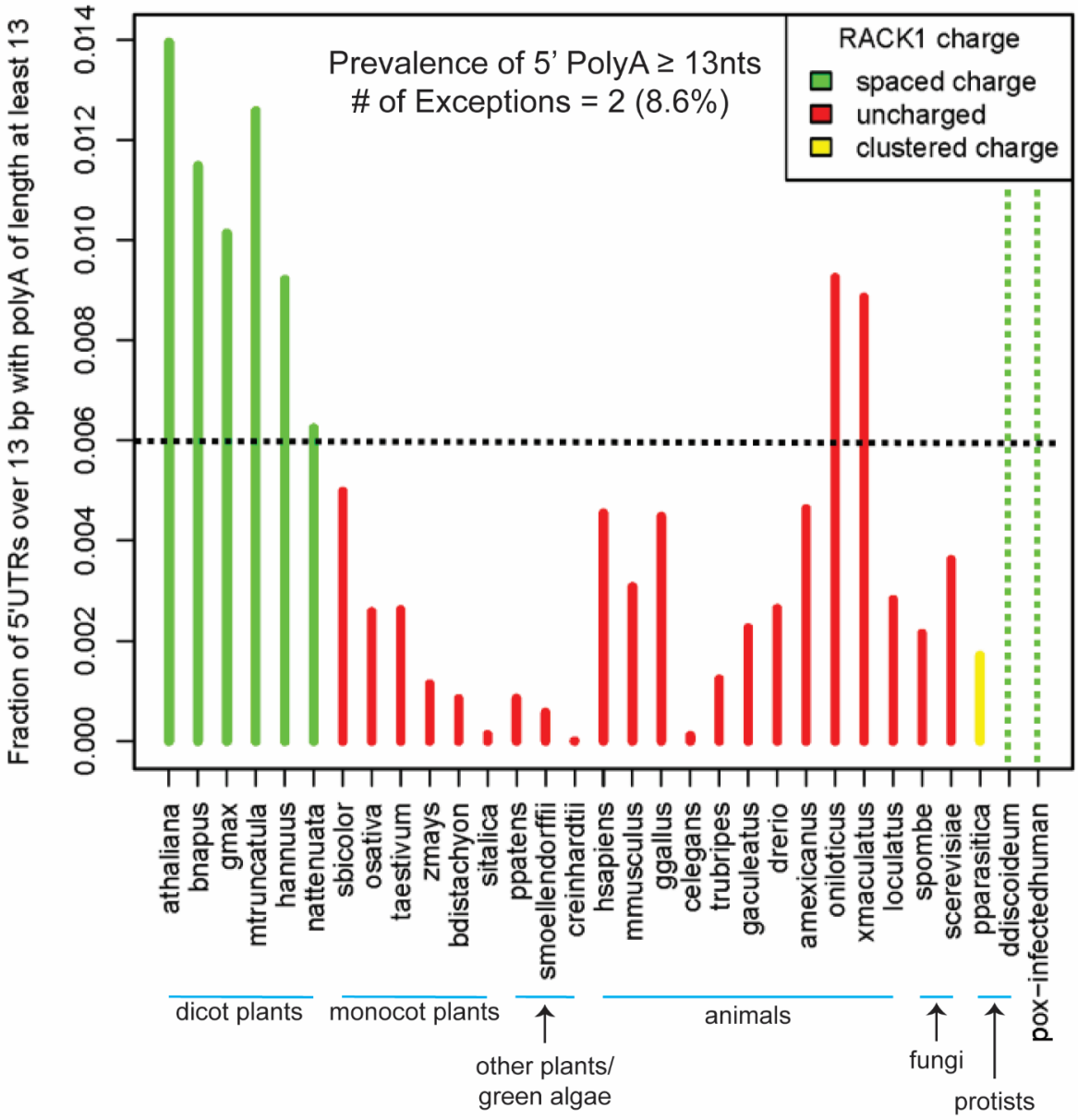


**Figure 9. Adenosine homopolymer and nucleotide use across different species**. The prevalence of polyA tracts ≥13nt across mRNA 5' UTRs of different species. Color coding matches that of Figure 7, indicating the negative charge status of each species' RACK1 loop: none (red), clustered (yellow) or spaced (green). Dotted black line highlights the lowest frequency of polyA use amongst dicots. Dotted green lines indicate additional contexts in which 5'polyA occurs in conjunction with RACK1 loop negative charge which includes poxvirus phosphorylation of human RACK1 and *D. discoideum* (see main text).

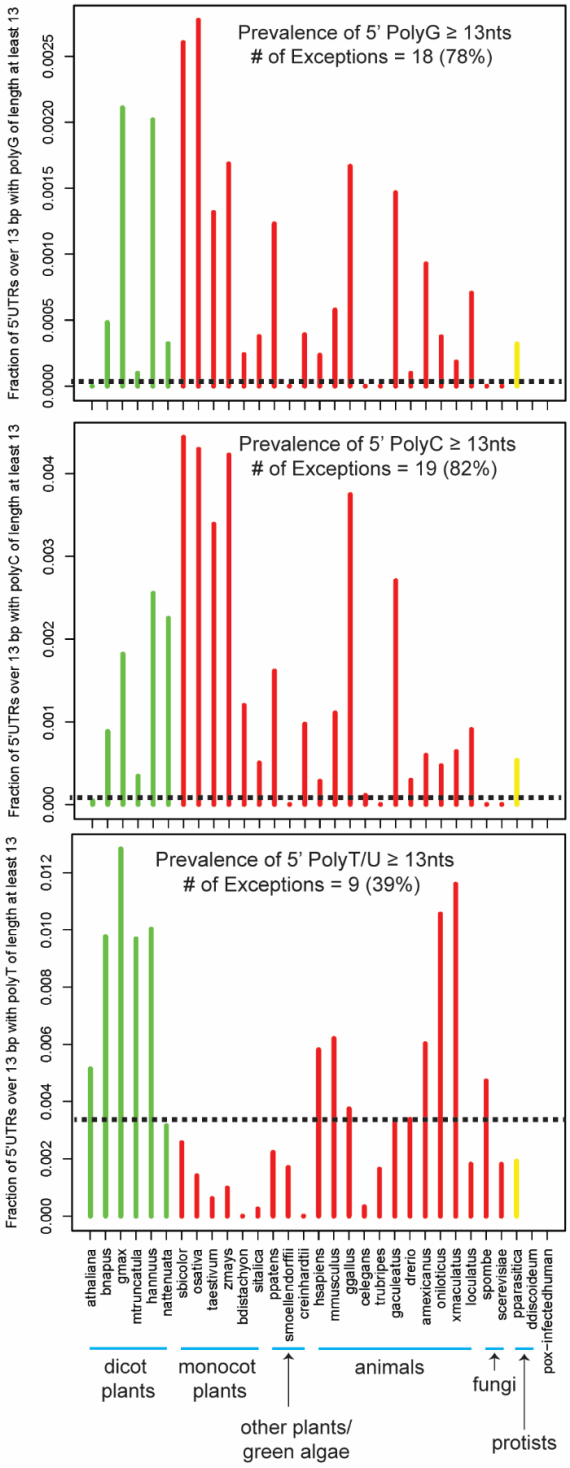


**Figure 10**. **Cytosine, guanine or thymine/uracil homopolymer use across different species**. The prevalence of polyG, polyC or polyT/U tracts ≥13nt in the UTRs of different species. Color coding matches that of Figure 7, indicating a lack of (red), clustered (yellow) or spaced (green) negatively charged amino acids in each species' RACK1 loop.

11). By contrast, despite having a similar number of genes and median 5' UTR length as humans, polyA tracts were found across all 5' UTR lengths in dicot plants with negatively charged loops, which suggests functional encoding (Figure 11). Moreover, Gene Ontology analysis of *A. thaliana* transcripts with 5' polyA tracts ≥13 nt revealed significant enrichment for mRNAs involved in responses to stimuli and single-organism processes (Figure 12). This aligns with the identification of A-rich "R-motifs" in the 5' UTRs of translationally upregulated genes during *A. thaliana* responses to microbial cues (182, 183). As an interesting parallel, dicot plant viruses also encode A-rich enhancer elements such as the tobacco mosaic virus (TMV) omega (Ω)-leader (210). For our controls, we observed no functional enrichment within the same number of genes grouped directly beneath polyA-rich gene sets, at the bottom of the polyA-ranked list, within *A. thaliana* genes with polyT tracts, nor within the smaller fraction of genes with 5' polyA tracts in the monocot rice plant *O. sativa* nor in humans – both of which possess uncharged loops. These observations suggest that longer A-rich elements likely have regulatory functions that are specific to dicot plants and may be functionally coupled to their use of negative charge in the RACK1 loop.

Two additional positive correlations between 5' polyA and RACK1 loop charge also occur, which are not recorded in databases but are graphically illustrated (Figure 9). First, poxvirus, mRNAs contain 5' polyA of 30-40 nt or longer (47, 48, 211), and poxviruses introduce a single phosphate into the short human RACK1 loop (179). Upon introduction of negative charge to the loop, the polyA leaders of poxviral transcripts function analogously to the A-rich enhancers present in the leader elements of transcripts from dicot plant viruses and their hosts. Second, protists, an unusual and diverse clade of eukaryotes, also encode negative charge in the RACK1 loop. Amongst these, *D. disocideum*, which we discussed earlier, has a longer loop with non-consecutive negatively charged residues similar to dicot plants (Figure 8, row two of RACK1 multiple sequence alignment). Although there is no 5' UTR database available, the majority of *D. discoideum* transcripts contain an unusual consensus motif comprised of polyA ≥15 nt preceding the initiator AUG, whose functional significance is unknown (212). It is also notable that mutations in the RACK1 loop impair *D. discoideum* growth and development (213), but precisely how the loop functions in these processes remains unknown. Intriguingly, the protist for which 5' UTR data was available, *P. parasitica* has a loop that is short yet contains two consecutive negatively charged amino acids (Figure 8, row three of

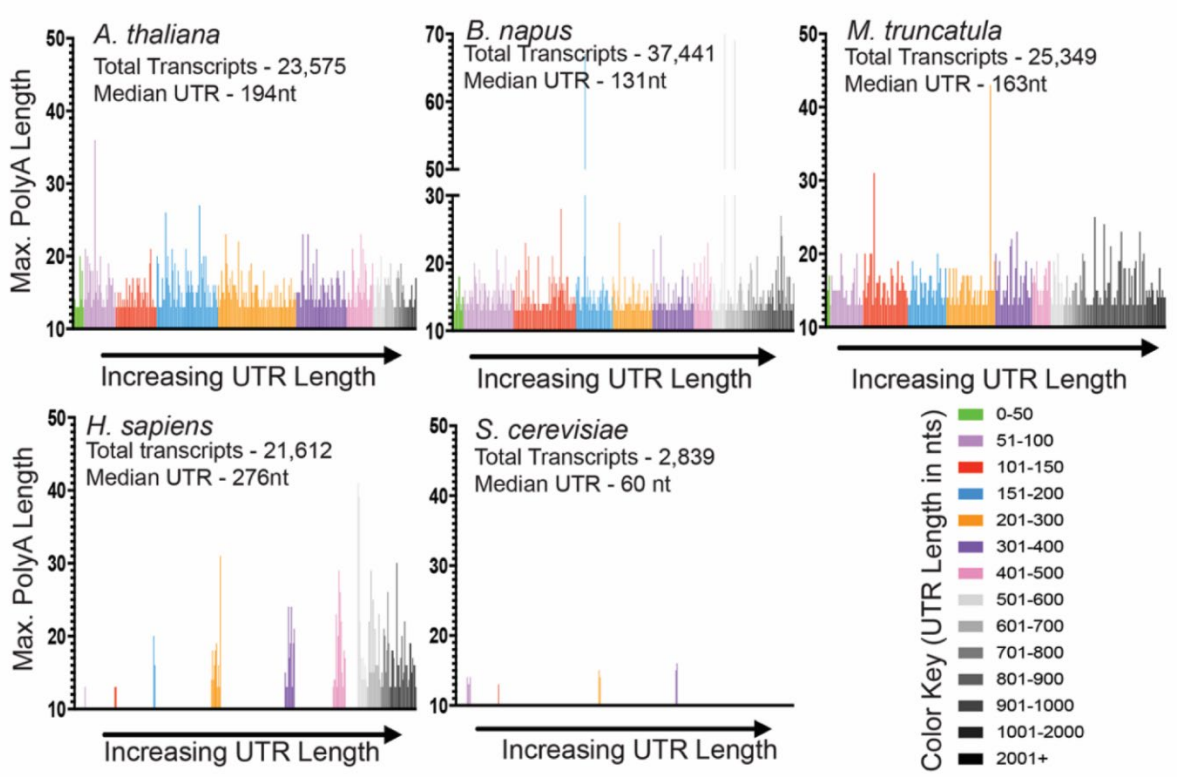


**Figure 11. Adenosine homopolymers ≥13nt are distributed across 5'UTRs of various lengths for dicots.** The distribution of polyA tracts ≥13nt as a function of 5' UTR length for representative dicot species (*A. thaliana*, *B. napus*, *M. truncatula*) compared to human (*H. sapiens*) and yeast (*S. cerevisiae)*. Color coding denotes UTR lengths as shown in the key. Total transcripts and median UTR length for each species is indicated.

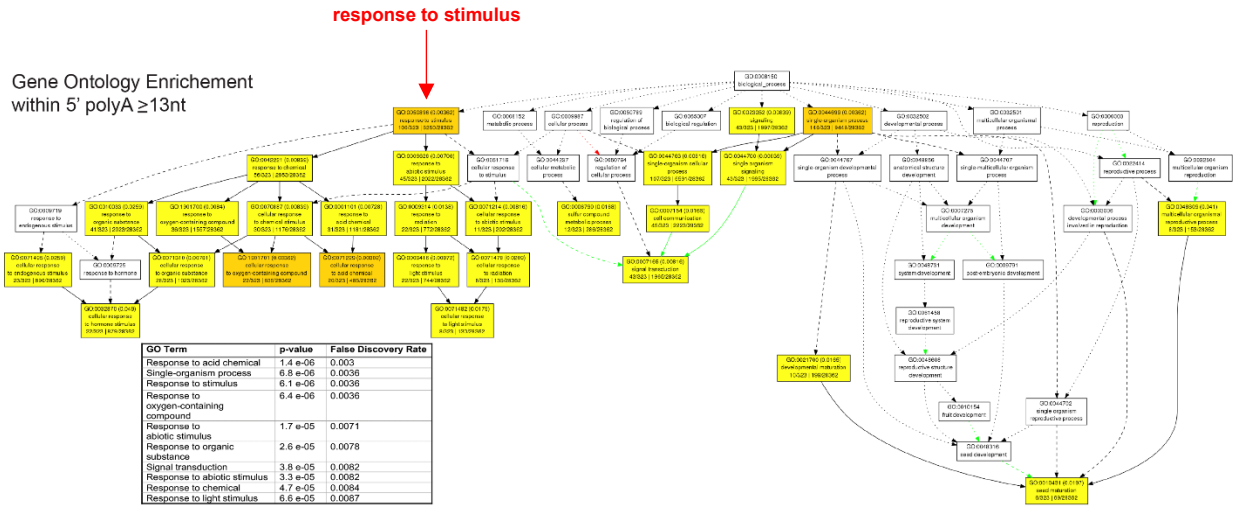


| GO Term | p-value | False Discovery Rate |
|---|---|---|
| Response to acid chemical | 1.4 e-06 | 0.003 |
| Single-organism process | 6.8 e-06 | 0.0036 |
| Response to stimulus | 6.1 e-06 | 0.0036 |
| Response to oxygen-containing compound | 6.4 e-06 | 0.0036 |
| Response to abiotic stimulus | 1.7 e-05 | 0.0071 |
| Response to organic substance | 2.6 e-05 | 0.0078 |
| Signal transduction | 3.8 e-05 | 0.0082 |
| Response to abiotic stimulus | 3.3 e-05 | 0.0082 |
| Response to chemical | 4.7 e-05 | 0.0084 |
| Response to light stimulus | 6.6 e-05 | 0.0087 |

**Figure 12. Agri-GO analysis for functional enrichment within *A. thaliana* genes with 5' polyA ≥13nts.** Significantly enriched processes are highlighted in yellow using the Agri-Go output. Table lists specific GO terms along with their respective p-value and False Discovery Rate.

RACK1 multiple sequence alignment). Despite being negatively charged, *P. parasitica* transcripts have a low frequency of UTRs with polyA ≥13 nt and no A-rich leaders like those of *D. discoideum* (Figure 9), suggesting that a tight threshold for appropriate charge spacing may exist in nature. Another possibility is that such species with alternate charge organization in the RACK1 loop may simply lack selective pressure(s) to drive both the evolution and retention of 5' polyA leaders as regulatory elements.

Despite the correlations that we uncovered, our 5' UTR database mining approach has some limitations. Notably, we cannot account for sequences with long polyA tracts that are interrupted by a single non-adenosine residue; such motifs may operate very similarly to the pure polyA tracts that we can extract with our current code. Therefore, there is a high likelihood that we are underestimating the number of A-rich domains present in dicot plants as well as other eukaryotic groups. To bypass this limitation, we could either incorporate a threshold or motif p-value to our code to permit a certain number of mismatches in our search for 5' UTR polyA tracts (214). We could also utilize a "sliding window" approach for 5' UTR analysis, where we shift a 13 nt frame along the length of the 5' UTR in single nucleotide increments to allow for a more careful inspection of the leader sequence. Regardless of our future approaches, our present phylogenetic analyses suggest that the use of negative charge in the RACK1 loop broadly correlates with and likely enables polyA leader enhancer activity among eukaryotes, even if many groups do not exploit the regulatory capacity of the loop.

**The RACK1 loop controls levels of 60S and 80S in a charge-independent manner**

To explore the potential functional significance of the loop sequence variability in different species, we created loop mutants and chimeras in the background of GFP-tagged human RACK1 and generated stably expressing pools of primary normal human dermal fibroblasts (NHDFs). We chose these cells as our model system for several important reasons. First, primary NHDFs retain normal translational control pathways that are typically dysregulated in most transformed cell lines (179, 215, 216). Second, GFP-tagged RACK1 is functional (179, 217) and allows us to both distinguish and directly compare the behaviors of exogenous and endogenous forms within the same cell. Indeed, expression of GFP-tagged wild-type (WT) RACK1 did not affect overall translation rates in NHDFs, distributed across polysomes similarly to the endogenous form and, as discussed later, produced polysome profiles within the normal range of variability

in these cells. Third, RACK1 has extra-ribosomal functions in several cell lines that might be linked to transformation or only operate in certain cellular contexts (168, 218). By contrast, several cell types – including primary fibroblasts – degrade extra-ribosomal RACK1 and restrict its function to the ribosome (165, 170, 177, 179, 196, 219, 220). For this reason, exogenous expression of RACK1 downregulates endogenous RACK1 levels such that RACK1 cannot be overexpressed in these cells (179). This homeostatic balance means that there is no supernumerary RACK1 in NHDFs, making these cells an ideal system to study RACK1 function on the ribosome.

We first investigated the effects of various RACK1 loop mutations and chimeras on the polysome profiles of NHDFs, prompted by our initial observation that a loop mutant in which we replaced the entire STSS motif with negatively charged phosphomimetic glutamic acid (E) residues (here on referred to as the STSS-EEEE mutant) shifted the profiles to an excess of free 40S subunits and reduced the levels of 80S initiation complexes and actively translating polyribosomes (179). Whether this phenomenon is specific to this clustered charge organization, which is underrepresented in nature, remains unknown. Western blot analysis showed that endogenous and GFP-tagged forms of human RACK1 were distributed across 40S, 80S and polysome fractions whereas the large ribosomal protein L11 (RPL11) was only detected on 60S, 80S and polysomes, as expected (Figure 13A). We observed similar distribution patterns in NHDFs expressing GFP-tagged human RACK1 in which the VISTSS motif was replaced by the yeast counterpart (*S. cerevisiae*; FAGYS) (Figure 8 and Figure 13A). However, expression of GFP-tagged human RACK1 in which the VISTSS motif was replaced with the loop sequence of a dicot plant (*A. thaliana*; LKAEAEKADNSGPAAT, where underlining denotes negatively charged residues) shifted the sedimentation of both endogenous and exogenous RACK1 to a predominance of 40S subunits and reduced the levels of RPL11 detected in 60S, 80S and polysome fractions (Figure 8 and Figure 13A). We observed similar profiles in NHDFs expressing human RACK1 with single ($S^{278}E$; also referred to as the poxvirus mimetic RACK1 form) and double (here on referred to as TS-DE) charge substitutions in the RACK1 loop (Figure 13B).

Surprisingly, the shift in polysome profiles that we first observed in the STSS-EEEE and later discovered in other negatively charged loop domains was also observed for an uncharged RACK1 loop

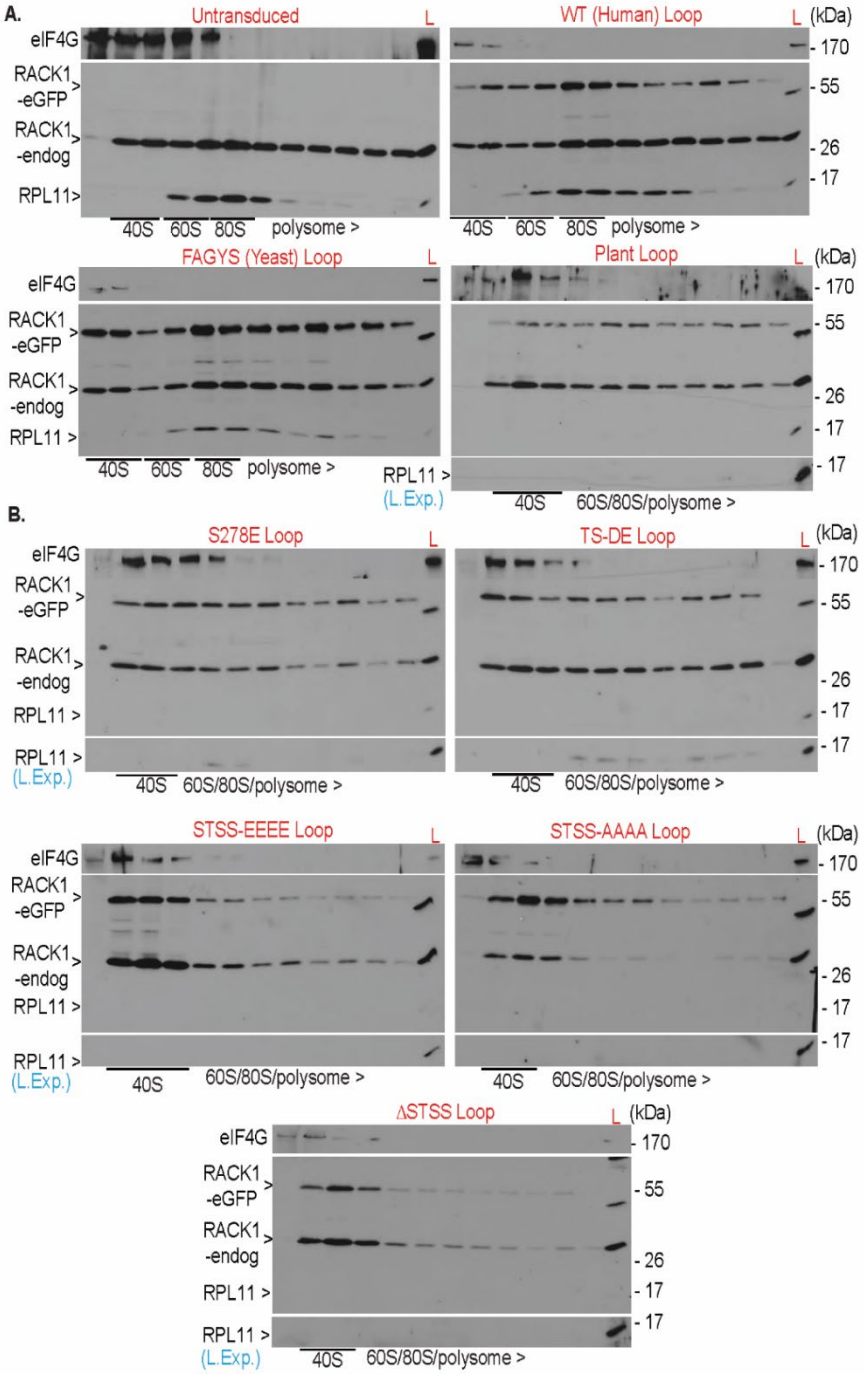


**Figure 13. Changes within the RACK1 loop sequence alter 60S, 80S and polyribosome levels.** (**A**) Western blot analysis of eIF4G, RACK1 and RPL11 distribution across ribosome fractions from non-transduced NHDFs or high-transduction NHDFs expressing GFP-tagged RACK1 harboring a human (WT), yeast or dicot plant loop. L, lysate. The longer exposure (L. Exp) shows RPL11 detection and reduced 60S and 80S ribosomes in NHDFs that express the plant loop chimera. (**B**) Western blot analysis of eIF4G, RACK1 and RPL11 distribution across ribosome fractions from high-transduction NHDFs that express GFP-tagged RACK1 harboring either negatively charged phosphomimetic or alanine substitutions within the STSS motif, as well as a mutant lacking the STSS motif (ΔSTSS). n≥3 for all experiments.

quadruple mutant in which the STSS motif was replaced with four uncharged alanine (A) residues (STSS-AAAA) (Figure 13B). Given the tendency of polyalanine tracts (i.e., 3-7 residues) to form alpha-helices (221, 222), we next examined the effects of deleting the STSS motif (ΔSTSS). Western blot analysis revealed that expression of the ΔSTSS deletion mutant also caused a shift towards 40S subunits and a decrease in 60S, 80S and polysome levels (Figure 13B). Representative traces further demonstrate the changes in the profiles that accompany the mutations producing these charged or uncharged loop forms (Figure 14).

Overall, these findings reveal that broader changes in loop sequence or structure, rather than negative charge affects the levels of assembled ribosomes and individual subunits. Our observation that the yeast FAGYS motif operates normally in human cells suggests that this function convergently evolved in these two distantly related eukaryotes, despite the difference in loop amino acid sequence. By contrast, the apparent lack of functionality of the *A. thaliana* plant loop in primary human fibroblasts indicates that the loop amino acid sequence is uniquely optimized for plant translational systems.

**The loop sequence controls RACK1 interactions with eIF6**

A serendipitous and initially perplexing clue as to why RACK1 loop mutations influence the ratio of free and ribosome-assembled subunits arose when we generated NHDF pools expressing a subset of the RACK1 mutants without using polybrene, which is used to increase retrovirus infection efficiency. These “moderately” transduced lines displayed a slight reduction in the levels of GFP-tagged RACK1 with either the $S^{278}E$ or ΔSTSS mutations as well as either the plant or yeast loop chimeras compared to the “highly” transduced lines we analyzed in the previous section (Figure 15). Despite this subtle difference, both endogenous and exogenous RACK1 were readily detected in the 40S, 80S and polysome fractions of moderately transduced fibroblasts as was RPL11 in the 60S, 80S and polysome fractions (Figure 16A). However, we discovered that 80S levels were elevated in fibroblasts that moderately expressed the RACK1 loop mutants whereas these same mutants lowered 80S levels in the highly transduced pools of NHDFs. These seemingly contradictory phenotypes in the high versus moderately transduced pools of NHDF mutants recapitulate the phenotypes reported from depletion studies performed on the RACK1-binding protein, eukaryotic translation initiation factor 6 (eIF6) (168, 219). eIF6 binds to 60S subunits and performs two key functions: (1) it controls 60S biogenesis and (2) it regulates 80S assembly by acting as a 60S anti-

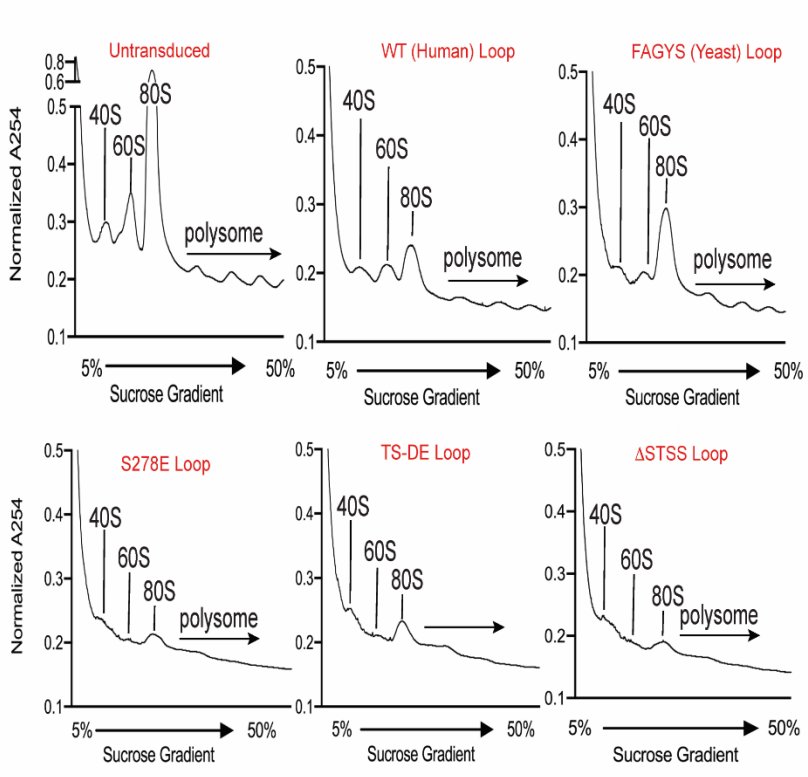


**Figure 14. Representative polysome traces of untransduced fibroblasts and pools expressing RACK1 forms.** Polysome traces from untransduced or high transduction NHDFs expressing RACK1 mutants that do or do not affect 60S and 80S ribosome levels. GFP-tagged RACK with WT (human) or a FAGYS (yeast) loop have no effect, while the effects of charged [$S^{278}$-E or TS-DE] or uncharged [ΔSTSS] loop mutants are shown as examples of the shift towards a predominance of 40S subunits accompanied by a decrease in 60S and 80S levels.

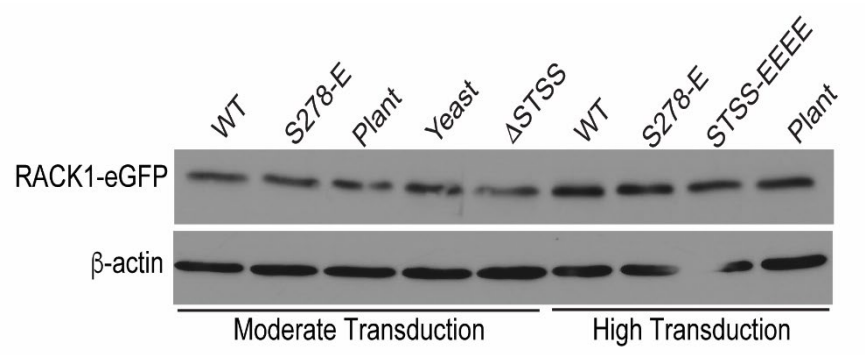


**Figure 15. Western blot analysis of moderate and high transduction RACK1-eGFP pools.** Representative western blot showing the relative expression levels of RACK1-eGFP variants in moderate transduction efficiency versus high transduction efficiency NHDF pools.

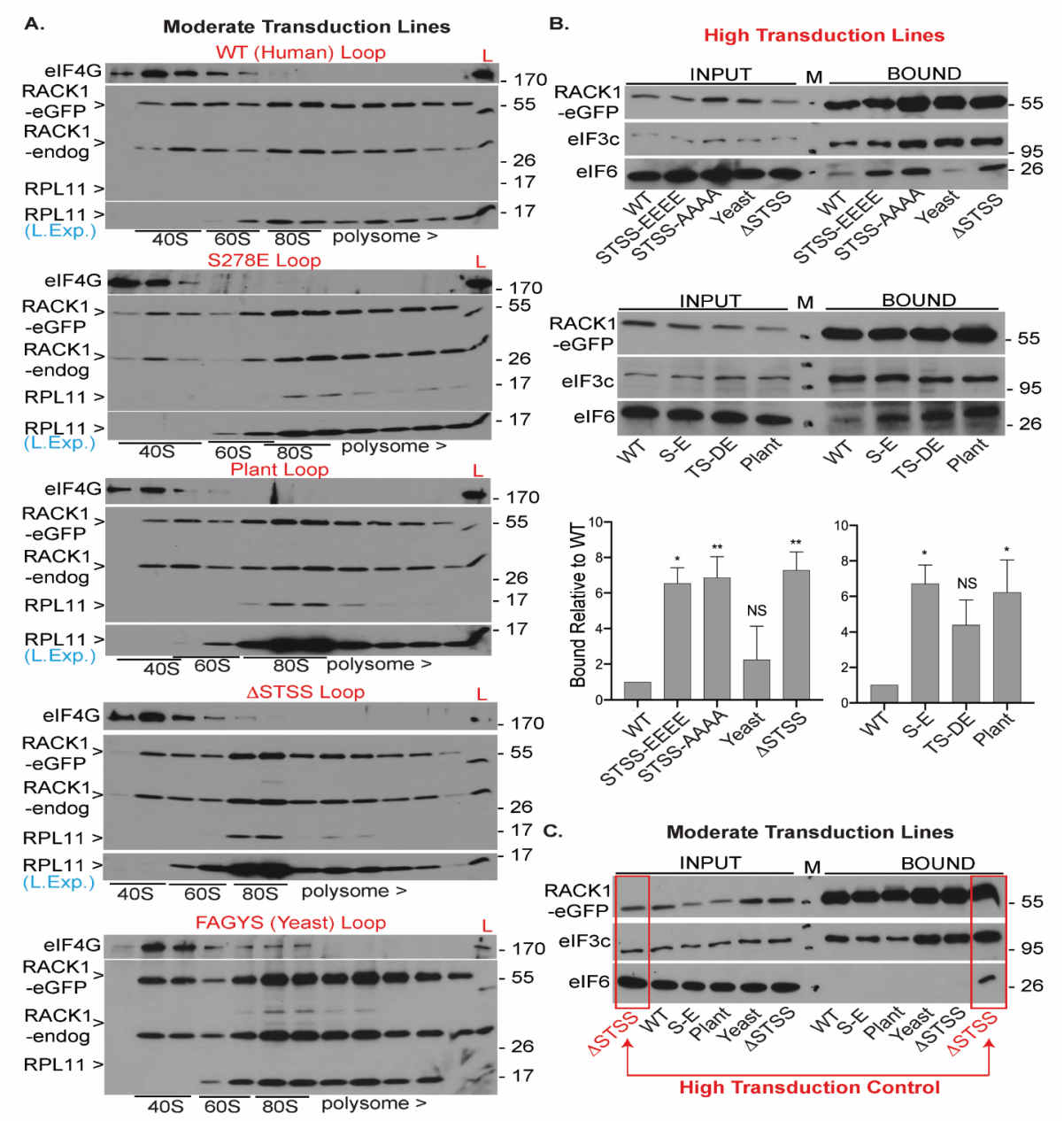


**Figure 16. The RACK1 loop regulates interactions with eIF6.** (**A**) Western blot analysis of eIF4G, RACK1 and RPL11 distribution across ribosome fractions from moderate-transduction NHDFs expressing GFP-tagged RACK1 harboring human wild type (WT), S-E ($S^{278}E$), dicot plant, ΔSTSS or yeast (FAGYS) loops. L, lysate; L. Exp., longer exposure. (**B**) Effects of RACK1 loop mutations or chimeras on RACK1 interactions with eIF3c or eIF6 in high-transduction NHDFs. RACK1-eGFP was recovered from soluble cell extracts by using GFP-Trap Sepharose, followed by western blot analysis of input and bound samples (top two panels). Quantification of the levels of eIF6 bound to each mutant relative to WT, normalized to 1 (bottom panels). Bars represent s.e.m., $n$=3 per group, except $n$=4 for S-E. *$P$≤0.05; **$P$≤0.01. One-way ANOVA with Dunnett's multiple comparisons test. (**C**) Effects of loop mutations or chimeras on interactions of RACK1 with eIF3c or eIF6 in moderate-transduction NHDFs. Flanking input and bound samples (boxed) are from a pulldown performed using lysates from high-transduction NHDFs expressing the ΔSTSS mutant as a control for eIF6 binding. Quantification of eIF6 binding in moderate transduction NHDFs could not be performed as binding was below reliable detection limits.

association factor that prevents 40S joining (223). Robust depletion of eIF6 or RACK1 reduces the levels of 60S subunits and impedes 80S assembly in mammals, yeast and plants (175, 224, 225), which is remarkably similar to the phenotypes we observe in our high transduction efficiency RACK1 loop mutant lines (Figure 13). By contrast, moderate reductions in eIF6 or RACK1 levels (e.g., mice that are heterozygous for either protein) do not impact 60S levels but instead increase in 80S levels (174, 226), which mirrors the profiles of our moderately transduced lines (Figure 16A). Although the reasons for this seemingly paradoxical effect of RACK1 and eIF6 levels remains unknown, the apparent dosing effect alludes to a dominant-negative function of diverse loop sequences in regulating the kinetics of subunit assembly.

To test whether changes to the loop sequence perturb eIF6 binding, we recovered RACK1-GFP complexes from both high and moderately transduced NHDFs using GFP-Trap Sepharose beads and compared eIF6 binding. Beginning with the high transduction lines, GFP binding assays showed that binding of eIF3c – which is mediated by the β-propeller blades of RACK1 (190) – was unaffected by loop mutations and reflected the level of RACK1-eGFP recovery across samples (Figure 16B). Furthermore, the amount of eIF3c enriched in the bound versus input samples mirrored RACK1 enrichment, suggesting that a large fraction of RACK1 binds a substantial fraction of the cellular eIF3c pool. This aligns with studies showing that RACK1 primarily functions on the 40S subunit where it interacts with initiation factors (227) and indicates that loop mutations do not affect these contacts. By contrast, although WT RACK1 bound to eIF6, eIF6 was not enriched in the bound samples compared to the input (Figure 16B). This suggest that only a small fraction of RACK1 binds eIF6, which confirms that RACK1 has limited extra-ribosomal activities in many cells, and that these interactions are likely transient. Strikingly, negatively charged (STSS-EEEE), uncharged (STSS-AAAA) or deletion (ΔSTSS) mutants of RACK1 increase eIF6 binding, whereas the yeast FAGYS motif functions analogously to the human STSS motif (Figure 16B). High transduction lines expressing either $S^{278}E$ or TS-DE RACK1 mutants or the plant loop chimeric RACK1 displayed similar increases in eIF6 binding compared to WT RACK1 (Figure 16B). Although the TS-DE mutant did not reach statistical significance due to variability in eIF6 binding, eIF6 bound to RACK1 in a similar range as the

other mutants. Thus, we established a direct correlation between high levels of eIF6 binding and defects in 60S and 80S levels in our high transduction pools of NHDFs expressing different RACK1 variants.

To test this further, we performed the same binding assay in our moderate transduction NHDF pools that did not display impaired 80S assembly in the profiles (Figure 16A). Remarkably, whereas eIF3c was enriched in bound fractions and its levels mirrored the recovery of RACK1 forms across samples, eIF6 binding was essentially undetectable in RACK1-GFP complexes isolated from the moderately transduced lines (Figure 16C). Direct comparison of the high transduction and moderate transduction lines expressing the ΔSTSS RACK1 mutant revealed the striking and specific difference in eIF6 recovery compared to eIF3c induced by seemingly negligible differences in exogenous RACK1 expression (Figure 16C). Based on our observed correlation between RACK1 loop mutant expression, eIF6 binding and 80S levels, we propose the following model (Figure 17): in non-transduced cells, most RACK1 stably binds to the 40S subunit while a small fraction of cycling RACK1 interacts with eIF6 (Figure 17A). This subpopulation of RACK1 regulates the function of eIF6 in 60S biogenesis and its release from 60S ribosomes to enable 80S assembly. The yeast loop complements the function of the human loop in our NHDF model, while the plant loop along with other charged or uncharged loop mutations bind tightly to eIF6 and impair its functions which reduces the levels of 60S and 80S (Figure 17B). Sequestration of key regulatory factors is a common mechanism in translational control, as exemplified by how limiting amounts of the eIF2 guanine nucleotide exchange factor eIF2B are sequestered through higher affinity binding by small amounts of the phosphorylated form of its own substrate, eIF2 (228). This parallels what we observe with RACK1, where a fractional subset of “free” RACK1 is responsible for eIF6 binding. Up to a certain threshold, all the exogenous RACK1 that is expressed is bound to ribosomes. However, exceeding this threshold shifts some of the exogenous RACK1 to the “free” RACK1 pool, which affects eIF6 binding (Figure 17B and Figure 17C). Taken together, our findings reveal that a secondary function of the RACK1 loop is to modulate interactions with eIF6 and that species-specific loop sequences are optimized to accomplish this activity in primary fibroblasts.

Given that a subset of RACK1 directly binds to eIF6 and that the loop affects this interaction, it is tempting to suggest that the RACK1 loop sequence co-evolves with eIF6 in certain species. In humans, RACK1 recruits activated protein kinase C beta II (PKCβII) and eIF6, which stimulates the PKCβII-

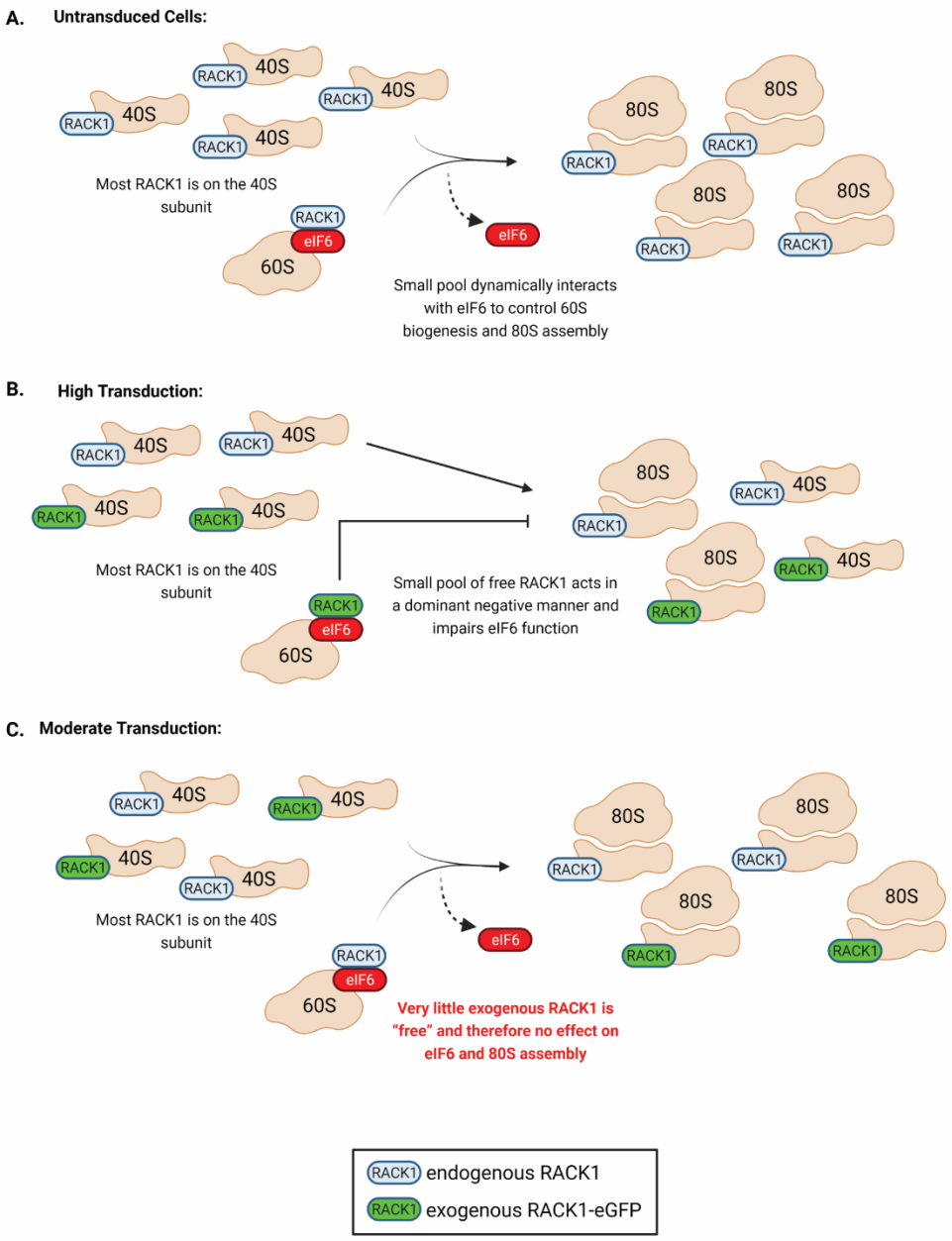


**Figure 17. Model for how the RACK1 loop regulates eIF6 activity.** (**A-C**) Models showing how high and moderate transduction levels differentially impact two distinct aspects of translation. (**A**) Under normal conditions (non-transduced), the vast majority of endogenous RACK1 (blue) is present on the 40S ribosome but a small fraction of "free" RACK1 binds eIF6 (red). eIF6 functions as a 60S anti-association factor, the release of which is required for efficient 80S assembly. (**B**) Under conditions of high exogenous RACK1-eGFP (green) transduction, the vast majority of RACK1-eGFP is present on the 40S ribosome. However, small amounts of exogenous RACK1 can also bind eIF6. When the exogenous RACK1 loop is mutated, eIF6 is bound too tightly, and impairs 60S biogenesis and 80S assembly, resulting in a profile shift towards a predominance of 40S subunits. (**C**) Under conditions of moderate RACK1-eGFP transduction, virtually all exogenously expressed RACK1 is present on the 40S ribosome due to high affinity; much less is available to bind eIF6, thereby, substantially minimizing the impact on 80S levels.

induced phosphorylation of eIF6 at Serine 235; this phosphorylation event releases the 60S subunit to enable 40S joining. Reports hypothesize that the loop region provides RACK1 with the structural flexibility required to accommodate PKCβII binding (205, 207); therefore, perturbations to the loop may impair PKCβII binding and, as a result, eIF6 phosphorylation. It is interesting to note that the PKCβII phosphorylation site in human eIF6 (i.e., Serine 235) is absent in non-mammalian animals, fungi, plants and protists (Figure 18), which indicates that other organisms might possess different phosphorylation sites or employ entirely different mechanisms to regulate 80S assembly (229). Strikingly, species whose loop domains cause defects in these phenotypes, such as the plant *A. thaliana*, do not possess a PKCβII ortholog, suggesting the activities of the RACK1 loop and PKCβII may have uniquely co-evolved in higher eukaryotes (224). It is also possible that plants utilize other protein kinases to phosphorylate eIF6 and interact with RACK1. Further studies are needed to characterize lineage-specific coevolution of RACK1, PKCβII and eIF6 interact as well as how these factors simultaneously interact to mediate 80S assembly.

**Negative charge in the RACK1 loop creates electrostatic repulsive forces against the 18S rRNA phosphate backbone**

Despite the small fraction of cycling RACK1 that interacts with eIF6, the majority of RACK1 tightly associates with the 40S subunit through an intricate interface comprised of contacts with small subunit proteins and 18S rRNA (165, 169, 177). This is reflected in our GFP binding assays, as RACK1 complexes are enriched with 40S-bound initiation factors such as eIF3c. By contrast, RACK1 interactions off the ribosome, as occurs with eIF6, are brief and transient and do not display any enrichment. On the ribosome, the loop region of RACK1 is proximal to 18S rRNA near the mRNA exit channel (165, 166); therefore, we hypothesized that the addition of negative charge in the loop creates repulsive forces against the phosphate backbone of 18S rRNA. To test this hypothesis, we homology-modeled varying extents of negative charge in the loop region of human RACK1 and counted the number interatomic clashes between residues of RACK1 and 18S RNA. There were no clash interactions between the uncharged STSS motif of WT RACK1 and 18S rRNA, while the $S^{278}E$ mutant, which mimics single-site phosphorylation during VacV infection, generated 15 clash interactions (Figure 19A). The count increased to 24 clashes for the STSS-EEEE phosphomimetic, which mimics the far less prevalent, clustered charge organization found in some protists

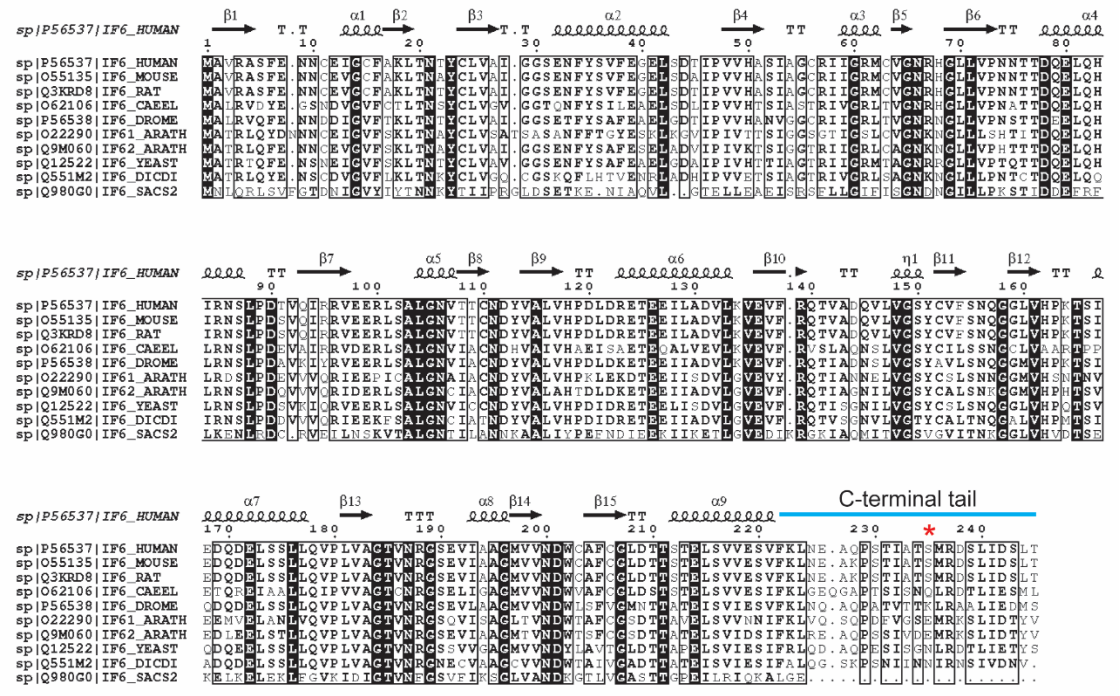


**Figure 18. Complete alignment of representative eukaryotic eIF6 sequences.** Sequences used in alignment were retrieved from UniProt, aligned in Clustal Omega and visualized using the black and white color scheme in ESPript. Black boxes with white letters depict strict sequence identity and bolded black letters show similarity. Yeast eIF6 (PDB: 1G62) was used to generate the secondary structure elements and sequence numbering shown at the top of the alignment. α, α-helices; η, $3_{10}$-helices; β, β-strands; TT, strict β-turns. Blue line indicates the C-terminal tail and the red asterisk highlights position 235 in the alignment, which marks the Serine residue phosphorylated by PKCβ in humans.

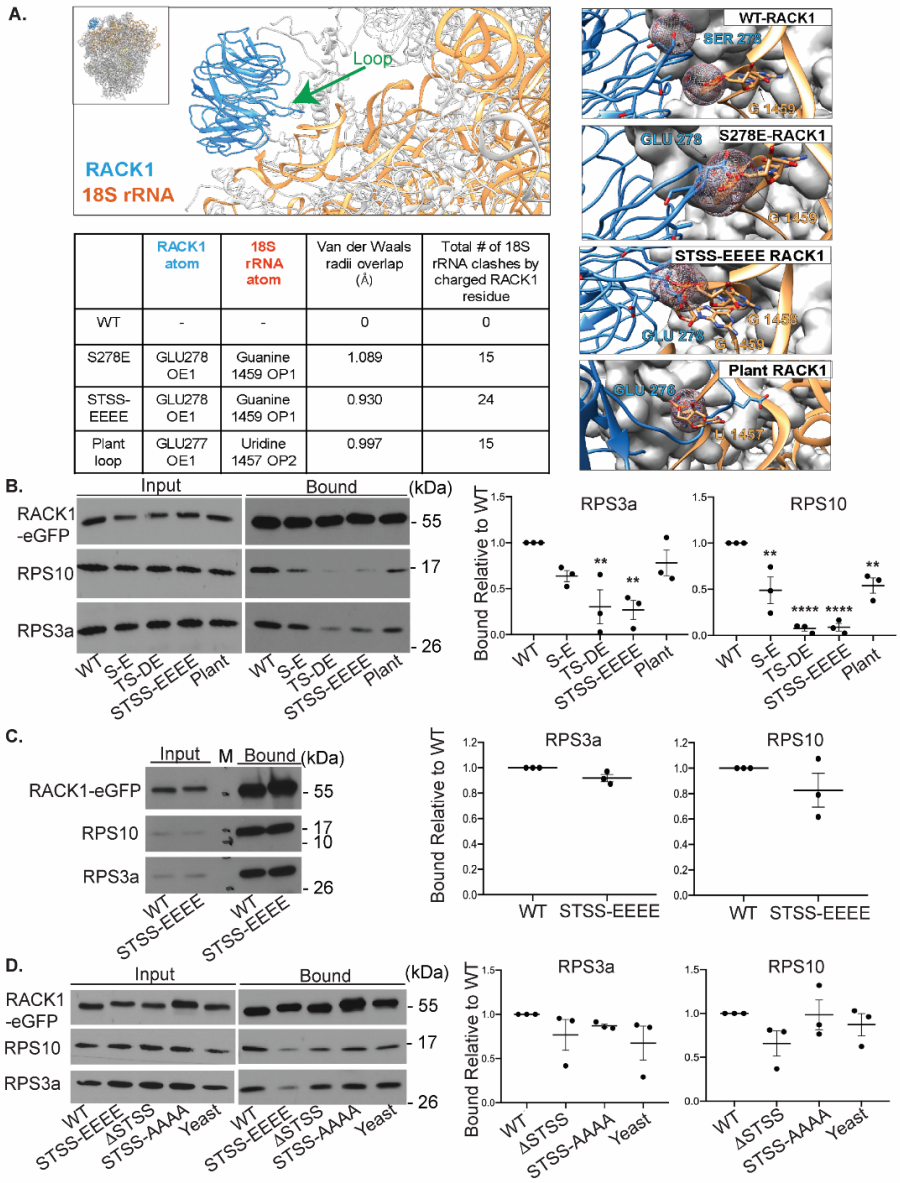


| | RACK1 atom | 18S rRNA atom | Van der Waals radii overlap (Å) | Total # of 18S rRNA clashes by charged RACK1 residue |
|---|---|---|---|---|
| WT | - | - | 0 | 0 |
| S278E | GLU278 OE1 | Guanine 1459 OP1 | 1.089 | 15 |
| STSS-EEEE | GLU278 OE1 | Guanine 1459 OP1 | 0.930 | 24 |
| Plant loop | GLU277 OE1 | Uridine 1457 OP2 | 0.997 | 15 |

**Figure 19. Negative charge within the RACK1 loop causes electrostatic repulsion against the 18S rRNA.** (**A**) Structure modeling of the RACK1 loop and clashes with 18S rRNA caused by negative charge. Electrostatic surfaces of select residues within the RACK1 loop and 18S rRNA visualize clash interactions (overlaps), if any. Table shows calculated values of van der Waals radii overlap, and specific atoms and molecules involved in clashes. (**B**) Effects of loop charge on association of RACK1 with RPSs. Quantification shows the mean ratio of bound RPS3a (black) or RPS10 (gray) to RACK1 relative to wild-type RACK1 (normalized to 1). Bars represent ±s.e.m., n=3 per group. RPS3a **P≤0.01; RPS10 **P≤0.01, ****P≤0.0001. One-way ANOVA followed by Sidak's or Dunnett's multiple comparisons test. (**C**) Rescue of apparent RPS-binding defects in the RACK1 STSS-EEEE mutant under changed buffer conditions. Assays and quantification were performed as described for panel B, except that polysome lysis buffer was used in C (instead of RACK1 isolation buffer). Bars represent ±s.e.m., n=3 per group. Unpaired t-test with Welch's correction was performed. No statistical significance was found. Welch's t-test used due to unequal variance between the two sample sets (**D**) Effects of uncharged loop mutations on RACK1 association with RPSs. Quantification shows mean ratio of bound RPS3a (black) or RPS10 (gray) as in B. Bars represent s.e.m., n=3 per group. No statistical significance was found. One-way ANOVA followed by Dunnett's multiple comparisons test. The STSS-EEEE loop mutant is shown in the western blot panel as a positive control, to detect reduced binding to RPSs.

(Figure 19A). Notably, the clash count dropped to 15 for *A. thaliana* plant loop chimeric RACK1 in which multiple negatively charged residues are separated by one or two uncharged residues (Figure 19A). Overall, the homology modeling suggests that the number and spatial organization of charged residues controls the electrostatic interactions between RACK1 and 18S rRNA.

To test these predictions biochemically, we examined how several GFP-tagged RACK1 loop mutants associated with other small subunit proteins as a readout for ribosome binding. We isolated the eGFP-tagged RACK1 forms from whole cell extracts using GFP-Trap Sepharose and our conventional high salt immunoprecipitation (IP) buffer followed by western blot analysis of the recovery of neighboring small subunit proteins RPS3a and RPS10. Compared with the unmodified WT human loop, the $S^{278}E$ phosphomimetic and the *A. thaliana* plant loop chimera yielded a modest decrease in RPS association (Figure 19B). By contrast, both the TS-DE and STSS-EEEE mutants produced a larger reduction in the recovery of both RPS3a and RPS10 (Figure 19B). These findings closely correlated with our clash modeling predictions. Taken together, the binding assays show that as few as two consecutive or “clustered” charged residues exert unfavorable electrostatic forces on the ribosome which may explain the high prevalence of single or spaced charge organizations found in the loop regions of many eukaryotes.

It is important to note that these assays utilize buffer conditions that differ from those used for the sucrose gradient centrifugation and polysome profiling and do not indicate that charge causes RACK1 to dissociate from the ribosome. For example, negatively charged RACK1 mutants are not detectable in the “free” fractions of our polysome profiling, where non-ribosomal RNA and proteins sediment (Figure 20). In addition, recent and independent biochemical studies show that the $S^{278}E$ RACK1 mutant remains bound to the 40S subunit (177). With these results in mind, we posit that our binding assays reflect differences in the strength of RACK1 contacts with the ribosome that stem from electrostatic forces. To confirm this, we performed GFP binding assays in which we replaced our standard high salt lysis buffer with the low salt lysis buffer used for polysome profiling. With this approach, we were able to preserve RPS3a and RPS10 binding to RACK1-eGFP complexes of the STSS-EEEE mutant, which initially produced the most severe defects in RPS recovery (Figure 19C). We also performed GFP binding assays with our conventional high salt lysis buffer using fibroblasts expressing uncharged STSS-AAAA, ΔSTSS or yeast loop chimera RACK1

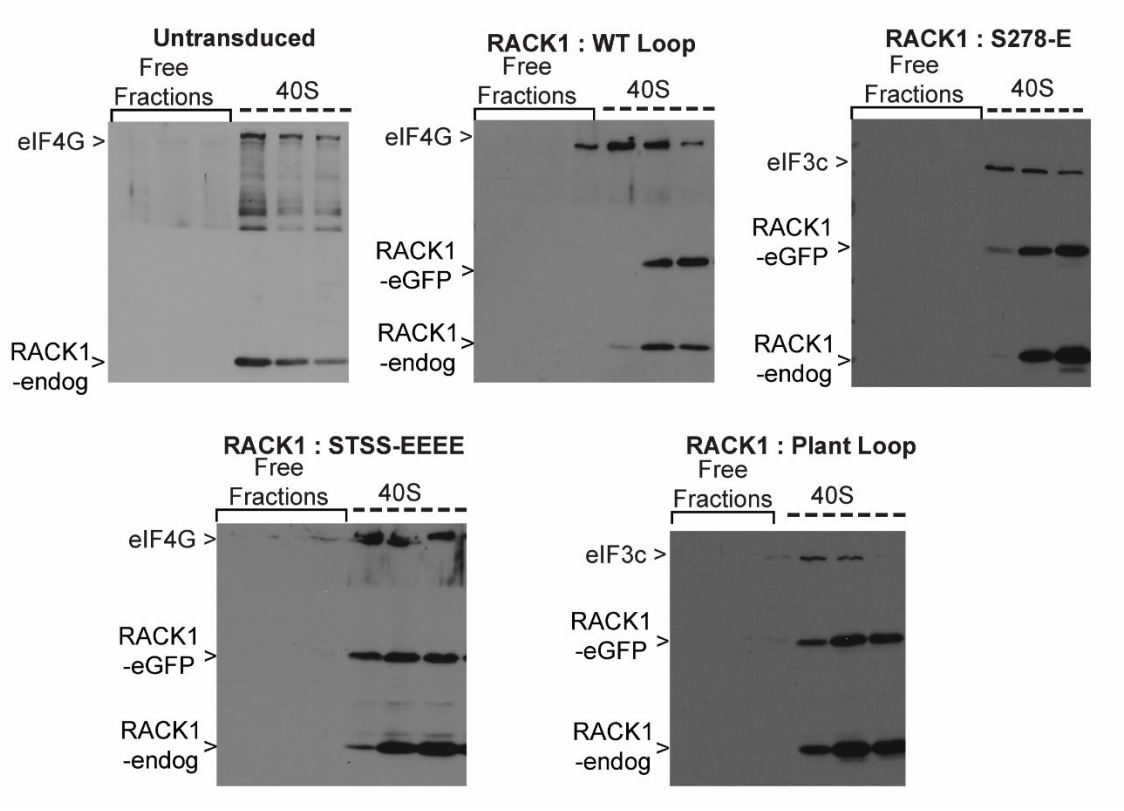


**Figure 20. RACK1 with a negatively charged loop remains associated with the ribosome.** WB analysis of the sedimentation of RACK1-eGFP loop mutants in high transduction lines compared with endogenous RACK1. Little or no RACK1 is found in free fractions while it is abundant in 40S fractions along with eukaryotic initiation factors (eIF4G or eIF3C).

forms, none of which displayed statistically significant defects in RPS recovery (Figure 19D). Taken together, these findings suggest that negative charge in the RACK1 loop exerts electrostatic repulsive forces on the 18S rRNA 40S subunit; these forces affect the normally tight binding of RACK1 with the ribosome (165, 230, 231) and become apparent under the different buffer conditions utilized by *in vitro* binding assays. In line with our observation that negative charge in the RACK1 loop mediates the polyA enhancer effect, we hypothesize that negative charge in the RACK1 loop remodels the local architecture of the 40S subunit near the mRNA exit channel to accommodate transcripts with unusual 5' leader elements, such as the helical polyA tracts of post-replicative poxviral transcripts (232).

**RACK1 loop enhances translation of 5' polyA mRNAs in a charge-dependent manner**

We next asked whether polyA leader activity is uniquely regulated by negative charge in the RACK1 loop. We compared the functionality of loops from species known to utilize polyA leaders, namely the dicot plant *A. thaliana*, to species in which long polyA tracts are underrepresented, specifically humans (*H. sapiens*) and yeast (*S. cerevisiae*). We used the moderately transduced NHDF pools which do not influence eIF6 activity to test the ability of diverse loop sequences to regulate polyA enhancer activity from the ribosome. However, as an additional control for potential contributions from the effects on eIF6, we also included the ΔSTSS mutant that binds eIF6 similarly to charged loop mutants. $^{35}$S-metabolic pulse labeling and western blot analysis showed that steady-state protein synthesis and the levels of several cellular proteins were not affected by any of these loop modifications compared with the WT human loop though there were certain proteins selectively upregulated upon expression of plant loop RACK1 but not with other loop forms (Figure 21, green arrow). This unexpected finding suggested that negative charge in the RACK1 loop may accommodate transcripts with diverse leader elements, which we explore in more detail in the next chapter. Furthermore, polyA enhancer activity was not observed with the uncharged yeast loop chimera nor with the ΔSTSS loop mutant. Only the plant loop chimera significantly enhanced production of a luciferase reporter with a 5' polyA leader (Figure 22); we and others have observed similar stimulation with expression of the S$^{278}$E pox-phosphomimetic RACK1 using various approaches (data not shown).

The objective of our luciferase reporter assay was to mechanistically couple negatively charged RACK1 loops with polyA leader functionality in human cells, as we know these leaders operate in pox-

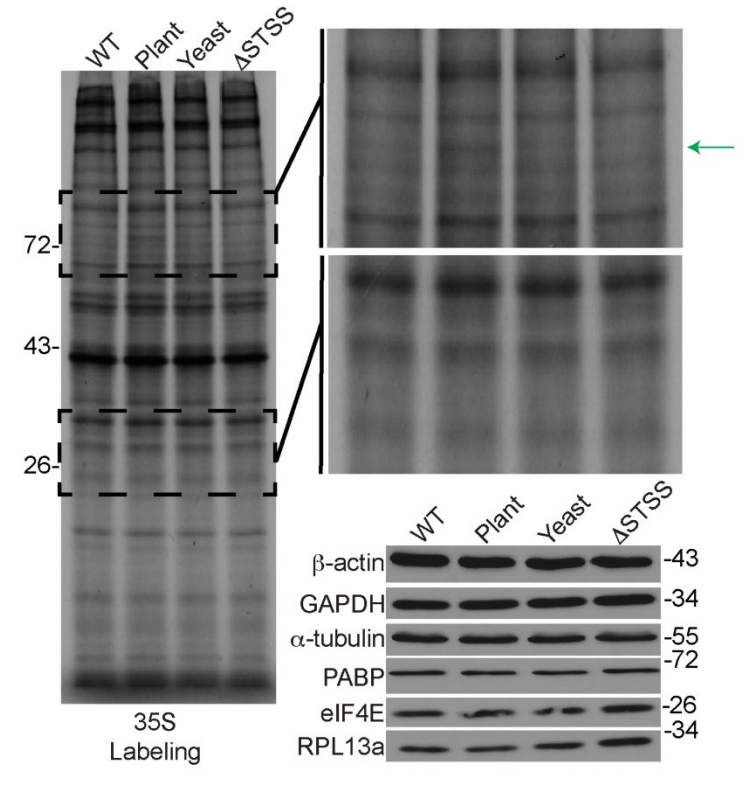


**Figure 21. $^{35}$S-metabolic labeling and western blot analysis of proteins expressed in a panel of moderately transduced NHDFs.** Green arrow marks a protein that is upregulated in fibroblasts expressing the RACK1 plant loop chimera but not RACK1 with the WT, yeast or ΔSTSS loops.

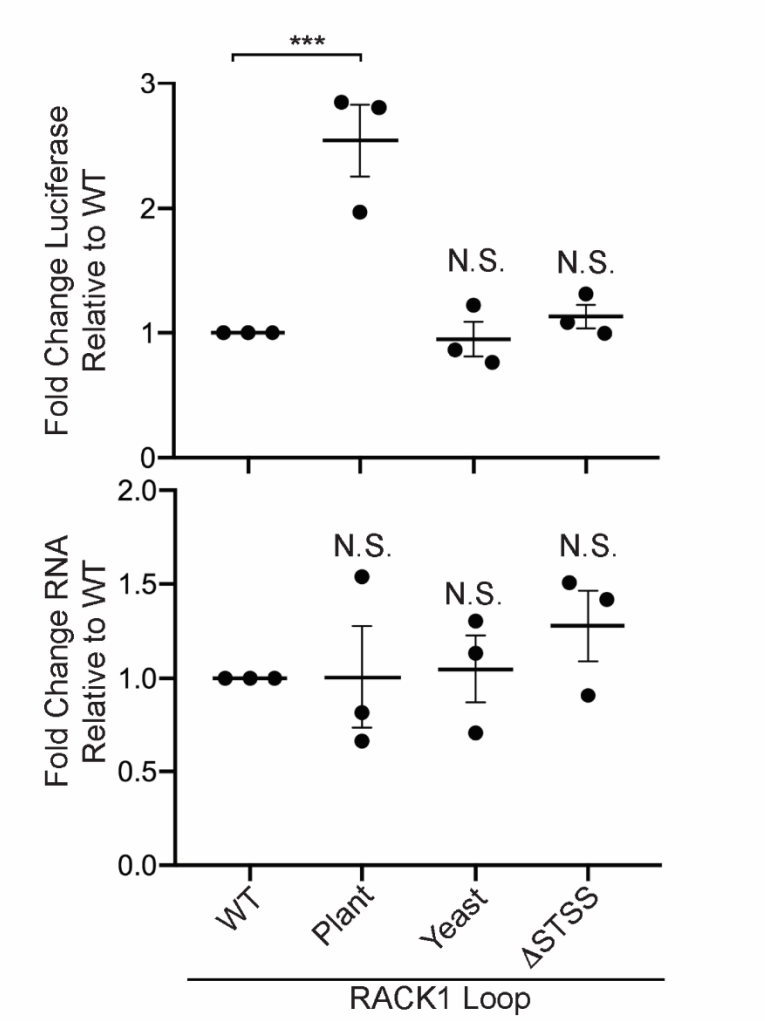


**Figure 22. Species-specific translational enhancement of 5′polyA mRNAs by a dicot plant RACK1 loop.** NHDFs as described for Figure 21 were electroporated with luciferase reporters harboring polyA leaders. Data are presented as mean luciferase activity (top) or mean RNA level (bottom) of each reporter relative to WT (arbitrarily set to 1). Bars represent ± s.e.m. Luciferase activity: n=3 per group, ***P=0.0005; one-way ANOVA followed by Dunnett's multiple comparisons test. RNA: n=3; N.S., not statistically significant.

infected human cells and dicot plants where the RACK1 loop is charged. However, choosing an appropriate control leader element to use as a comparison for polyA enhancer activity requires us to assume that these “control” leaders are not regulated by negative charge in the RACK1 loop. In our early reporter assays, we randomly selected a leader segment comprised of a 30 nt portion of the β-actin 5’ UTR as a control leader. Surprisingly, in transient expression assays this artificial leader element displayed modest enhancer activity in the presence of a negatively charged RACK1 loop (not shown). This finding, in addition to the protein whose synthesis was upregulated in fibroblasts expressing the plant loop RACK1 chimera (Figure 21, green arrow), suggests that the regulatory functions of negative charge in the RACK1 loop is not restricted to polyA leaders, which we will address in more detail in the next chapter.

# Chapter 4

## Negative charge in the RACK1 loop broadens the translational capacity of the human ribosome

*Parts of this chapter appeared as the published article "Negative charge in the RACK1 loop broadens the translational capacity of the human ribosome."*

### INTRODUCTION

There is growing evidence that the ribosome can structurally and functionally diversify to regulate translation (124-126). For example, cell-type-specific expression of the large ribosomal subunit protein L38 (RPL38) (138, 139) and ribosomal expansion segments (140) regulate homeobox (Hox) mRNA translation during cytoskeletal patterning. Ribosomal protein (RP) paralogs diversify ribosome activity during gonad development (133) , and intracellular heterogeneity in ribosomes regulates translation (134). However, the structural basis by which these subunit differences alter ribosome specificity remains unclear.

Beyond subunit differences, post-translational modifications (PTMs) to RPs also control ribosome activity. Several RPs are mono- or polyubiquitinated during cell stress and ribosome quality control (RQC) (159, 233-235). RQC senses aberrant translation events or mis-processed transcripts (236). For example, ribosomes are inherently designed to stall on polyA stretches to detect mRNAs that are erroneously internally polyadenylated; therefore, polyA tracts are heavily selected against outside of the 3′ untranslated region (UTR) (160, 181). Upon encountering poly(A) stretches, ribosomes stall, collide, and activate stress signals, along with destruction of the mRNA and nascent peptide (151-154). In the earliest stages of stalling, the ubiquitin E3 ligase zinc finger protein 598 (ZNF598), with the aid of receptor for activated C kinase 1 (RACK1), monoubiquitinates several small RP subunits (RPSs) (147, 155-159). RACK1 also prevents stalled ribosomes from frameshifting and enables endonucleolytic cleavage on mRNA lacking stop codons (162, 202, 203). Structures of stall-inducing sequences (161, 237) and ribosomes in various RQC stages have been solved (236), and extensive polyubiquitination traps the ribosome in a rotated and inactive state (238). However, beyond the broad inactivation effects of ubiquitination during RQC, how other PTMs to RPs affect ribosome structure and customize its output remains unknown.

Beyond its role in RQC, RACK1 regulates several other aspects of translation. RACK1 is a conserved Trp-Asp (WD) repeat protein that largely consists of seven β-propeller blades that

mediate protein binding (163, 164). RACK1 is a core RP that is located on the head domain of the 40S subunit near the mRNA exit channel, with much of its surface solvent exposed (165, 166). This enables RACK1 to act as a docking site for eukaryotic translation initiation factors (eIFs) and kinases, thereby integrating signaling with translational output (167, 169). There is strong evidence that in many cell types and like other RPs, extra-ribosomal RACK1 is degraded to restrict its signaling and other activities to the ribosome (169-173, 179, 239, 240). In terms of effects on translation, RACK1 can stimulate overall rates of protein synthesis (169), as well as control translation of specific mRNA subsets (175, 176). RACK1 also contributes to noncanonical cap-independent initiation by viral internal ribosome entry sites (IRESs) (86, 92, 93, 177, 178).

RACK1 also contains a short interconnecting loop between blades six and seven that is not required for ribosome binding and whose amino acid sequence varies across species (165, 166, 179, 240). The human loop sequence consists of uncharged amino acids, but during poxvirus infection, a viral kinase introduces negative charge into the loop through single-site phosphorylation at serine 278 ($S^{278}$) to enhance translation of viral mRNAs that harbor unusual 5′ poly(A) leaders (179, 240). This phosphorylation of human RACK1 mimics negatively charged amino acids that are present in the RACK1 loops of dicot plants and protists (179, 240), which unlike mammals also encode adenosine-rich 5′ UTRs (182, 212). Expression of RACK1 in which $S^{278}$ is replaced with a glutamic acid ($S^{278}E$), which mimics poxvirus phosphorylation of human RACK1, as well as the negatively charged loops of many other species, is sufficient to enhance translation of mRNAs with adenosine-rich 5′ UTRs (179, 240). But beyond this, how a charged RACK1 loop affects ribosome structure and translational output remains unknown. Here, we show that negative charge in the RACK1 loop does not affect its ability to transmit ribotoxin signals but alters the swivel motion of the 40S head domain and enables the human ribosome to broadly support noncanonical modes of translation.

## RESULTS

### WT and $S^{278}E$ RACK1 form stable interactions with eEF2, SERBP1 and Ebp1

Understanding how $S^{278}E$ RACK1 influences ribosome structure and function necessitated the development of a new cell system. Our prior approaches involved expression of exogenous forms of RACK1 against a background of competition with endogenous RACK1 for ribosome binding

and protein stabilization, which results in a 50:50 expression ratio in primary normal human fibroblasts (179, 240). Although this was sufficient to study the enhancer effect of $S^{278}E$ RACK1 on specific 5′ polyA leader-containing reporters and transcripts, the continued presence of endogenous RACK1 confounded attempts to understand its broader impact on translation. Indeed, in this system, negatively charged RACK1 does not impair overall translation as measured by $^{35}S$-methionine/cysteine pulse labeling or luciferase expression from a β-actin reporter; yet RiboTag assays, specifically isolating green fluorescent protein (GFP)-tagged wild-type (WT) or $S^{278}E$ RACK1 forms away from endogenous RACK1, suggested that $S^{278}E$ RACK1 had reduced affinity for β-actin mRNA compared with WT RACK1 (179). However, commonly used ribosome profiling and RiboTag RNA affinity assays do not discern transcripts associated with active versus inactive ribosomes. Moreover, our subsequent studies revealed that negative charge in the loop weakens RACK1's association with the ribosome in a buffer-dependent manner, which further confounds the interpretation of such *in vitro* RiboTag assays while hinting at the potential structural impact of a charged RACK1 loop (179, 240). Stemming from these biochemical observations, clash modeling suggested that negatively charged RACK1 loops create electrostatic repulsive interactions with the negatively charged phosphate backbone of 18S rRNA (240). From this, we hypothesized that this repulsion may alter local contacts that RACK1 makes on the 40S. As such, key questions as to whether $S^{278}E$ RACK1 truly affects ribosome structure and regarding its broader effects on translation remain unanswered.

To address this, we developed a HAP1 cell-based knockout and rescue system to analyze the effects of negative charge in the loop on global translation and enable large-scale ribosome isolation for cryo-EM. The HAP1 model system provides three key benefits. First, HAP1 cells are fibroblast-like and are not as translationally hyper-activated as many commonly used transformed cell lines. Second, they recapitulate the strict ribosome association and homeostatic control of RACK1 expression that we observe in our primary fibroblasts (Figure 23A) (179, 239). Finally, we previously made RACK1 knockout HAP1 cells (179) that have been shown by others to be phenotypically rescued using Flag-tagged RACK1 (177, 178, 241). Therefore, we generated our own RACK1 knockout rescue pools stably expressing Flag-tagged WT or $S^{278}E$ forms of RACK1 (Figure 23B). The minimal impact of RACK1 depletion in our HAP1 RACK1 knockout cells, here on referred to as "no rescue" cells, on polysome profiles (Figure 24A) confirms the

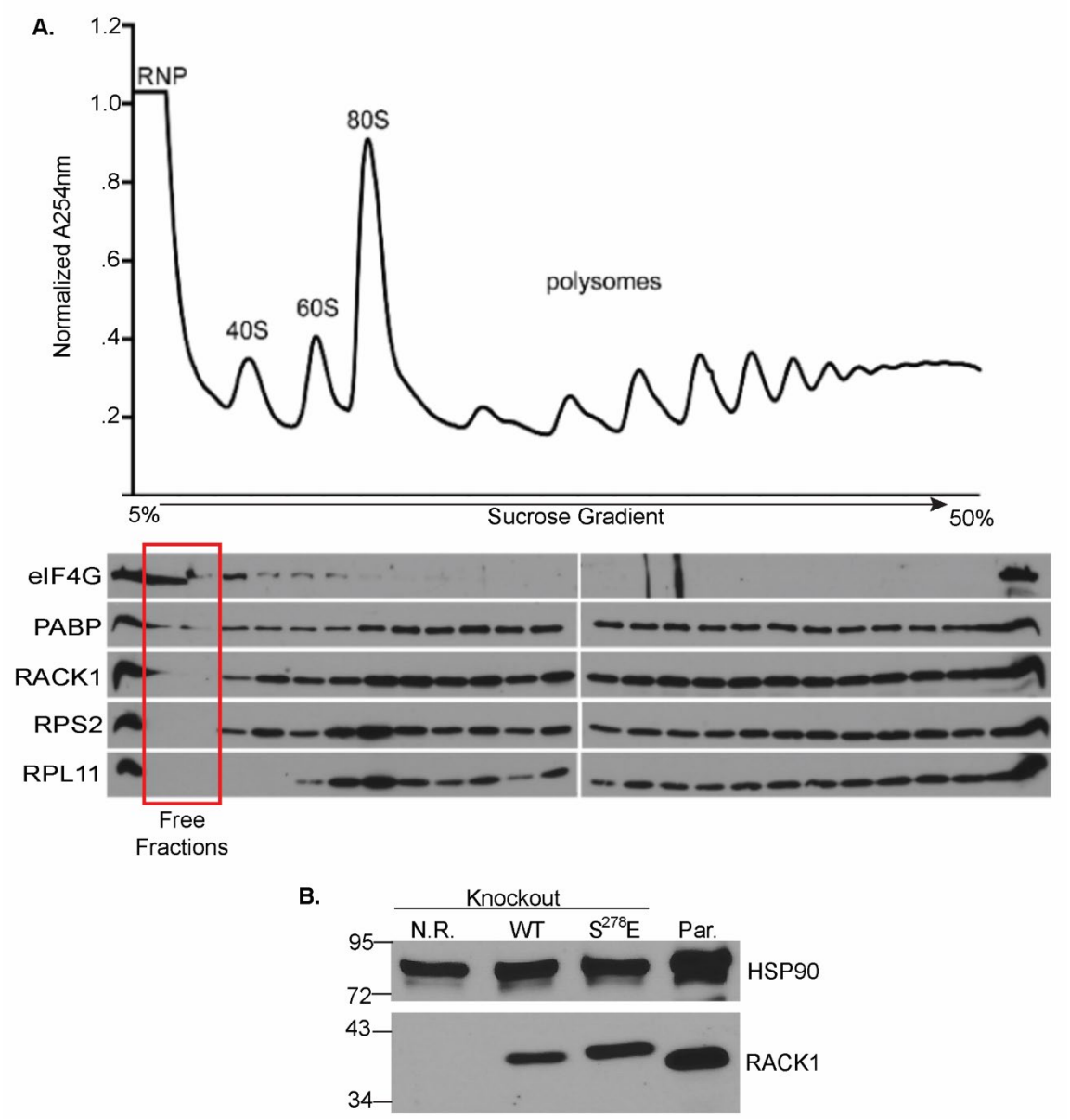


**Figure 23. Ribosome sedimentation and rescue of RACK1 expression in HAP1 cells.** (**A**) Absorbance traces and Western blot analysis of free, 40S, 60S, 80S and polysome fractions from parental HAP1 cells. L = Lysate. Free or extra-ribosomal fractions are indicated by the red box; initiation factor eIF4G is readily detected in both free and initiating 40S/80S fractions. RNA binding proteins such as PABP are detectable in all fractions, while RPs including RACK1 are restricted to ribosomal fractions. (**B**) Western blot analysis showing the relative expression of RACK1 in parental (Par.) HAP1 cells from A. compared with no rescue (N.R.) RACK1 knockouts that were rescued with either WT or $S^{278}E$ forms of RACK1.

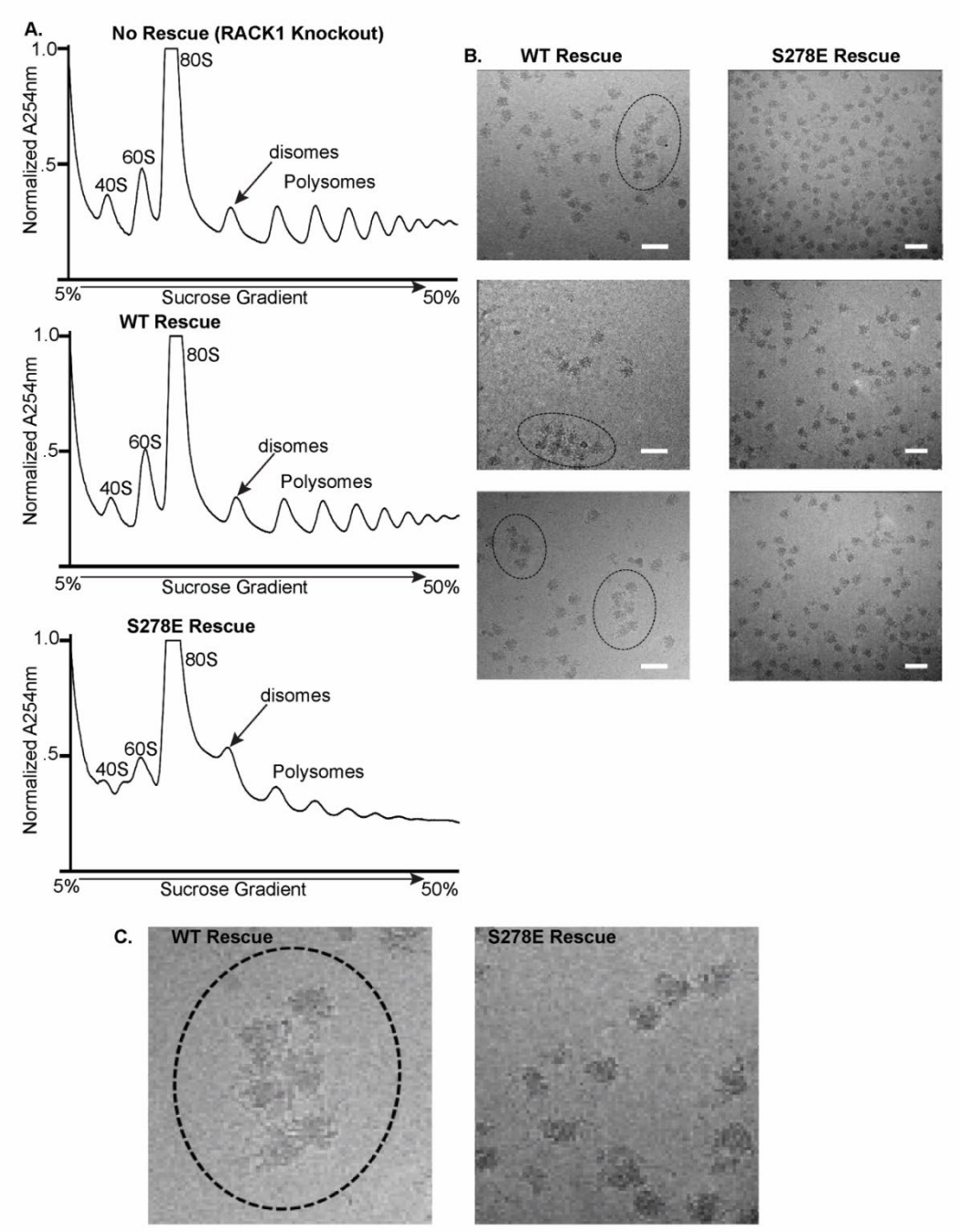


**Figure 24. S$^{278}$E RACK1 expression induces monosome and disome accumulation in HAP1 cells.** (**A**) Labeling highlights 40S and 60S subunits, 80S monosomes, disomes and polysomes in RACK1 knockout cells that were either not rescued or were rescued with WT or S$^{278}$E forms of RACK1. There is a notable reduction in polysomes and an increase in monosomes and disomes specifically in cells expressing S$^{278}$E RACK1. (**B-C**) Cryo-EM micrographs of ribosomes isolated by anti-Flag rapid purification from cells expressing Flag-tagged WT or S$^{278}$E RACK1. Scale bars = 50 nm. Zoom shown in C. highlights polysomes readily observed in WT RACK1 samples, and monosome and disomes that are prevalent in S$^{278}$E samples.

non-essentiality of RACK1 to global protein synthesis, which has been previously reported (177-179). In addition, the rescue lines reproduce known phenotypes of primary fibroblasts expressing GFP-tagged forms of RACK1 (240), such as monosome and disome accumulation induced by $S^{278}E$ RACK1 which we observe in both polysome profiles and cryo-EM micrographs (Figure 24B and Figure 24C). Sucrose gradient density centrifugation confirmed that both the WT and $S^{278}E$ RACK1 forms are restricted to the ribosome in our rescue cells and are detected along with other RPs on the 40S subunit, monosomes and disomes but not in free fractions (Figure 25A). As expected, translation factors like eIF4G and eukaryotic elongation factor 2 (eEF2) as well as RNA binding proteins like Serpine mRNA binding protein 1 (SERBP1) and ErbB3-binding protein 1 (Ebp1) are found in both ribosome-bound and free fractions (Figure 25A).

To assess the effects of the different RACK1 loop forms on translation, we first analyzed the large-scale “ratcheting” rotation of the 40S relative to the 60S that occurs during elongation (81, 82, 242). Cryo-EM structure analysis revealed that of the Flag-RACK1-bound ribosome particles recovered, an expected balance of 40S rotated (40%) and 40S non-rotated (60%) ribosomes were observed in WT RACK1 rescue cells (Figure 25B). By contrast, 78% of $S^{278}E$ RACK1-bound ribosomes were in a 40S rotated state. 40S rotated ribosomes were associated with eEF2, E-site tRNA, SERBP1 and Ebp1 (Figure 25B), with well-defined SERBP1 density observed on $S^{278}E$ RACK1 ribosomes (Figure 26A). In line with this, polysome analyses also suggested that SERBP1, EBP1 and eEF2 shifted distribution from free fractions to ribosome fractions (Figure 25A). Previous reports have identified SERBP1-eEF2-Ebp1-80S complexes as one of two classes of translationally inactive ribosomes (243, 244). These ribosomes are thought to be primarily inactivated by the binding behavior of SERBP1; similar to the yeast ortholog, Stm1, human SERBP1 binds to the head domain of the 40S subunit, inserts into mRNA entry channel and extends along the mRNA path up to the peptidyl (P) tRNA binding site where it makes contacts with the 60S. This mode of binding inactivates the ribosome by blocking transcript entry (62, 244, 245). SERBP1 also traps eEF2 on these inactive ribosomes (244, 246); as eEF2 typically functions in elongation, its contribution to ribosome inactivation remains unknown. Ebp1 is a particularly perplexing factor; this protein functions in ribosome biogenesis and binds near the peptide exit tunnel on the 60S subunit (247, 248). It is also unclear how it contributes to ribosome inactivation though its positioning is hypothesized to prevent ubiquitination of

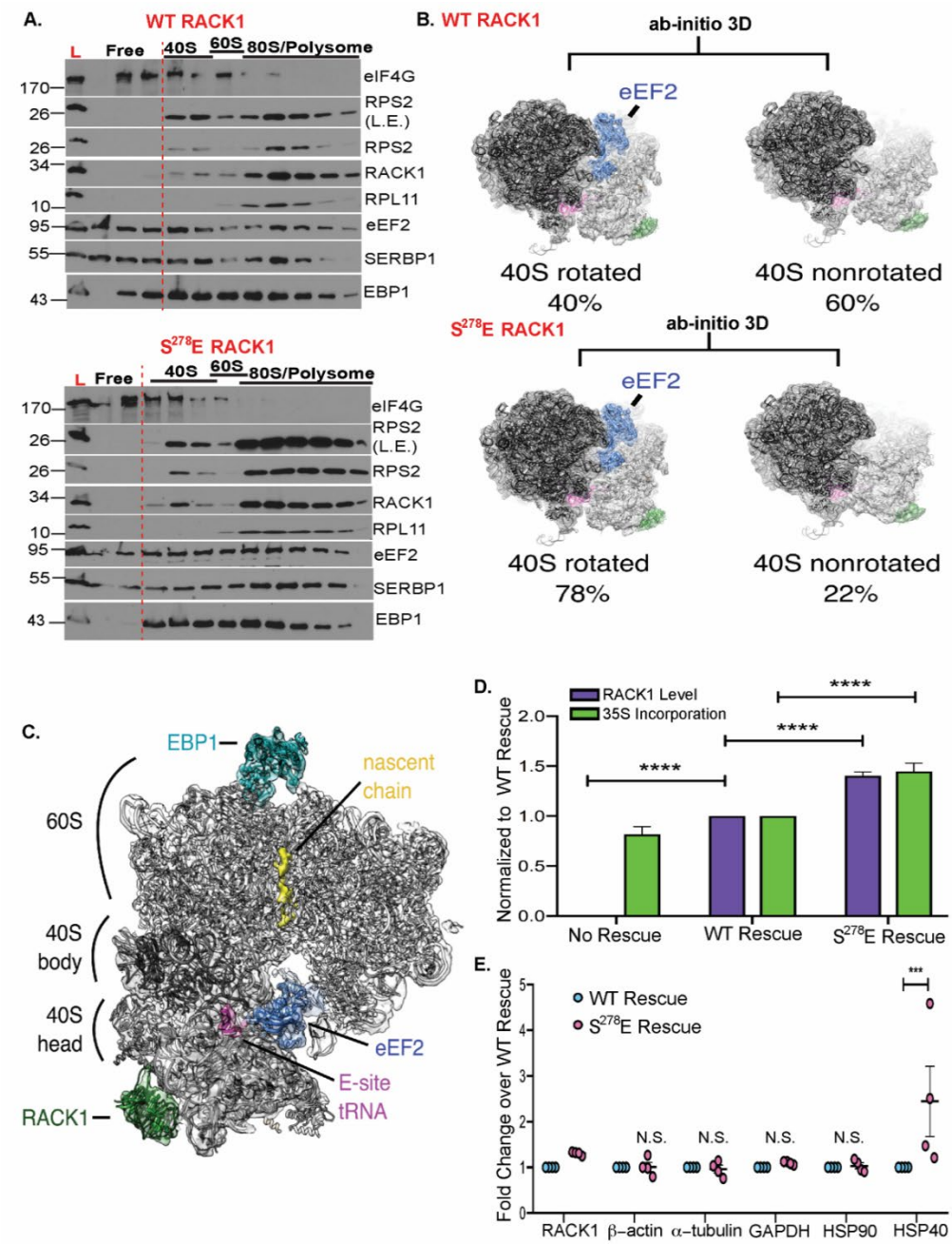


**Figure 25. Effects of $S^{278}E$ RACK1 on ribosome rotation and translational output.** (**A**) Western blot analysis of free and ribosomal fractions. L = lysate. L.E. = Long Exposure. Representative of 3 independent replicates. (**B**) Ab-initio 3D classification of 80S ribosomes from WT RACK1 and $S^{278}E$ RACK1 purifications reveal a shift toward 40S-rotated, eEF2-bound particles in the presence of RACK1-$S^{278}E$. (**C**) Reconstruction of rotated ribosomes from $S^{278}E$ RACK1 purifications reveal densities ascribed to eEF2, E-site tRNA, EBP1, and a nascent chain. (**D**) Quantification of RACK1 protein levels (n = 22) and $^{35}$S-Met/Cys incorporation (n ≥ 4). Bars represent s.e.m, ****P ≤ 0.0001; Two-way ANOVA with Sidak's multiple comparisons test. (**E**) Densitometry-based quantification of the indicated protein levels (n = 4). Bars represent ± s.e.m, ***P = 0.0004, N.S. = not significant; Two-way ANOVA with Sidak's multiple comparisons test.

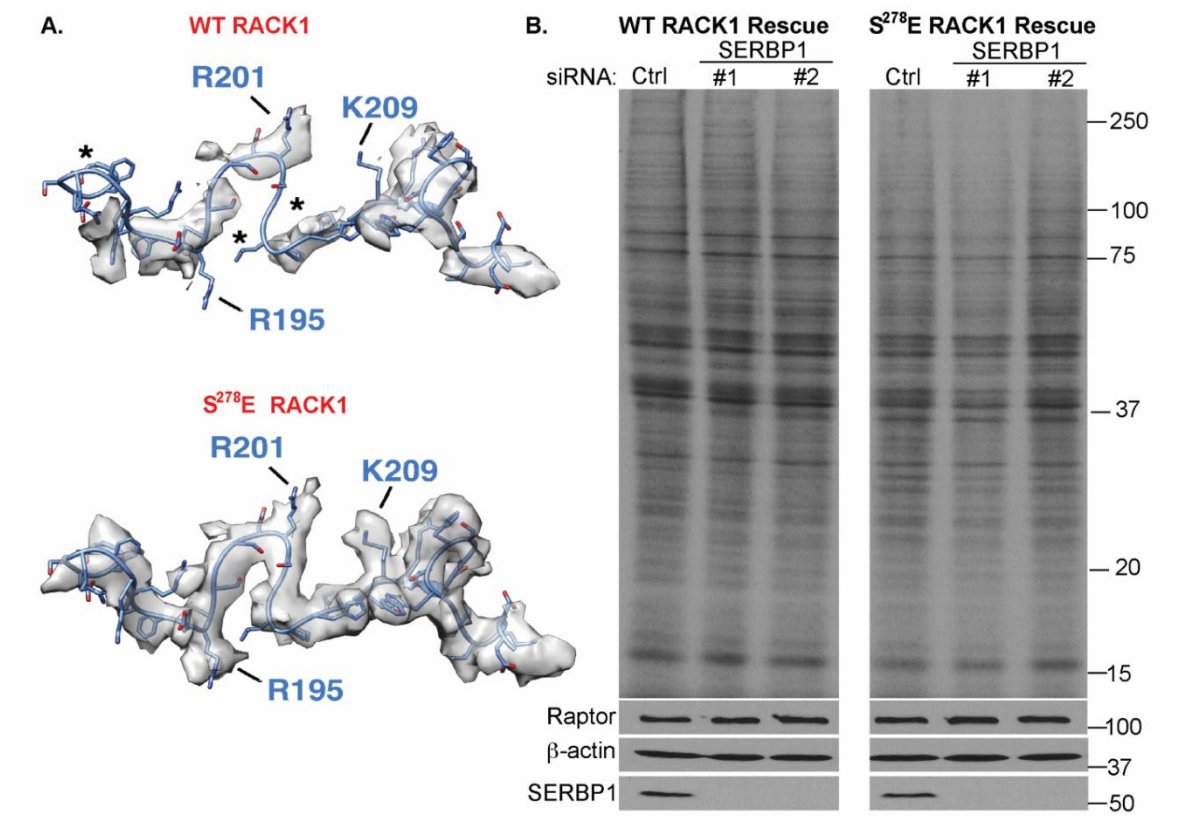


**Figure 26. SERBP1 depletion does not de-repress protein synthesis.** (**A**) View of SERBP1 model fitted in RACK1-WT (top) and $S^{278}E$ RACK1 (bottom) reconstructions indicate more ordered SERBP1 density in $S^{278}E$ RACK1. (**B**) siRNA-mediated depletion suggests that SERBP1 does not enhance translation in either WT or $S^{278}E$ RACK1-expressing cells. Cells were treated with control (ctrl) or either of two independent SERBP1 siRNAs prior to $^{35}$S-Met/Cys pulse labeling. $^{35}$S-Met/Cys labeling gel (top panels) and Western blot analysis (bottom panels) is shown. Representative of 3 independent replicates.

ribosomal protein uL29 (RPL35) thus priming inactive ribosomes for ribophagy (152, 243). Despite the presence of these factors on our WT and $S^{278}E$ RACK1 rescue ribosomes, we observe nascent chain density in our ribosome reconstructions (Figure 25C), which suggests that these ribosomes were translationally active at or near the time of isolation. Furthermore, $^{35}S$-methionine/cysteine labeling demonstrated that the rescue of RACK1 knockout cells with either WT or $S^{278}E$ RACK1 stimulates overall translation, and that each form does so in proportion to the level of RACK1 expression (Figure 25D). In addition, despite minor differences in overall translation rates, there were no significant differences in the steady-state levels of certain cellular proteins, although elevated HSP40 levels in the $S^{278}E$ RACK1-expressing cells hinted that negative charge in the loop may selectively regulate the translation of certain transcripts (Figure 25E).

We also discovered that SERBP1 depletion does not stimulate translation in either cell line, which suggests that it does not have a substantial repressive effect in HAP1 cells (Figure 26B). There are many other contexts in which SERBP1 does not repress translation (249-252). For example, SERBP1 is required for translation in budding yeast and creates rapidly reactivatable ribosome pools during stress, suggesting that it functions *in vivo* to modulate rather than fully inactivate ribosomes (249, 253-256). Furthermore, SERBP1 binds to pre-ternary complexes and 48S PICs in rabbit reticulocyte lysates (RRLs) *in vitro* (250) as well as actively translating ribosomes in mammalian cells (257), suggesting that the abundant SERBP1 that we detect in our structures is not unusual. One possibility is that SERBP1 adopts two distinct conformations when bound to the ribosome, one of which allows the N-terminus to bind to the 40S head without inserting the C-terminal tail into the mRNA channel (250). Regardless, the increased abundance of the SERBP1-eEF2-Ebp1 ribosome pool in our HAP1 system is likely an indirect consequence of cell-type specific differences in ribosome dynamics, and our data shows that it is not a key factor in modulating translation in our system.

**Negative charge in the RACK1 loop remodels the ribosome A and E sites**

To further investigate how negative charge in the RACK1 loop alters ribosome activity, we evaluated the sensitivity of our no rescue and rescue cells to ribosome targeting drugs (Figure 27A). We first treated cells with anisomycin, an elongation inhibitor that binds to the 60S aminoacyl tRNA acceptor

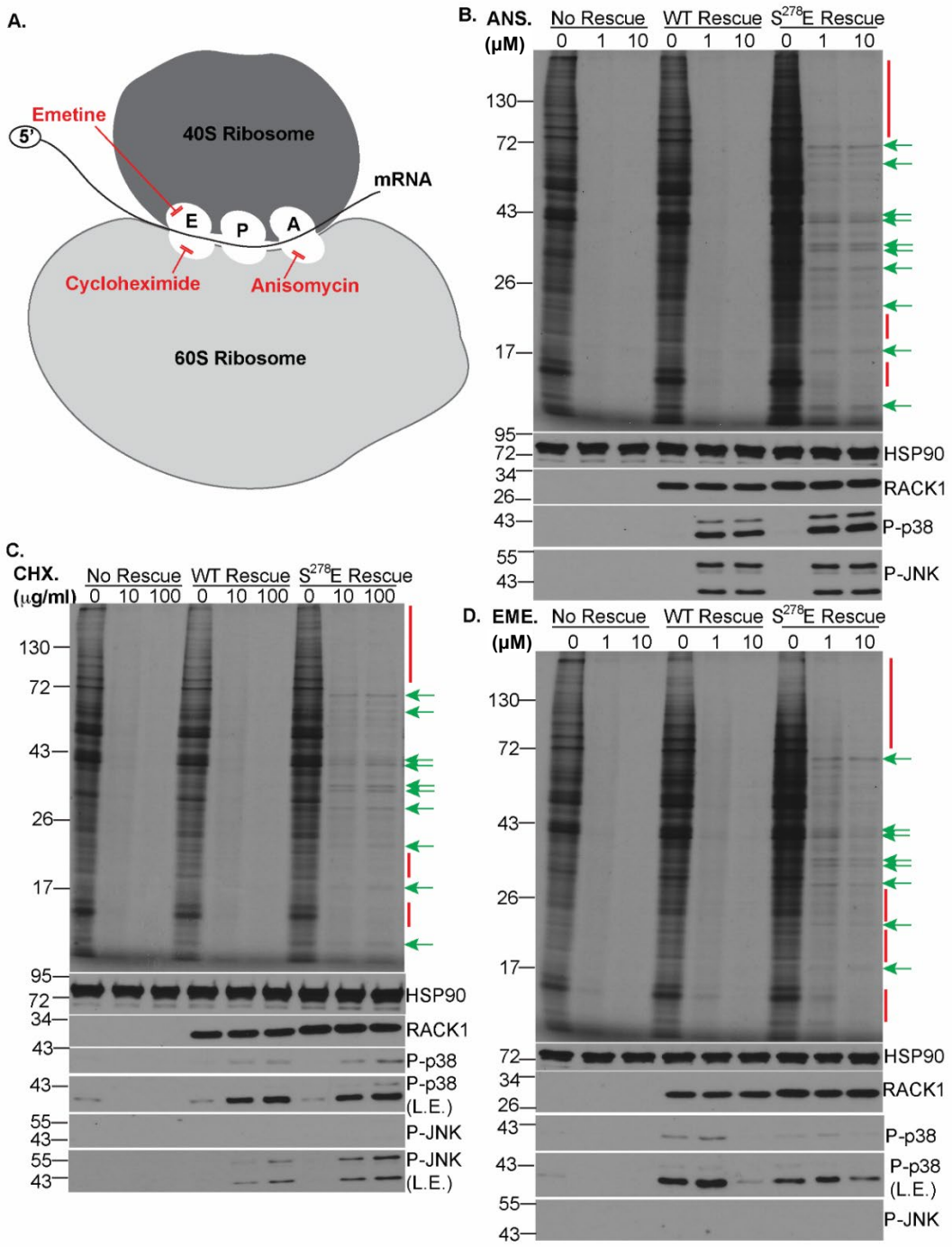


**Figure 27. Negative charge in the RACK1 loop confers resistance to ribosome-targeting drugs.** (**A**) Schematic of the ribosome and target sites of inhibitors used in B-D. (**B-D**) $^{35}$S-Met/Cys labeling gels (top panel) and Western blot analysis (bottom panels) of cells treated with the indicated concentrations of anisomycin (ANS; B.), cycloheximide (CHX; C.) or emetine (EME; D.). Red bars/arrows highlight examples of proteins whose synthesis is repressed by inhibitors. Green arrows highlight examples of proteins whose synthesis is sustained. P-p38 = phosphorylated p38, P-JNK = phosphorylated JNK. L.E. = Long Exposure. Representative of 3 independent replicates.

(A) site. $^{35}$S-methionine/cysteine labeling showed that anisomycin effectively repressed translation in our no rescue and WT RACK1 rescue cells (Figure 27B). In the S$^{278}$E RACK1 rescue cells, anisomycin treatment similarly impaired the synthesis of most proteins (Figure 27B, red bars). However, the production of a subset of proteins persisted even with a ten-fold increase in drug concentration (Figure 27B, green arrows). We obtained similar results by treating cells with cycloheximide, an elongation inhibitor that binds to the 60S exit (E)-site (Figure 27C), and emetine, another E-site targeting elongation inhibitor that binds to the 40S subunit (Figure 27D). The sensitivity of global protein synthesis in both the WT and S$^{278}$E RACK1 rescue cells suggests that the selective translation that we observe is not due to the slight differences in RACK1 expression between the two lines. Furthermore, the sustained synthesis of specific proteins in the S$^{278}$E RACK1 cells with a ten-fold increase in drug concentration demonstrates that this phenomenon is not the product of an inhibitor-dosing effect.

Ribosome impairment activates stress-response pathways, such as the ribotoxic stress response (RSR), that reprogram translational output to maintain cellular homeostasis. The RSR is primarily activated by 60S-targeting drugs that damage the conserved alpha-sarcin loop of 28S rRNA which inhibits or partially inhibits protein synthesis, activates the stress kinases JNK/SAPK1 and p38 and induces transcription of immediate-early genes such as *c-fos* and *c-jun* (154, 258-262). To determine whether the drug resistance that we observe upon introduction of negative charge in the loop correlates with defects in the RSR response, we probed for the activated phospho-forms of JNK/SAPK1 and p38 in our metabolic labeling samples. We found that the RSR is not activated in RACK1 knockout cells, which validates previous studies identifying RACK1 as a critical factor in ribotoxic stress signaling (263) (Figure 27B-D). Rescue with either WT or S$^{278}$E RACK1 restored the RSR, and in line with prior studies, anisomycin elicited the most potent response while cycloheximide did so but to a lesser extent (259, 264, 265) (Figure 27B-C). Further in line with other systems, emetine is not a potent activator of the RSR but lower concentrations of it modestly activate p38 above basal levels (154, 259, 266) (Figure 27D). In the absence of differential effects on RSR signaling between the two rescue lines, these findings suggest that the inhibitor resistance that we observe can likely be attributed to the effects of RACK1 loop charge on ribosome structure.

To test this hypothesis, we performed rigid-body fitting of emetine- and anisomycin-bound ribosome structures into our reconstructions of the WT and $S^{278}E$ RACK1 ribosomes. For emetine fitting, densities from Guanine 961 (G961) of 18S rRNA, a key residue of the 40S E-site (267, 268), partially occlude emetine binding through a pronounced interaction with the E-site tRNA which we do not detect in the reconstruction of the WT RACK1-bound ribosome (Figure 28A-B). Anisomycin fitting also reveals clashes between uridine 4452 (U4452) and pseudouridine 4531 (ψ4531) of the 60S subunit 28S rRNA that overlap with anisomycin in the A-site binding pocket (Figure 28C-D). Uridine 4452 (U4452) and pseudouridine 4531 (ψ4531) are also key functional residues of the 60S peptidyl transferase center (PTC) (269-271). To determine whether displacement of these residues alters PTC activity, we treated cells with puromycin which is incorporated into nascent chains in the PTC. Puromycin treatment effectively halted translation in all lines tested, as represented by the “smear” of puromycin-terminated peptides in samples treated with lower concentrations (Figure 29A). Notably, a persistent protein roughly 72 kDa in size continued to be synthesized in the puromycin-treated $S^{278}E$ RACK1 samples. Puromycin-fitting into the $S^{278}E$ RACK1 reconstruction suggests that densities including that of the nascent chain may also affect puromycin binding to some extent (Figure 29B), which partially explains continued protein synthesis but not the extreme selectivity, as only a single protein product persists. However, this finding is not an irregularity of our $S^{278}E$ RACK1 rescue cells as previous studies have also identified distinct bands amidst a smear of puromycin-terminated peptides in whole cell lysates from HeLa cells; these bands represent full length protein products that were translated and terminated normally without puromycin incorporation (272). Regardless of the identity of this protein, we can conclude that $S^{278}E$ RACK1-bound ribosomes are largely puromycin-sensitive and PTC activity is not drastically altered. Given the competitive nature of these elongation inhibitors, certain transcripts and proteins likely escape their effects due to altered rRNA densities in drug binding sites on $S^{278}E$ RACK1-containing ribosomes that reduce inhibitor efficacy. These altered densities and the resulting partial drug resistance are again likely to be reflective of broader changes in ribosome structure and dynamics caused by negative charge in the RACK1 loop, which we will explore later.

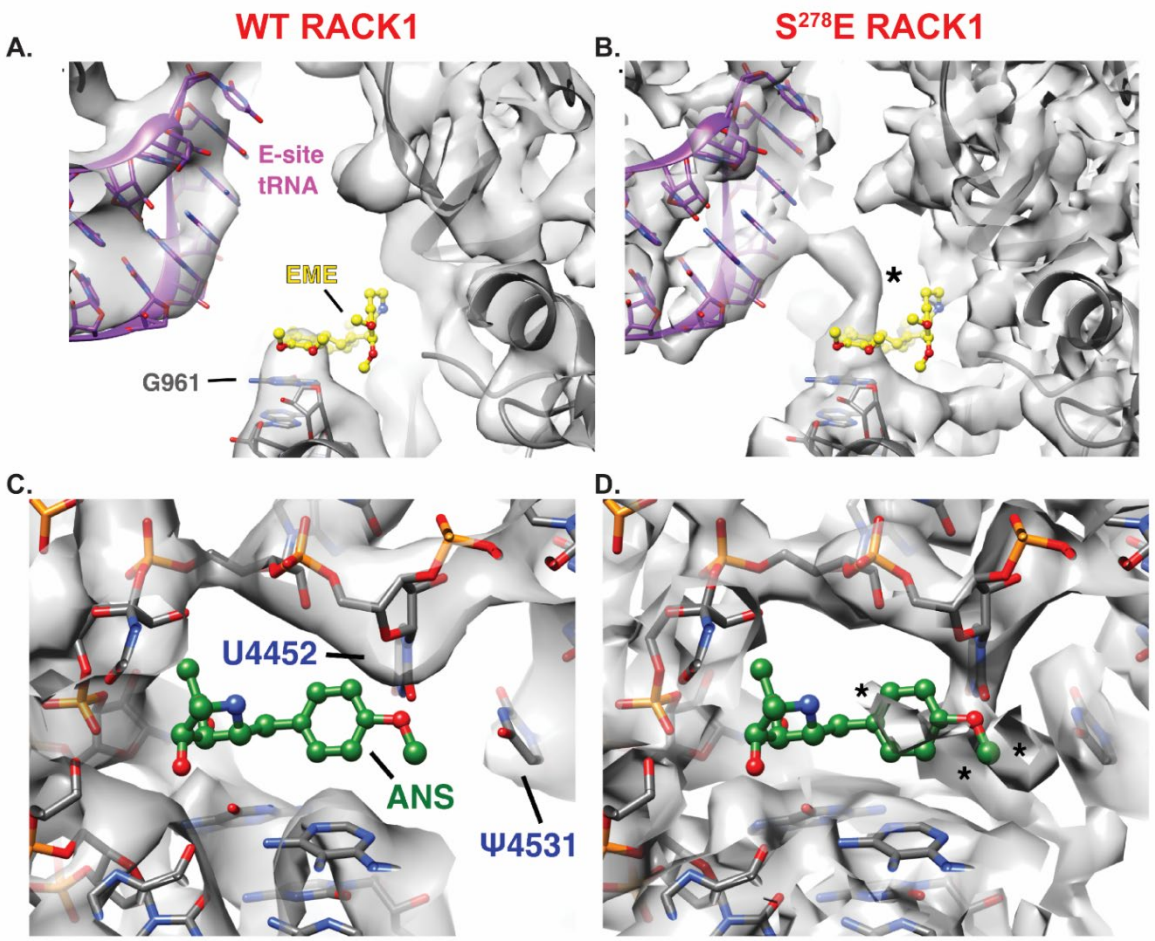


**Figure 28. A negatively charged RACK1 loop affects ribosomal E-site and A-site residues.** (**A-B**) Views of the emetine (EME) binding site in WT RACK1 (A) and $S^{278}E$ RACK1 (B) 80S reconstructions (rotated state shown). In $S^{278}E$ RACK1, an unidentified density connects G961 of the 18S rRNA with the E-site tRNA (asterisk). EME modeling based on PDB 3J7A (273). (**C-D**) Views of anisomycin (ANS) binding site WT RACK1 (C) and $S^{278}E$ RACK1 (D) indicate unidentified clashing densities in the reconstruction of $S^{278}E$ RACK1 that is not observed in WT RACK1. ANS modeling based on PDB 4U3M (274).

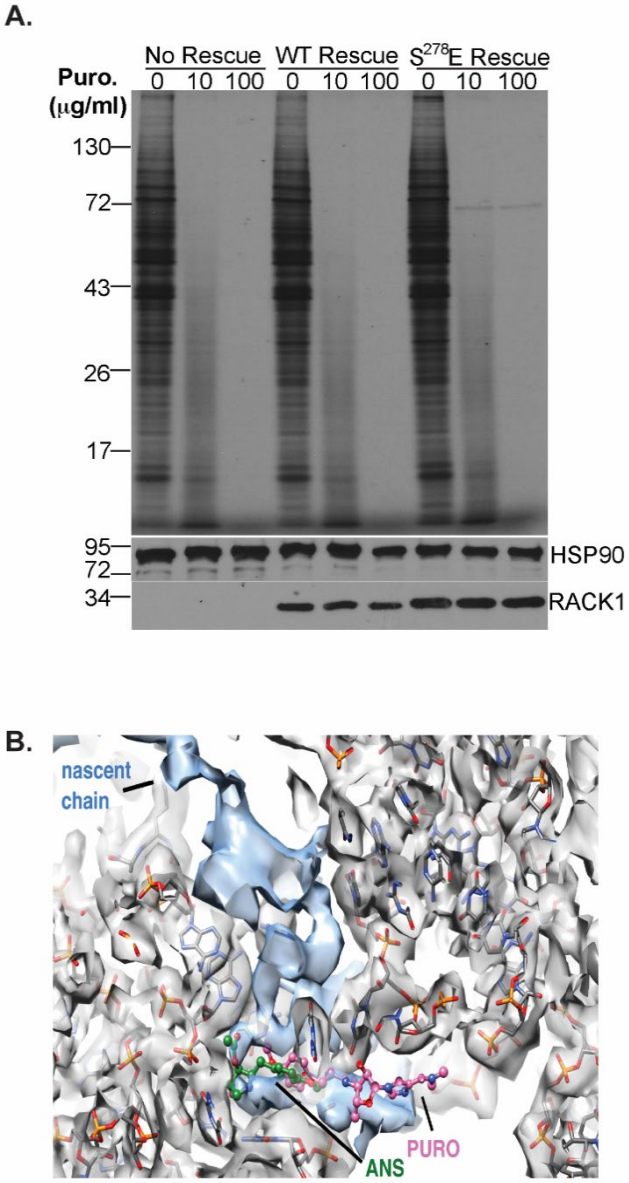


**Figure 29. S$^{278}$E RACK1 loop does not affect puromycin sensitivity or peptidyl transferase activity.** (**A**) $^{35}$S-Met/Cys labeling gels (top panel) and Western blot analysis (bottom panels) of cells treated with the indicated concentrations of puromycin (Puro). Representative of 3 independent replicates. (**B**) Zoomed out view of the S$^{278}$E reconstruction showing putative nascent chain density (blue) and its proximity to anisomycin (green) and puromycin (pink) binding sites.

**Negative charge in the RACK1 loop alters ribosome behavior towards polyA sequences and enables eIF4A-independent translation**

Given the effects of a negatively charged RACK1 loop on A-site remodeling, we next investigated whether $S^{278}E$ RACK1 influences stall resolution of polyA tracts which interact with A-site rRNA residues (161, 237). We transfected our no rescue and rescue cells with dual fluorescence translational stall reporters (156, 157). The reporter contains an N-terminal GFP and C-terminal RFP flanked by 2A protease sites to generate individual as opposed to fusion proteins, which are separated by either a control linker or 60 adenosine stall sequence (Figure 30A, top). In mammalian cells, both GFP and RFP are produced from the control linker reporter but due to ribosome stalling on the polyA tract, more GFP than RFP is made from the polyA stall reporters. Densitometry of GFP and RFP detected by Western blotting revealed that as expected, the polyA stall reporter produced less RFP relative to GFP than the control linker reporter in both the no rescue and WT RACK1 rescue lines (Figure 30A, bottom). Although we do not explore the potential for differences in frameshifting on these polyA constructs, prior studies using the same reporter and readouts found a requirement for RACK1 in regulating RFP levels from this stall reporter in HEK293T cells. However, these studies also showed that stalling was dependent on the levels of polyA reporter expression and depends more on ZNF598 than RACK1 (156, 157). As such, our failure to observe a significant requirement for RACK1 in HAP1 cells likely reflects differences in translation rates or cell type specific differences in requirements for RACK1 in ribosome quality control pathway activities.

By contrast, the difference in GFP to RFP expression with the polyA reporter and between the control linker and polyA linker transfections was notably smaller in the $S^{278}E$ RACK1 rescue cells (Figure 30A, bottom) suggesting that there is something fundamentally different in how charged loop RACK1 interacts with the polyA stall reporter. To explore this in more detail, we performed single-cell fluorescence analysis and quantified GFP and RFP intensity in individual cells. Presented as violin plots, we observe that WT and $S^{278}E$ RACK1 increase GFP and RFP expression from the control linker reporter compared to no rescue cells (Figure 30B) which aligns with the stimulatory effect of RACK1 expression on global protein synthesis that we observed earlier using $^{35}S$-methionine/cysteine labeling. We also observed the expected reduction in expression of RFP relative to GFP with transfection of the polyA reporter in no rescue and WT

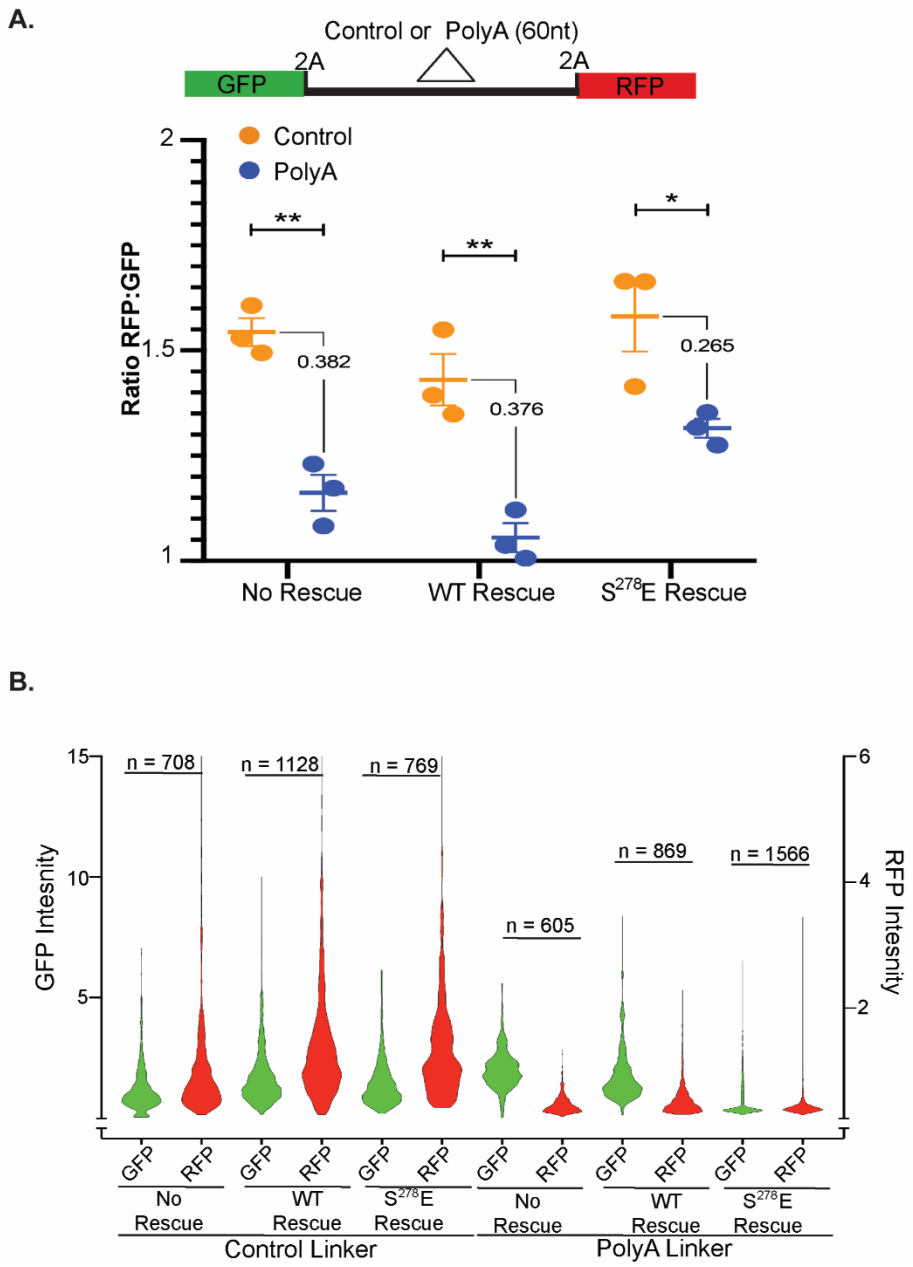


**Figure 30. A negatively charged RACK1 loop affects RQC reporter activity** (**A**) Top: Schematic of control or polyA RQC reporters, with 2A protease and linker sites indicated. Bottom: Densitometry-based quantification of GFP and RFP from Western blot analysis of cells transfected with RQC reporters, presented as RFP:GFP ratio. n = 3, No Rescue **P = 0.002, WT Rescue **P = 0.006, S278E Rescue *P = 0.037; unpaired t-test between control and polyA reporter. The numeric difference in ratio between each reporter is also shown. (**B**) Fluorescence intensity measurements of GFP or RFP (reported as arbitrary units) in cells transfected with RQC reporters, presented as violin plots. n = number of fluorescent cells analyzed over 3 independent replicates.

RACK1 rescue cells. However, while GFP and RFP levels were more equivalent in the $S^{278}E$ RACK1 cells transfected with the polyA reporter, in line with our densitometric analysis, this effect appeared to be at least in part due to reduced GFP expression (Figure 30B).

To explore potential cell population dynamics that could explain this phenotype, we presented each cell as a single data point based on its GFP and RFP fluorescence. The distribution of cells shows that $S^{278}E$ RACK1-expressing cells exhibit normal stalling behavior, as we observe a reduced slope in plots for all three lines transfected with the polyA reporter (Figure 31A). However, more detailed analysis of this data showed that while some cells expressed high levels of GFP and low levels of RFP in line with conventional stalling, a larger fraction of $S^{278}E$ RACK1-expressing cells produced RFP with relatively little or no GFP (Figure 31B-D). This finding suggests that $S^{278}E$ RACK1 favors internal initiation from the polyA sequence. Several viruses that infect dicot plants encode long polyA tracts that support internal initiation (275-277). However, unlike classical IRESs, these polyA elements are unstructured and their ability to act in an IRES-like manner may be linked to the negative charge present in the RACK1 loops of dicot plants.

These dual fluorescence stall reporter assays are indirect measures of translation and are limited in scope for assessing how charge in the loop may impact the translation of other transcripts. We initially planned to utilize cellular stressors, such as heat shock, to reprogram the cell to use alternative modes of initiation. However, the robust stress response in HAP1 cells hampers our ability to reliably detect any regulatory contribution from negative charge in the loop (data not shown). To determine whether negative charge in the loop more broadly enables alternative initiation, we instead treated cells with either hippuristanol or silvestrol, two inhibitors that block eIF4A activity using distinct mechanisms (278, 279). eIF4A is an RNA helicase that is essential for cap-dependent scanning, the primary mode of initiation used in mammalian cells (65, 67, 280). Both inhibitors repressed translation in a dose-dependent manner in the no rescue and rescue cells as it would be expected for increasingly impaired eIF4A activity (Figure 32A-B, red bars). However, $S^{278}E$ RACK1 sustained the synthesis of several proteins even at higher inhibitor concentrations (Figure 32A-B and Figure 33, green arrows). These results demonstrate that negative charge in the RACK1 loop reprograms the ribosome to enable eIF4A-independent translation of subsets of cellular transcripts.

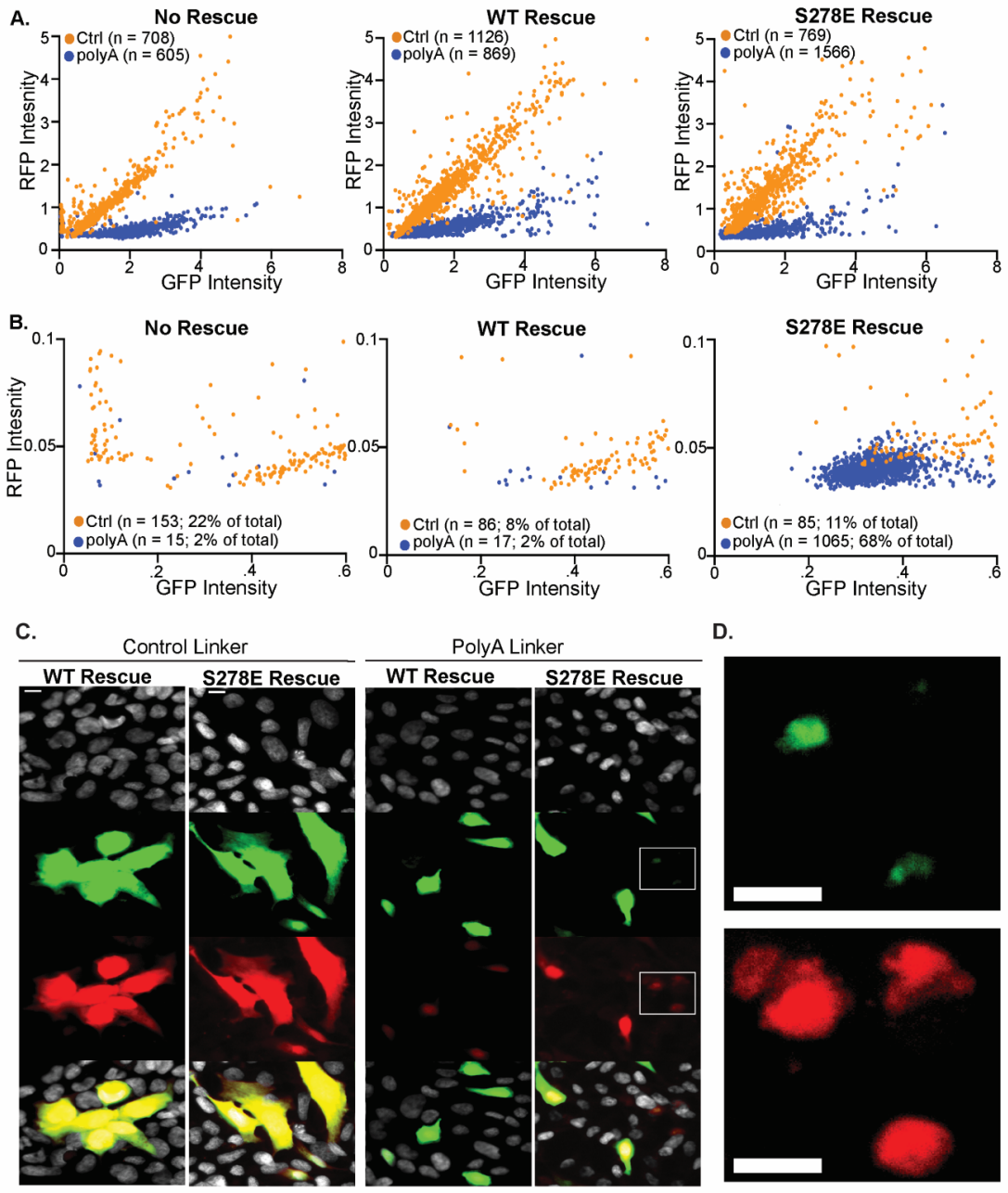


**Figure 31. RQC reporter activity in WT and S$^{278}$E RACK1-expressing cells.** (**A-B**) Fluorescence intensity measurements of GFP and RFP (reported as arbitrary units) in cells transfected with control (Ctrl) or polyA RQC reporters as in Figure 30B. Each cell is presented as an individual data point. n = number of fluorescent cells analyzed over 3 independent replicates. Whole data set is shown in A. Zoomed data set in B highlights the large population of cells in S$^{278}$E RACK1 rescue lines that express RFP but very little GFP. (**C-D**) Representative images of GFP and RFP expression from control or polyA stall reporters analyzed in Figures 30B and 31A. Note that in the control reporter, cells expressing either WT or S$^{278}$E RACK1 express equivalent levels of GFP and RFP. As expected, less RFP is produced relative to GFP from the polyA stall reporter in cells expressing WT RACK1. However, two cell populations are observed in cells expressing S$^{278}$E RACK1; as shown in larger scale analysis in Figure 31A, a smaller subset of cells produce less RFP compared to GFP, as expected. However, in a larger fraction of cells, very little GFP is made despite notable levels of RFP expression; zooms in D. highlight these cells. Bar = 10µm.

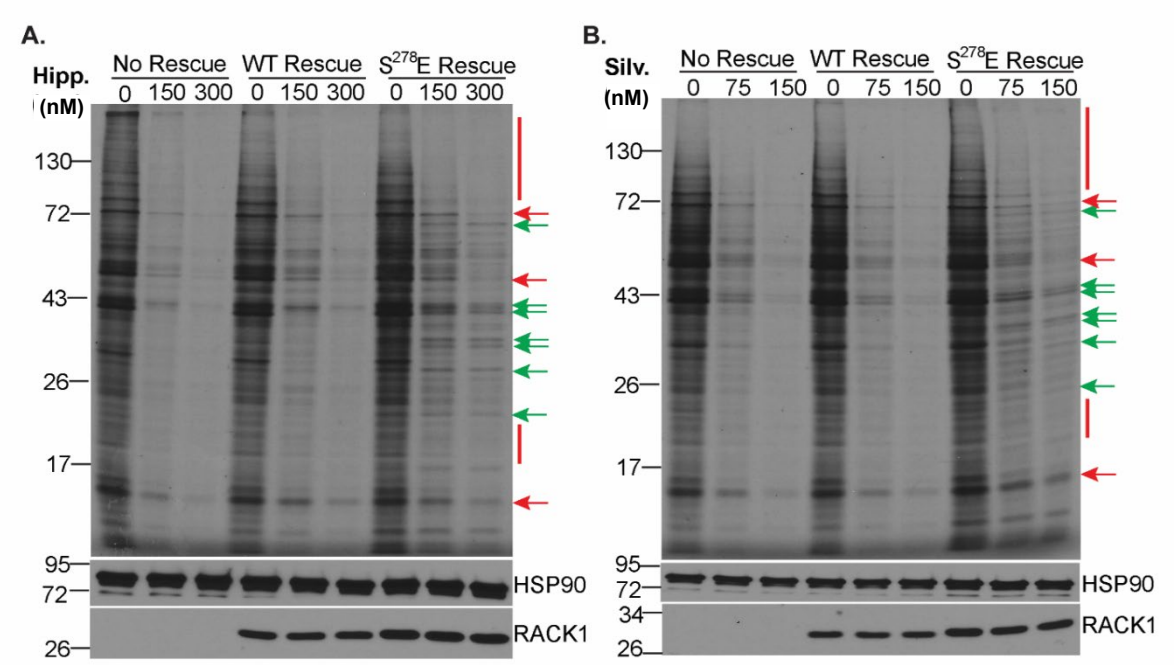


**Figure 32. A negatively charged RACK1 loop broadly enables eIF4A-independent translation.** (**A-B**) $^{35}$S-Met/Cys labeling gels (top panel) and Western blot analysis (bottom panels) of cells treated with the indicated concentrations of Hippuristanol (Hipp; A.) or Silvestrol (Silv; B.). Red bars/arrows highlight examples of proteins whose synthesis is repressed by inhibitors. Green arrows highlight examples of proteins whose synthesis is sustained. Representative of 3 independent replicates.

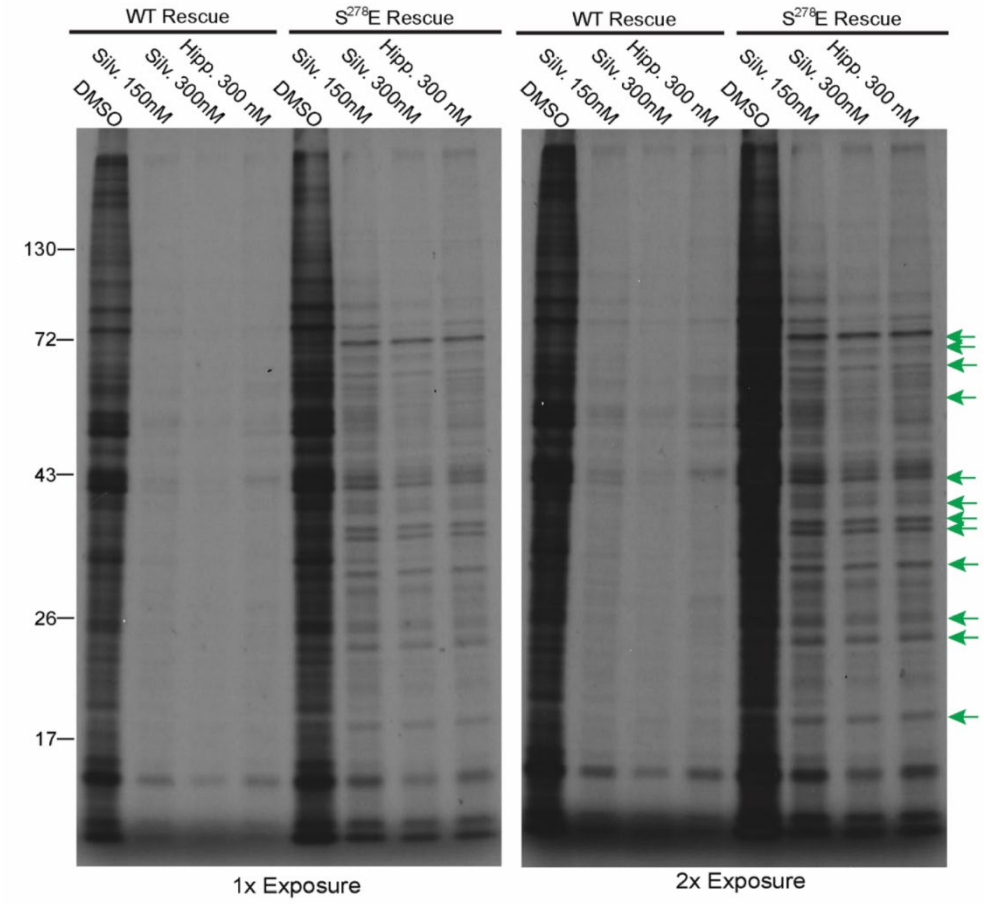


**Figure 33. Specificity of resistant proteins with two different eIF4A inhibitor treatments.** WT RACK1 or $S^{278}E$ RACK1 rescue cells were treated with the indicated concentrations of the eIF4A inhibitors, silvestrol (Silv.) or hippuristanol (Hipp.) prior to $^{35}S$-methionine/cysteine pulse labeling. Complementing data in Figure 32, this data provides a direct comparison of the effects of both inhibitors and enlarged autoradiograms make it easier to see resistant proteins in $S^{278}E$ RACK1 rescue cells (indicated with green arrows). Two exposures are provided side-by-side with the longer exposures illustrating the specificity of the resistant proteins in $S^{278}E$ RACK1 rescue cells.

**Negative charge in the RACK1 loop affects 40S head rotation**

We further analyzed our cryo-EM datasets to determine if there are structural changes to $S^{278}E$ RACK1-bound ribosomes that might explain the correlation between charge in the loop and eIF4A-independent initiation. We first revisited the effects negative charge in the loop exerts on the large-scale "ratcheting" rotation of the 40S relative to the 60S that occurs during elongation (81, 82, 242). Earlier, we mentioned that ribosomes in WT RACK1 cells display the expected balance of 40S rotated (40%) and 40S non-rotated (60%) ribosomes whereas 78% of $S^{278}E$ RACK1-bound ribosomes were found to be in a 40S rotated state (Figure 25B). The structures of our WT RACK1-bound 80S particles are consistent with published structures of the human 80S ribosome in both rotated (PDB 6Z6M) and non-rotated states (PDB 4UG0) (61, 243). In addition, ribosomes in the rotated state structurally superimposed between WT and $S^{278}E$ RACK1 datasets (Figure 34A). As such, the addition of negative charge to the RACK1 loop does not alter the normal trajectory of ribosome ratcheting, as the rotated states of both WT and $S^{278}E$ RACK1 80S are superimposable and consistent with published structures of the 80S ribosome (244). However, within non-rotated datasets an overlay of the WT and $S^{278}E$ RACK1 bound ribosomes revealed striking differences. The structures overlaid well at the 60S subunit and 40S body, but not at the 40S head (Figure 34B). The non-rotated $S^{278}E$ RACK1 reconstruction exhibits an unusually greater degree of swiveling in which it becomes shifted towards the 60S subunit and alters contacts with other RPs (Figure 34B-D). These structural changes and the substantially lower percentage of $S^{278}E$ RACK1 particles in the non-rotated state (Figure 34B) suggest that negative charge in the loop destabilizes the non-rotated 40S state and drives it towards a rotated state.

Strikingly, the type III or IV IRES elements of RNA viruses such as Hepatitis C virus (HCV), Israeli acute paralysis virus (IAPV) or Cricket paralysis virus (CrPV) manipulate 40S head rotation to enable cap- and scanning-independent initiation (281-285). These IRESs also interact with RACK1 and require RACK1 for their translation (86, 92, 93, 177, 178). Given that IRESs are not particularly prevalent in cellular mRNAs and alternative initiation was unique to $S^{278}E$ RACK1-expressing cells, we next tested whether the 40S head rotation induced by $S^{278}E$ RACK1 mimics that induced by IRES elements. Our superimpositions revealed that the $S^{278}E$ RACK1 40S only-reconstructions are consistent with the structures of 40S subunits

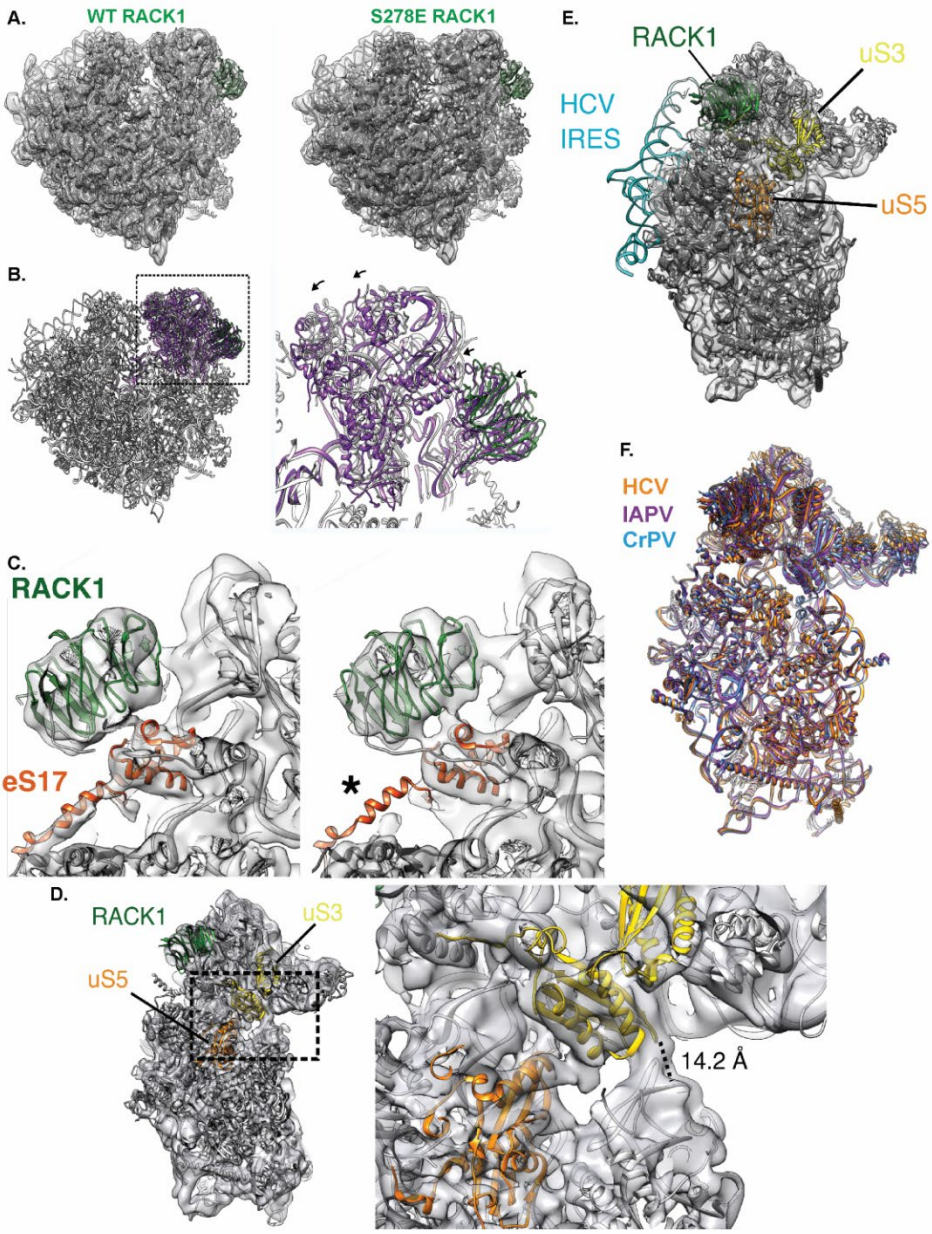


**Figure 34. The 40S head is displaced in S$^{278}$E RACK1-containing ribosomes.** (**A**) Rigid-body fits of the human 80S ribosome in the non-rotated state (PDB 4UG0) shows agreement in 60S and 40S body for both WT and S$^{278}$E RACK1 reconstructions (**B**) In contrast, the fitting is inconsistent at the 40S head between the two reconstructions (WT, gray; S$^{278}$E, purple). Arrows indicate direction of S$^{278}$E 40S head displacement towards the 60S (**C**) Closeup views of RACK1-eS17 interface in WT (left) and S$^{278}$E (right) reconstructions of nonrotated 80S particles. eS17 contains a connecting helix between the 40S body and head, which is less pronounced in the S$^{278}$E reconstruction (asterisk) (**D**) Reconstruction of 40S particles isolated from S$^{278}$E RACK1 purifications (left). Zoomed-in view of the "latch" separating the 40S head and body. Distance between Q179 of uS3 and G610 of the 18S rRNA is indicated and consistent with the 40S "latch" in the closed conformation (**E**) Reconstruction of S$^{278}$E 40S particles shows agreement with the rigid-body fit of the 40S ribosome bound to HCV IRES (PDB 5A2Q) (**F**) Overlaid models of IRES-bound 40S subunits are generally superimposable (HCV, orange, PDB 5A2Q; IAPV, purple, PDB 6P4G; CrPV, blue, PDB 7JQC; IRES models removed for clarity).

bound to HCV, CrPV and IAPV IRESs (Figure 34D-F). Taken together, these data suggest that similar to IRESs, negative charge in the RACK1 loop remodels the 40S to enable the use atypical modes of initiation.

While the finer structural and mechanistic details remain to be determined, our findings reveal the broad extent to which a single charged residue in the RACK1 loop can alter ribosome structure, dynamics and translational capacity. The range of effects of $S^{278}E$ RACK1 on ribosome structure and function was somewhat unexpected but undoubtedly linked to RACK1's position on the 40S head. Charge in the RACK1 loop altered local contacts in the "latch," a key structural feature of the 40S subunit that, when closed, ensures the mRNA remains in the channel during initiation (286-289). This would undoubtedly affect translational output and may disproportionately affect certain transcripts over others. Negative charge in the loop also alters 40S head rotation, which would influence 60S joining and 80S assembly as well as the rate of ribosome assembly. Changes to 40S and 60S contacts may also alter the conformation of residues in the tRNA binding sites leading to the inhibitor resistance we observe.

Viruses often evolve strategies to dysregulate tightly controlled processes and, in this case, negative charge in the human RACK1 loop appears to broaden the functionality of the human ribosome to support non-canonical modes of translation which many RNA viruses utilize. Indeed, $S^{278}E$ RACK1 mimics the 40S remodeling induced by structurally complex HCV, CrPV and IAPV IRES elements that drive 80S assembly with minimal dependence on eIFs (281, 283-285, 290). By contrast, poxviruses are DNA viruses that generate mRNAs with fairly short 5' polyA-leaders (97). Early studies reported that such leaders have reduced dependence on eIFs or scanning but lack the structural complexity of true IRES elements (118, 119, 180, 237, 291, 292). Yet, polyA leaders are foreign to their mammalian hosts and their maximal activity requires either poxvirus infection or expression of phosphomimetic $S^{278}E$ RACK1 (118, 119, 179, 180, 237, 240, 291, 292). Our findings suggest that $S^{278}E$ RACK1 likely primes 40S subunits in a similar way to IRESs to initiate on mRNAs with little to no scanning. Beyond our earlier focus on 5' polyA leaders, data here shows that a negatively charged RACK1 loop more broadly enables eIF4A-independent translation of many cellular mRNAs. Given that human mRNAs do not contain 5' polyA tracts and bona-fide IRESs are rare, this demonstrates that poxviruses introduce negative charge to the RACK1 loop not to control a process unique to their polyA leaders, but to maximize the capacity of ribosomes to accommodate transcripts with

different types of leaders. Overall, our findings suggest that in lieu of more complex IRES structures, modifications to RPs such as RACK1 can achieve similar effects to unlock non-canonical modes of translation by the human ribosome.

# Chapter 5

## Discussion

Cells utilize a variety of post-transcriptional control mechanisms to regulate gene expression in response to various stimuli. Functional ribosome heterogeneity is a unique approach to translation regulation achieved by varying subunit protein composition or post-translational modifications to ribosomal components. Certain ribosomal proteins specify the translational output of ribosomes by interacting with 5' leader elements in subsets of transcripts, with RPL38 and RACK1 being two of the most well-studied examples (93, 138, 139). RACK1 is a highly conserved core ribosomal protein that utilizes the blades of its beta propeller structure to bind to a wide range of signaling proteins, which mediates different cellular processes. Though the blades endow RACK1 with the bulk of its regulatory capacity, until recently, the contribution of other RACK1 structural domains remained unexplored. We used phylogenetic, biochemical and structural approaches to determine that a C-terminal flexible loop in RACK1 that varies among eukaryotes regulates subunit joining in mammalian cells and, when phosphorylated during poxvirus infection, maximizes the adaptive potential of the ribosome. Our findings provide insight into how a single domain or residue in RACK1 exerts immense regulatory control over ribosome activity.

Our phylogenetic analyses revealed that the RACK1 loop region displays broad sequence plasticity among eukaryotes; however only contexts in which the loop was negatively charged, such as dicot plant loops or pox-modified human loops, enabled polyA enhancer activity. The correlation between loop charge usage and polyA leader activity hints at the coevolution of these features in species that encode functional adenosine-rich leader elements, though recent studies show that this relationship may be more complex. For example, long 5' polyA leaders repress translation and are underrepresented in the transcripts of most yeast species (209), which also vary widely in RACK1 loop charge usage and organization. However, a small fraction (1-2%) of budding yeast strains produce toxins expressed from linear cytoplasmic DNA virus-like elements (VLEs) with short (≤12 nt) non-templated polyA leaders that resemble the polyA leaders found in post-replicative poxviral transcripts (293-295). Both poxviral transcripts and yeast VLEs also display a reduced requirement for canonical cap-dependent initiation factors such as eIF4E (118, 119, 293, 296). However, it remains unknown whether RACK1 contributes to the molecular mechanism that governs the

expression of these unusual extrachromosomal elements. The unicellular parasite *Plasmodium falciparum* also possesses a highly adenosine and thymine rich genome that encodes long polyA tracts (297). Recent studies have confirmed that RACK1 binds to actively translating ribosomes in *P. falciparum* (298), which resolves long-standing questions prompted by the absence of RACK1 in previous cryo-EM ribosome reconstructions (297, 299). However, *P. falciparum* RACK1 lacks negative charge in its C-terminal loop region, which may suggest that other specialized structural domains of the ribosome, such as *P. falciparum*-specific ribosomal rRNA expansion segments may recruit other proteins that facilitate the scanning and/or decoding of polyA tracts (273, 299). Taken together, RACK1 is likely one of many proteins – both ribosomal and non-ribosomal – that regulate the translation of 5' adenosine-rich transcripts in different eukaryotic organisms.

Mass-spectrometry studies of pox-infected ribosome complexes also indicate that RACK1 is just one of many subunit proteins that are post-translationally modified during infection (239); we hypothesize that these modifications act in concert to structurally and functionally reprogram the ribosome to accommodate transcripts with diverse leader elements. In addition to performing RNA-seq to identify the cellular transcripts regulated by negative charge in the RACK1 loop, it will be particularly valuable to determine the full extent of ribosome structural remodeling that occurs during poxvirus infection. These studies will provide important insights into how poxviruses customize the translational machinery and how these modifications impact protein synthesis and other fundamental biological processes.

**References**


1. Koonin EV, Yutin N. Evolution of the Large Nucleocytoplasmic DNA Viruses of Eukaryotes and Convergent Origins of Viral Gigantism. Adv Virus Res. 2019;103:167-202. Epub 2019/01/13. doi: 10.1016/bs.aivir.2018.09.002. PubMed PMID: 30635076.
2. Iyer LM, Balaji S, Koonin EV, Aravind L. Evolutionary genomics of nucleo-cytoplasmic large DNA viruses. Virus Res. 2006;117(1):156-84. Epub 2006/02/24. doi: 10.1016/j.virusres.2006.01.009. PubMed PMID: 16494962.
3. Iyer LM, Aravind L, Koonin EV. Common origin of four diverse families of large eukaryotic DNA viruses. J Virol. 2001;75(23):11720-34. Epub 2001/11/02. doi: 10.1128/JVI.75.23.11720-11734.2001. PubMed PMID: 11689653; PMCID: PMC114758.
4. Yutin N, Koonin EV. Hidden evolutionary complexity of Nucleo-Cytoplasmic Large DNA viruses of eukaryotes. Virol J. 2012;9(161):161. Epub 2012/08/16. doi: 10.1186/1743-422X-9-161. PubMed PMID: 22891861; PMCID: PMC3493329.
5. Koonin EV, Yutin N. Nucleo-cytoplasmic Large DNA Viruses (NCLDV) of Eukaryotes. eLS. 2012. doi: https://doi.org/10.1002/9780470015902.a0023268.
6. Filee J, Pouget N, Chandler M. Phylogenetic evidence for extensive lateral acquisition of cellular genes by Nucleocytoplasmic large DNA viruses. BMC Evol Biol. 2008;8(1):320. Epub 2008/11/28. doi: 10.1186/1471-2148-8-320. PubMed PMID: 19036122; PMCID: PMC2607284.
7. Schulz F, Roux S, Paez-Espino D, Jungbluth S, Walsh DA, Denef VJ, McMahon KD, Konstantinidis KT, Eloe-Fadrosh EA, Kyrpides NC, Woyke T. Giant virus diversity and host interactions through global metagenomics. Nature. 2020;578(7795):432-6. Epub 2020/01/23. doi: 10.1038/s41586-020-1957-x. PubMed PMID: 31968354; PMCID: PMC7162819.
8. Galindo I, Alonso C. African Swine Fever Virus: A Review. Viruses. 2017;9(5). Epub 2017/05/11. doi: 10.3390/v9050103. PubMed PMID: 28489063; PMCID: PMC5454416.
9. Andreani J, Khalil JYB, Sevvana M, Benamar S, Di Pinto F, Bitam I, Colson P, Klose T, Rossmann MG, Raoult D, La Scola B. Pacmanvirus, a New Giant Icosahedral Virus at the Crossroads between Asfarviridae and Faustoviruses. J Virol. 2017;91(14):e00212-17. Epub 2017/04/28. doi: 10.1128/JVI.00212-17. PubMed PMID: 28446673; PMCID: PMC5487549.
10. Bajrai LH, Benamar S, Azhar EI, Robert C, Levasseur A, Raoult D, La Scola B. Kaumoebavirus, a New Virus That Clusters with Faustoviruses and Asfarviridae. Viruses. 2016;8(11):278. Epub 2016/11/02. doi: 10.3390/v8110278. PubMed PMID: 27801826; PMCID: PMC5127008.
11. McFadden G. Poxvirus tropism. Nat Rev Microbiol. 2005;3(3):201-13. Epub 2005/03/02. doi: 10.1038/nrmicro1099. PubMed PMID: 15738948; PMCID: PMC4382915.
12. Oliveira GP, Rodrigues RAL, Lima MT, Drumond BP, Abrahao JS. Poxvirus Host Range Genes and Virus-Host Spectrum: A Critical Review. Viruses. 2017;9(11):331. Epub 2017/11/08. doi: 10.3390/v9110331. PubMed PMID: 29112165; PMCID: PMC5707538.
13. Burrell CJ, Howard CR, Murphy FA. Poxviruses. In: Burrell CJ, Howard CR, Murphy FA, editors. Fenner and White's Medical Virology. London: Academic Press; 2017. p. 229-36.
14. Pauli G, Blumel J, Burger R, Drosten C, Groner A, Gurtler L, Heiden M, Hildebrandt M, Jansen B, Montag-Lessing T, Offergeld R, Seitz R, Schlenkrich U, Schottstedt V, Strobel J, Willkommen H, von Konig CH. Orthopox Viruses: Infections in Humans. Transfus Med Hemother. 2010;37(6):351-64. Epub 2010/01/01. doi: 10.1159/000322101. PubMed PMID: 21483466; PMCID: PMC3048946.
15. National Advisory Committee on I. An advisory committee statement (ACS). National Advisory Committee on Immunization (NACI). Statement on smallpox vaccination. Can Commun Dis Rep. 2002;28(ACS-1):1-12. Epub 2003/05/06. PubMed PMID: 12728646.
16. Baxby D. The origins of vaccinia virus. J Infect Dis. 1977;136(3):453-5. Epub 1977/09/01. doi: 10.1093/infdis/136.3.453. PubMed PMID: 198484.
17. Baxby D. Jenner's smallpox vaccine: the riddle of vaccinia virus and its origin. London: Heinemann Educational Books; 1981. xiv, 214 p. p.
18. Esparza J, Nitsche A, Damaso CR. Beyond the myths: Novel findings for old paradigms in the history of the smallpox vaccine. PLoS Pathog. 2018;14(7):e1007082. Epub 2018/07/27. doi: 10.1371/journal.ppat.1007082. PubMed PMID: 30048524; PMCID: PMC6062137.

19. de Freitas LFD, Oliveira RP, Miranda MCG, Rocha RP, Barbosa-Stancioli EF, Faria AMC, da Fonseca FG. The Virulence of Different Vaccinia Virus Strains Is Directly Proportional to Their Ability To Downmodulate Specific Cell-Mediated Immune Compartments In Vivo. J Virol. 2019;93(6):e02191-18. Epub 2018/12/21. doi: 10.1128/JVI.02191-18. PubMed PMID: 30567985; PMCID: PMC6401461.
20. Jacobs BL, Langland JO, Kibler KV, Denzler KL, White SD, Holechek SA, Wong S, Huynh T, Baskin CR. Vaccinia virus vaccines: past, present and future. Antiviral Res. 2009;84(1):1-13. Epub 2009/07/01. doi: 10.1016/j.antiviral.2009.06.006. PubMed PMID: 19563829; PMCID: PMC2742674.
21. Qin L, Upton C, Hazes B, Evans DH. Genomic analysis of the vaccinia virus strain variants found in Dryvax vaccine. J Virol. 2011;85(24):13049-60. Epub 2011/10/07. doi: 10.1128/JVI.05779-11. PubMed PMID: 21976639; PMCID: PMC3233142.
22. Zeh HJ, Downs-Canner S, McCart JA, Guo ZS, Rao UN, Ramalingam L, Thorne SH, Jones HL, Kalinski P, Wieckowski E, O'Malley ME, Daneshmand M, Hu K, Bell JC, Hwang TH, Moon A, Breitbach CJ, Kirn DH, Bartlett DL. First-in-man study of western reserve strain oncolytic vaccinia virus: safety, systemic spread, and antitumor activity. Mol Ther. 2015;23(1):202-14. Epub 2014/10/09. doi: 10.1038/mt.2014.194. PubMed PMID: 25292189; PMCID: PMC4426804.
23. Rosenthal SR, Merchlinsky M, Kleppinger C, Goldenthal KL. Developing new smallpox vaccines. Emerg Infect Dis. 2001;7(6):920-6. Epub 2001/12/19. doi: 10.3201/eid0706.010602. PubMed PMID: 11747717; PMCID: PMC2631916.
24. Moss B. Vaccinia virus: a tool for research and vaccine development. Science. 1991;252(5013):1662-7. Epub 1991/06/21. doi: 10.1126/science.2047875. PubMed PMID: 2047875.
25. Moss B. Genetically engineered poxviruses for recombinant gene expression, vaccination, and safety. Proc Natl Acad Sci U S A. 1996;93(21):11341-8. Epub 1996/10/15. doi: 10.1073/pnas.93.21.11341. PubMed PMID: 8876137; PMCID: PMC38059.
26. Fenner F. Smallpox and its eradication. Geneva: World Health Organization; 1988. xvi, 1460 p. p.
27. O'Connell CM, Jasperse B, Hagen CJ, Titong A, Verardi PH. Replication-inducible vaccinia virus vectors with enhanced safety in vivo. PLoS One. 2020;15(4):e0230711. Epub 2020/04/03. doi: 10.1371/journal.pone.0230711. PubMed PMID: 32240193; PMCID: PMC7117657.
28. Katsafanas GC, Moss B. Colocalization of transcription and translation within cytoplasmic poxvirus factories coordinates viral expression and subjugates host functions. Cell Host Microbe. 2007;2(4):221-8. Epub 2007/11/17. doi: 10.1016/j.chom.2007.08.005. PubMed PMID: 18005740; PMCID: PMC2084088.
29. Tolonen N, Doglio L, Schleich S, Krijnse Locker J. Vaccinia virus DNA replication occurs in endoplasmic reticulum-enclosed cytoplasmic mini-nuclei. Mol Biol Cell. 2001;12(7):2031-46. Epub 2001/07/14. doi: 10.1091/mbc.12.7.2031. PubMed PMID: 11452001; PMCID: PMC55651.
30. Chung CS, Chen CH, Ho MY, Huang CY, Liao CL, Chang W. Vaccinia virus proteome: identification of proteins in vaccinia virus intracellular mature virion particles. J Virol. 2006;80(5):2127-40. Epub 2006/02/14. doi: 10.1128/JVI.80.5.2127-2140.2006. PubMed PMID: 16474121; PMCID: PMC1395410.
31. Baldick CJ, Jr., Moss B. Characterization and temporal regulation of mRNAs encoded by vaccinia virus intermediate-stage genes. J Virol. 1993;67(6):3515-27. Epub 1993/06/01. doi: 10.1128/JVI.67.6.3515-3527.1993. PubMed PMID: 8098779; PMCID: PMC237698.
32. Gershon PD, Moss B. Early transcription factor subunits are encoded by vaccinia virus late genes. Proc Natl Acad Sci U S A. 1990;87(11):4401-5. Epub 1990/06/01. doi: 10.1073/pnas.87.11.4401. PubMed PMID: 2190222; PMCID: PMC54118.
33. Broyles SS, Fesler BS. Vaccinia virus gene encoding a component of the viral early transcription factor. J Virol. 1990;64(4):1523-9. Epub 1990/04/01. doi: 10.1128/JVI.64.4.1523-1529.1990. PubMed PMID: 2138681; PMCID: PMC249286.
34. Joklik WK. The Intracellular Uncoating of Poxvirus DNA. I. The Fate of Radioactively-Labeled Rabbitpox Virus. J Mol Biol. 1964;8:263-76. Epub 1964/02/01. doi: 10.1016/s0022-2836(64)80136-4. PubMed PMID: 14126295.

35. Joklik WK. The Intracellular Uncoating of Poxvirus DNA. Ii. The Molecular Basis of the Uncoating Process. J Mol Biol. 1964;8:277-88. Epub 1964/02/01. doi: 10.1016/s0022-2836(64)80137-6. PubMed PMID: 14126296.
36. Broyles SS. Vaccinia virus transcription. J Gen Virol. 2003;84(Pt 9):2293-303. Epub 2003/08/15. doi: 10.1099/vir.0.18942-0. PubMed PMID: 12917449.
37. Keck JG, Baldick CJ, Jr., Moss B. Role of DNA replication in vaccinia virus gene expression: a naked template is required for transcription of three late trans-activator genes. Cell. 1990;61(5):801-9. Epub 1990/06/01. doi: 10.1016/0092-8674(90)90190-p. PubMed PMID: 2344616.
38. Yang Z, Maruri-Avidal L, Sisler J, Stuart CA, Moss B. Cascade regulation of vaccinia virus gene expression is modulated by multistage promoters. Virology. 2013;447(1-2):213-20. Epub 2013/11/12. doi: 10.1016/j.virol.2013.09.007. PubMed PMID: 24210117; PMCID: PMC3840034.
39. Moss B, Earl PL. Overview of the Vaccinia Virus Expression System. Current Protocols in Molecular Biology. 2002;60(1):16.5.1-.5.5. doi: https://doi.org/10.1002/0471142727.mb1615s60.
40. Bidgood SR, Mercer J. Cloak and Dagger: Alternative Immune Evasion and Modulation Strategies of Poxviruses. Viruses. 2015;7(8):4800-25. doi: 10.3390/v7082844. PubMed PMID: 26308043.
41. De Clercq E. Vaccinia Virus Inhibitors as a Paradigm for the Chemotherapy of Poxvirus Infections. Clinical Microbiology Reviews. 2001;14(2):382. doi: 10.1128/CMR.14.2.382-397.2001.
42. Yang Z, Bruno DP, Martens CA, Porcella SF, Moss B. Simultaneous high-resolution analysis of vaccinia virus and host cell transcriptomes by deep RNA sequencing. Proc Natl Acad Sci U S A. 2010;107(25):11513-8. Epub 2010/06/11. doi: 10.1073/pnas.1006594107. PubMed PMID: 20534518; PMCID: PMC2895082.
43. Yang Z, Reynolds SE, Martens CA, Bruno DP, Porcella SF, Moss B. Expression profiling of the intermediate and late stages of poxvirus replication. J Virol. 2011;85(19):9899-908. Epub 2011/07/29. doi: 10.1128/JVI.05446-11. PubMed PMID: 21795349; PMCID: PMC3196450.
44. de Magistris L, Stunnenberg HG. Cis-acting sequences affecting the length of the poly(A) head of vaccinia virus late transcripts. Nucleic Acids Res. 1988;16(8):3141-56. Epub 1988/04/25. doi: 10.1093/nar/16.8.3141. PubMed PMID: 2897657; PMCID: PMC336484.
45. Rosel JL, Earl PL, Weir JP, Moss B. Conserved TAAATG sequence at the transcriptional and translational initiation sites of vaccinia virus late genes deduced by structural and functional analysis of the HindIII H genome fragment. J Virol. 1986;60(2):436-49. Epub 1986/11/01. doi: 10.1128/JVI.60.2.436-449.1986. PubMed PMID: 3021979; PMCID: PMC288911.
46. Schwer B, Vista P, Vos JC, Stunnenberg HG. Discontinuous Transcription or RNA Processing of Vaccinia Virus Late Messengers Results in a 5 ' Poly ( A ) Leader. Cell. 1986;50:163-9.
47. Bertholet C, Van Meir E, ten Heggeler-Bordier B, Wittek R. Vaccinia virus produces late mRNAs by discontinuous synthesis. Cell. 1987;50(2):153-62. Epub 1987/07/17. doi: 10.1016/0092-8674(87)90211-x. PubMed PMID: 3036368; PMCID: PMC7133321.
48. Schwer B, Stunnenberg HG. Vaccinia virus late transcripts generated in vitro have a poly(A) head. EMBO J. 1988;7(4):1183-90. Epub 1988/04/01. doi: 10.1002/j.1460-2075.1988.tb02929.x. PubMed PMID: 3402436; PMCID: PMC454454.
49. Yang Z, Martens CA, Bruno DP, Porcella SF, Moss B. Pervasive initiation and 3'-end formation of poxvirus postreplicative RNAs. J Biol Chem. 2012;287(37):31050-60. Epub 2012/07/26. doi: 10.1074/jbc.M112.390054. PubMed PMID: 22829601; PMCID: PMC3438937.
50. Wang Z, Gerstein M, Snyder M. RNA-Seq: a revolutionary tool for transcriptomics. Nat Rev Genet. 2009;10(1):57-63. Epub 2008/11/19. doi: 10.1038/nrg2484. PubMed PMID: 19015660; PMCID: PMC2949280.
51. Wright CF, Moss B. In vitro synthesis of vaccinia virus late mRNA containing a 5' poly(A) leader sequence. Proc Natl Acad Sci U S A. 1987;84(24):8883-7. Epub 1987/12/01. doi: 10.1073/pnas.84.24.8883. PubMed PMID: 2827158; PMCID: PMC299655.
52. Filipowicz W. Functions of the 5,-terminal m7G cap in eukaryotic mRNA. FEBS Lett. 1978;96(1):1-11. Epub 1978/12/01. doi: 10.1016/0014-5793(78)81049-7. PubMed PMID: 729775.
53. Shatkin AJ. Capping of eucaryotic mRNAs. Cell. 1976;9(4 PT 2):645-53. Epub 1976/12/01. doi: 10.1016/0092-8674(76)90128-8. PubMed PMID: 1017010.

54. Brawerman G. The Role of the poly(A) sequence in mammalian messenger RNA. CRC Crit Rev Biochem. 1981;10(1):1-38. Epub 1981/01/01. doi: 10.3109/10409238109114634. PubMed PMID: 6111419.
55. Bernstein P, Ross J. Poly(A), poly(A) binding protein and the regulation of mRNA stability. Trends Biochem Sci. 1989;14(9):373-7. Epub 1989/09/01. doi: 10.1016/0968-0004(89)90011-x. PubMed PMID: 2688202.
56. Shuman S, Hurwitz J. Mechanism of mRNA capping by vaccinia virus guanylyltransferase: characterization of an enzyme--guanylate intermediate. Proc Natl Acad Sci U S A. 1981;78(1):187-91. Epub 1981/01/01. doi: 10.1073/pnas.78.1.187. PubMed PMID: 6264433; PMCID: PMC319016.
57. Gershon PD. mRNA 3′ End Formation by Vaccinia Virus: Mechanism of Action of a Heterodimeric Poly(A) Polymerase. Seminars in Virology. 1998;8(4):343-50. doi: 10.1006/smvy.1997.0137. PubMed PMID: WOS:000081695400008.
58. Banerjee AK. 5'-terminal cap structure in eucaryotic messenger ribonucleic acids. Microbiol Rev. 1980;44(2):175-205. Epub 1980/06/01. PubMed PMID: 6247631; PMCID: PMC373176.
59. Ghosh A, Komar AA. Eukaryote-specific extensions in ribosomal proteins of the small subunit: Structure and function. Translation (Austin). 2015;3(1):e999576. Epub 2016/01/19. doi: 10.1080/21690731.2014.999576. PubMed PMID: 26779416; PMCID: PMC4682806.
60. Ramakrishnan V. Ribosome structure and the mechanism of translation. Cell. 2002;108(4):557-72. Epub 2002/03/23. doi: 10.1016/s0092-8674(02)00619-0. PubMed PMID: 11909526.
61. Khatter H, Myasnikov AG, Natchiar SK, Klaholz BP. Structure of the human 80S ribosome. Nature. 2015;520(7549):640-5. Epub 2015/04/23. doi: 10.1038/nature14427. PubMed PMID: 25901680.
62. Ben-Shem A, Garreau de Loubresse N, Melnikov S, Jenner L, Yusupova G, Yusupov M. The structure of the eukaryotic ribosome at 3.0 A resolution. Science. 2011;334(6062):1524-9. Epub 2011/11/19. doi: 10.1126/science.1212642. PubMed PMID: 22096102.
63. Klinge S, Voigts-Hoffmann F, Leibundgut M, Arpagaus S, Ban N. Crystal structure of the eukaryotic 60S ribosomal subunit in complex with initiation factor 6. Science. 2011;334(6058):941-8. Epub 2011/11/05. doi: 10.1126/science.1211204. PubMed PMID: 22052974.
64. Wilson DN, Doudna Cate JH. The structure and function of the eukaryotic ribosome. Cold Spring Harb Perspect Biol. 2012;4(5):1-18. Epub 2012/05/03. doi: 10.1101/cshperspect.a011536. PubMed PMID: 22550233; PMCID: PMC3331703.
65. Hinnebusch AG. The scanning mechanism of eukaryotic translation initiation. Annu Rev Biochem. 2014;83:779-812. Epub 2014/02/07. doi: 10.1146/annurev-biochem-060713-035802. PubMed PMID: 24499181.
66. Jenner L, Melnikov S, de Loubresse NG, Ben-Shem A, Iskakova M, Urzhumtsev A, Meskauskas A, Dinman J, Yusupova G, Yusupov M. Crystal structure of the 80S yeast ribosome. Current Opinion in Structural Biology. 2012;22(6):759-67. doi: https://doi.org/10.1016/j.sbi.2012.07.013.
67. Hinnebusch AG. Molecular mechanism of scanning and start codon selection in eukaryotes. Microbiol Mol Biol Rev. 2011;75(3):434-67, first page of table of contents. Epub 2011/09/03. doi: 10.1128/MMBR.00008-11. PubMed PMID: 21885680; PMCID: PMC3165540.
68. Pestova TV, Lorsch JR, Hellen CUT. The Mechanism of Translation Initiation in Eukaryotes. In: Mathews M, Sonenberg N, Hershey JWB, editors. Translational Control in Biology and Medicine Cold Spring Harbor, N.Y.: Cold Spring Harbor Laboratory. 2007. p. 87-128.
69. Goss DJ, Kleiman FE. Poly(A) binding proteins: are they all created equal? Wiley Interdiscip Rev RNA. 2013;4(2):167-79. Epub 2013/02/21. doi: 10.1002/wrna.1151. PubMed PMID: 23424172; PMCID: PMC3580857.
70. Kahvejian A, Roy G, Sonenberg N. The mRNA closed-loop model: the function of PABP and PABP-interacting proteins in mRNA translation. Cold Spring Harb Symp Quant Biol. 2001;66:293-300. Epub 2003/05/24. doi: 10.1101/sqb.2001.66.293. PubMed PMID: 12762031.
71. Kozak M. Point mutations define a sequence flanking the AUG initiator codon that modulates translation by eukaryotic ribosomes. Cell. 1986;44(2):283-92. Epub 1986/01/31. doi: 10.1016/0092-8674(86)90762-2. PubMed PMID: WOS:A1986AZC2900011.
72. Svitkin YV, Pause A, Haghighat A, Pyronnet S, Witherell G, Belsham GJ, Sonenberg N. The requirement for eukaryotic initiation factor 4A (eIF4A) in translation is in direct proportion to the

degree of mRNA 5' secondary structure. RNA. 2001;7(3):382-94. Epub 2001/05/03. doi: 10.1017/s135583820100108x. PubMed PMID: 11333019; PMCID: PMC1370095.

73. Parsyan A, Svitkin Y, Shahbazian D, Gkogkas C, Lasko P, Merrick WC, Sonenberg N. mRNA helicases: the tacticians of translational control. Nat Rev Mol Cell Biol. 2011;12(4):235-45. Epub 2011/03/24. doi: 10.1038/nrm3083. PubMed PMID: 21427765.
74. Nanda JS, Saini AK, Munoz AM, Hinnebusch AG, Lorsch JR. Coordinated movements of eukaryotic translation initiation factors eIF1, eIF1A, and eIF5 trigger phosphate release from eIF2 in response to start codon recognition by the ribosomal preinitiation complex. J Biol Chem. 2013;288(8):5316-29. Epub 2013/01/08. doi: 10.1074/jbc.M112.440693. PubMed PMID: 23293029; PMCID: PMC3581429.
75. Unbehaun A, Borukhov SI, Hellen CU, Pestova TV. Release of initiation factors from 48S complexes during ribosomal subunit joining and the link between establishment of codon-anticodon base-pairing and hydrolysis of eIF2-bound GTP. Genes Dev. 2004;18(24):3078-93. Epub 2004/12/17. doi: 10.1101/gad.1255704. PubMed PMID: 15601822; PMCID: PMC535918.
76. Llacer JL, Hussain T, Saini AK, Nanda JS, Kaur S, Gordiyenko Y, Kumar R, Hinnebusch AG, Lorsch JR, Ramakrishnan V. Translational initiation factor eIF5 replaces eIF1 on the 40S ribosomal subunit to promote start-codon recognition. Elife. 2018;7:e39273. Epub 2018/11/27. doi: 10.7554/eLife.39273. PubMed PMID: 30475211; PMCID: PMC6298780.
77. Acker MG, Shin BS, Dever TE, Lorsch JR. Interaction between eukaryotic initiation factors 1A and 5B is required for efficient ribosomal subunit joining. J Biol Chem. 2006;281(13):8469-75. Epub 2006/02/08. doi: 10.1074/jbc.M600210200. PubMed PMID: 16461768.
78. Acker MG, Shin BS, Nanda JS, Saini AK, Dever TE, Lorsch JR. Kinetic analysis of late steps of eukaryotic translation initiation. J Mol Biol. 2009;385(2):491-506. Epub 2008/11/04. doi: 10.1016/j.jmb.2008.10.029. PubMed PMID: 18976658; PMCID: PMC2654283.
79. Guo Z, Noller HF. Rotation of the head of the 30S ribosomal subunit during mRNA translocation. Proc Natl Acad Sci U S A. 2012;109(50):20391-4. Epub 2012/11/29. doi: 10.1073/pnas.1218999109. PubMed PMID: 23188795; PMCID: PMC3528506.
80. Mohan S, Donohue JP, Noller HF. Molecular mechanics of 30S subunit head rotation. Proc Natl Acad Sci U S A. 2014;111(37):13325-30. Epub 2014/09/05. doi: 10.1073/pnas.1413731111. PubMed PMID: 25187561; PMCID: PMC4169957.
81. Frank J, Agrawal RK. A ratchet-like inter-subunit reorganization of the ribosome during translocation. Nature. 2000;406(6793):318-22. Epub 2000/08/05. doi: 10.1038/35018597. PubMed PMID: 10917535.
82. Zhang W, Dunkle JA, Cate JH. Structures of the ribosome in intermediate states of ratcheting. Science. 2009;325(5943):1014-7. Epub 2009/08/22. doi: 10.1126/science.1175275. PubMed PMID: 19696352; PMCID: PMC2919209.
83. Pisarev AV, Kolupaeva VG, Yusupov MM, Hellen CU, Pestova TV. Ribosomal position and contacts of mRNA in eukaryotic translation initiation complexes. EMBO J. 2008;27(11):1609-21. Epub 2008/05/10. doi: 10.1038/emboj.2008.90. PubMed PMID: 18464793; PMCID: PMC2426728.
84. Rabl J, Leibundgut M, Ataide SF, Haag A, Ban N. Crystal structure of the eukaryotic 40S ribosomal subunit in complex with initiation factor 1. Science. 2011;331(6018):730-6. Epub 2011/01/06. doi: 10.1126/science.1198308. PubMed PMID: 21205638.
85. Dever TE, Green R. The elongation, termination, and recycling phases of translation in eukaryotes. Cold Spring Harb Perspect Biol. 2012;4(7):a013706. Epub 2012/07/04. doi: 10.1101/cshperspect.a013706. PubMed PMID: 22751155; PMCID: PMC3385960.
86. Qin X, Sarnow P. Preferential translation of internal ribosome entry site-containing mRNAs during the mitotic cycle in mammalian cells. J Biol Chem. 2004;279(14):13721-8. Epub 2004/01/24. doi: 10.1074/jbc.M312854200. PubMed PMID: 14739278.
87. Lacerda R, Menezes J, Romao L. More than just scanning: the importance of cap-independent mRNA translation initiation for cellular stress response and cancer. Cell Mol Life Sci. 2017;74(9):1659-80. Epub 2016/12/04. doi: 10.1007/s00018-016-2428-2. PubMed PMID: 27913822.
88. Holcik M, Sonenberg N. Translational control in stress and apoptosis. Nat Rev Mol Cell Biol. 2005;6(4):318-27. Epub 2005/04/02. doi: 10.1038/nrm1618. PubMed PMID: 15803138.

89. Yueh A, Schneider RJ. Selective translation initiation by ribosome jumping in adenovirus-infected and heat-shocked cells. Genes Dev. 1996;10(12):1557-67. Epub 1996/06/15. doi: 10.1101/gad.10.12.1557. PubMed PMID: 8666238.
90. Yueh A, Schneider RJ. Translation by ribosome shunting on adenovirus and hsp70 mRNAs facilitated by complementarity to 18S rRNA. Genes Dev. 2000;14(4):414-21. Epub 2000/02/26. PubMed PMID: 10691734; PMCID: PMC316380.
91. Futterer J, Kiss-Laszlo Z, Hohn T. Nonlinear ribosome migration on cauliflower mosaic virus 35S RNA. Cell. 1993;73(4):789-802. Epub 1993/05/21. doi: 10.1016/0092-8674(93)90257-q. PubMed PMID: 8500171.
92. Jackson RJ. The current status of vertebrate cellular mRNA IRESs. Cold Spring Harb Perspect Biol. 2013;5(2):a011569. Epub 2013/02/05. doi: 10.1101/cshperspect.a011569. PubMed PMID: 23378589; PMCID: PMC3552511.
93. Majzoub K, Hafirassou ML, Meignin C, Goto A, Marzi S, Fedorova A, Verdier Y, Vinh J, Hoffmann JA, Martin F, Baumert TF, Schuster C, Imler JL. RACK1 controls IRES-mediated translation of viruses. Cell. 2014;159(5):1086-95. Epub 2014/11/25. doi: 10.1016/j.cell.2014.10.041. PubMed PMID: 25416947; PMCID: PMC4243054.
94. Waldron JA, Tack DC, Ritchey LE, Gillen SL, Wilczynska A, Turro E, Bevilacqua PC, Assmann SM, Bushell M, Le Quesne J. mRNA structural elements immediately upstream of the start codon dictate dependence upon eIF4A helicase activity. Genome Biol. 2019;20(1):300. Epub 2020/01/01. doi: 10.1186/s13059-019-1901-2. PubMed PMID: 31888698; PMCID: PMC6936103.
95. Jan E, Mohr I, Walsh D. A Cap-to-Tail Guide to mRNA Translation Strategies in Virus-Infected Cells. Annu Rev Virol. 2016;3(1):283-307. Epub 2016/08/09. doi: 10.1146/annurev-virology-100114-055014. PubMed PMID: 27501262.
96. Mailliot J, Martin F. Viral internal ribosomal entry sites: four classes for one goal. Wiley Interdiscip Rev RNA. 2018;9(2). Epub 2017/12/02. doi: 10.1002/wrna.1458. PubMed PMID: 29193740.
97. Meade N, DiGiuseppe S, Walsh D. Translational control during poxvirus infection. Wiley Interdiscip Rev RNA. 2019;10(2):e1515. Epub 2018/11/02. doi: 10.1002/wrna.1515. PubMed PMID: 30381906; PMCID: PMC6375802.
98. Mader S, Lee H, Pause A, Sonenberg N. The translation initiation factor eIF-4E binds to a common motif shared by the translation factor eIF-4 gamma and the translational repressors 4E-binding proteins. Mol Cell Biol. 1995;15(9):4990-7. Epub 1995/09/01. doi: 10.1128/mcb.15.9.4990. PubMed PMID: 7651417; PMCID: PMC230746.
99. Walsh D, Arias C, Perez C, Halladin D, Escandon M, Ueda T, Watanabe-Fukunaga R, Fukunaga R, Mohr I. Eukaryotic translation initiation factor 4F architectural alterations accompany translation initiation factor redistribution in poxvirus-infected cells. Mol Cell Biol. 2008;28(8):2648-58. Epub 2008/02/06. doi: 10.1128/MCB.01631-07. PubMed PMID: 18250159; PMCID: PMC2293122.
100. Zaborowska I, Kellner K, Henry M, Meleady P, Walsh D. Recruitment of host translation initiation factor eIF4G by the Vaccinia Virus ssDNA-binding protein I3. Virology. 2012;425(1):11-22. Epub 2012/01/28. doi: 10.1016/j.virol.2011.12.022. PubMed PMID: 22280895.
101. Walsh D, Mohr I. Assembly of an active translation initiation factor complex by a viral protein. Genes Dev. 2006;20(4):461-72. Epub 2006/02/17. doi: 10.1101/gad.1375006. PubMed PMID: 16481474; PMCID: PMC1369048.
102. Su MJ, Bablanian R. Polyadenylated RNA sequences from vaccinia virus-infected cells selectively inhibit translation in a cell-free system: structural properties and mechanism of inhibition. Virology. 1990;179(2):679-93. Epub 1990/12/01. doi: 10.1016/0042-6822(90)90135-e. PubMed PMID: 1700540.
103. Lu C, Bablanian R. Characterization of small nontranslated polyadenylylated RNAs in vaccinia virus-infected cells. Proc Natl Acad Sci U S A. 1996;93(5):2037-42. Epub 1996/03/05. doi: 10.1073/pnas.93.5.2037. PubMed PMID: 8700881; PMCID: PMC39905.
104. Bablanian R, Scribani S, Esteban M. Amplification of polyadenylated nontranslated small RNA sequences (POLADS) during superinfection correlates with the inhibition of viral and cellular protein synthesis. Cell Mol Biol Res. 1993;39(3):243-55. Epub 1993/01/01. PubMed PMID: 7507390.
105. Bablanian R, Goswami SK, Esteban M, Banerjee AK, Merrick WC. Mechanism of selective translation of vaccinia virus mRNAs: differential role of poly(A) and initiation factors in the

translation of viral and cellular mRNAs. J Virol. 1991;65(8):4449-60. Epub 1991/08/01. doi: 10.1128/JVI.65.8.4449-4460.1991. PubMed PMID: 2072458; PMCID: PMC248885.

106. Cacoullos N, Bablanian R. Polyadenylated RNA sequences produced in vaccinia virus-infected cells under aberrant conditions inhibit protein synthesis in vitro. Virology. 1991;184(2):747-51. Epub 1991/10/01. doi: 10.1016/0042-6822(91)90445-h. PubMed PMID: 1716028.
107. Bablanian R, Banerjee AK. Poly(riboadenylic acid) preferentially inhibits in vitro translation of cellular mRNAs compared with vaccinia virus mRNAs: possible role in vaccinia virus cytopathology. Proc Natl Acad Sci U S A. 1986;83(5):1290-4. Epub 1986/03/01. doi: 10.1073/pnas.83.5.1290. PubMed PMID: 3456588; PMCID: PMC323061.
108. Cacoullos N, Bablanian R. Role of polyadenylated RNA sequences (POLADS) in vaccinia virus infection: correlation between accumulation of POLADS and extent of shut-off in infected cells. Cell Mol Biol Res. 1993;39(7):657-64. Epub 1993/01/01. PubMed PMID: 7519942.
109. Dhungel P, Cantu FM, Molina JA, Yang Z. Vaccinia Virus as a Master of Host Shutoff Induction: Targeting Processes of the Central Dogma and Beyond. Pathogens. 2020;9(5):400. Epub 2020/05/28. doi: 10.3390/pathogens9050400. PubMed PMID: 32455727; PMCID: PMC7281567.
110. Cao S, Dhungel P, Yang Z. Going against the Tide: Selective Cellular Protein Synthesis during Virally Induced Host Shutoff. J Virol. 2017;91(17):e00071-17. Epub 2017/06/24. doi: 10.1128/JVI.00071-17. PubMed PMID: 28637757; PMCID: PMC5553178.
111. Parrish S, Moss B. Characterization of a second vaccinia virus mRNA-decapping enzyme conserved in poxviruses. J Virol. 2007;81(23):12973-8. Epub 2007/09/21. doi: 10.1128/JVI.01668-07. PubMed PMID: 17881455; PMCID: PMC2169080.
112. Parrish S, Resch W, Moss B. Vaccinia virus D10 protein has mRNA decapping activity, providing a mechanism for control of host and viral gene expression. Proc Natl Acad Sci U S A. 2007;104(7):2139-44. Epub 2007/02/07. doi: 10.1073/pnas.0611685104. PubMed PMID: 17283339; PMCID: PMC1793903.
113. Parrish S, Moss B. Characterization of a vaccinia virus mutant with a deletion of the D10R gene encoding a putative negative regulator of gene expression. J Virol. 2006;80(2):553-61. Epub 2005/12/28. doi: 10.1128/JVI.80.2.553-561.2006. PubMed PMID: 16378957; PMCID: PMC1346865.
114. Liu SW, Wyatt LS, Orandle MS, Minai M, Moss B. The D10 decapping enzyme of vaccinia virus contributes to decay of cellular and viral mRNAs and to virulence in mice. J Virol. 2014;88(1):202-11. Epub 2013/10/25. doi: 10.1128/JVI.02426-13. PubMed PMID: 24155373; PMCID: PMC3911708.
115. Walsh D, Mathews MB, Mohr I. Tinkering with translation: protein synthesis in virus-infected cells. Cold Spring Harb Perspect Biol. 2013;5(1):a012351. Epub 2012/12/05. doi: 10.1101/cshperspect.a012351. PubMed PMID: 23209131; PMCID: PMC3579402.
116. Person A, Ben-Hamida F, Beaud G. Inhibition of 40S--Met--tRNAfMet ribosomal initiation complex formation by vaccinia virus. Nature. 1980;287(5780):355-7. Epub 1980/09/25. doi: 10.1038/287355a0. PubMed PMID: 6968407.
117. Person-Fernandez A, Beaud G. Purification and characterization of a protein synthesis inhibitor associated with vaccinia virus. J Biol Chem. 1986;261(18):8283-9. Epub 1986/06/25. PubMed PMID: 3636342.
118. Mulder J, Robertson ME, Seamons RA, Belsham GJ. Vaccinia virus protein synthesis has a low requirement for the intact translation initiation factor eIF4F, the cap-binding complex, within infected cells. J Virol. 1998;72(11):8813-9. Epub 1998/10/10. doi: 10.1128/JVI.72.11.8813-8819.1998. PubMed PMID: 9765426; PMCID: PMC110298.
119. Dhungel P, Cao S, Yang Z. The 5'-poly(A) leader of poxvirus mRNA confers a translational advantage that can be achieved in cells with impaired cap-dependent translation. PLoS Pathog. 2017;13(8):e1006602. Epub 2017/08/31. doi: 10.1371/journal.ppat.1006602. PubMed PMID: 28854224; PMCID: PMC5595341.
120. Strnadova P, Ren H, Valentine R, Mazzon M, Sweeney TR, Brierley I, Smith GL. Inhibition of Translation Initiation by Protein 169: A Vaccinia Virus Strategy to Suppress Innate and Adaptive Immunity and Alter Virus Virulence. PLoS Pathog. 2015;11(9):e1005151. Epub 2015/09/04. doi: 10.1371/journal.ppat.1005151. PubMed PMID: 26334635; PMCID: PMC4559412.

121. Alberts B. The cell as a collection of protein machines: preparing the next generation of molecular biologists. Cell. 1998;92(3):291-4. Epub 1998/02/26. doi: 10.1016/s0092-8674(00)80922-8. PubMed PMID: 9476889.
122. Frank J. The ribosome--a macromolecular machine par excellence. Chem Biol. 2000;7(6):R133-41. Epub 2000/06/30. doi: 10.1016/s1074-5521(00)00127-7. PubMed PMID: 10873840.
123. Ferretti MB, Karbstein K. Does functional specialization of ribosomes really exist? RNA. 2019;25(5):521-38. Epub 2019/02/09. doi: 10.1261/rna.069823.118. PubMed PMID: 30733326; PMCID: PMC6467006.
124. Gilbert WV. Functional specialization of ribosomes? Trends Biochem Sci. 2011;36(3):127-32. Epub 2011/01/19. doi: 10.1016/j.tibs.2010.12.002. PubMed PMID: 21242088; PMCID: PMC3056915.
125. Sulima SO, Dinman JD. The Expanding Riboverse. Cells. 2019;8(10):1205. Epub 2019/10/09. doi: 10.3390/cells8101205. PubMed PMID: 31590378; PMCID: PMC6829380.
126. Xue S, Barna M. Specialized ribosomes: a new frontier in gene regulation and organismal biology. Nat Rev Mol Cell Biol. 2012;13(6):355-69. Epub 2012/05/24. doi: 10.1038/nrm3359. PubMed PMID: 22617470; PMCID: PMC4039366.
127. Ramagopal S, Ennis HL. Regulation of synthesis of cell-specific ribosomal proteins during differentiation of Dictyostelium discoideum. Proc Natl Acad Sci U S A. 1981;78(5):3083-7. Epub 1981/05/01. doi: 10.1073/pnas.78.5.3083. PubMed PMID: 16593020; PMCID: PMC319504.
128. Szick-Miranda K, Bailey-Serres J. Regulated heterogeneity in 12-kDa P-protein phosphorylation and composition of ribosomes in maize (Zea mays L.). J Biol Chem. 2001;276(14):10921-8. Epub 2001/03/30. doi: 10.1074/jbc.M011002200. PubMed PMID: 11278810.
129. Chang IF, Szick-Miranda K, Pan S, Bailey-Serres J. Proteomic characterization of evolutionarily conserved and variable proteins of Arabidopsis cytosolic ribosomes. Plant Physiol. 2005;137(3):848-62. Epub 2005/03/01. doi: 10.1104/pp.104.053637. PubMed PMID: 15734919; PMCID: PMC1065386.
130. Giavalisco P, Wilson D, Kreitler T, Lehrach H, Klose J, Gobom J, Fucini P. High heterogeneity within the ribosomal proteins of the Arabidopsis thaliana 80S ribosome. Plant Mol Biol. 2005;57(4):577-91. Epub 2005/04/12. doi: 10.1007/s11103-005-0699-3. PubMed PMID: 15821981.
131. Gazda HT, Kho AT, Sanoudou D, Zaucha JM, Kohane IS, Sieff CA, Beggs AH. Defective ribosomal protein gene expression alters transcription, translation, apoptosis, and oncogenic pathways in Diamond-Blackfan anemia. Stem Cells. 2006;24(9):2034-44. Epub 2006/06/03. doi: 10.1634/stemcells.2005-0554. PubMed PMID: 16741228; PMCID: PMC3372914.
132. Boria I, Garelli E, Gazda HT, Aspesi A, Quarello P, Pavesi E, Ferrante D, Meerpohl JJ, Kartal M, Da Costa L, Proust A, Leblanc T, Simansour M, Dahl N, Frojmark AS, Pospisilova D, Cmejla R, Beggs AH, Sheen MR, Landowski M, Buros CM, Clinton CM, Dobson LJ, Vlachos A, Atsidaftos E, Lipton JM, Ellis SR, Ramenghi U, Dianzani I. The ribosomal basis of Diamond-Blackfan Anemia: mutation and database update. Hum Mutat. 2010;31(12):1269-79. Epub 2010/10/21. doi: 10.1002/humu.21383. PubMed PMID: 20960466; PMCID: PMC4485435.
133. Hopes T, Norris K, Agapiou M, McCarthy CGP, Lewis PA, O'Connell MJ, Fontana J, Aspden JL. Ribosome heterogeneity in Drosophila melanogaster gonads through paralog-switching. Nucleic Acids Res. 2021. Epub 2021/07/21. doi: 10.1093/nar/gkab606. PubMed PMID: 34283226.
134. Shi Z, Fujii K, Kovary KM, Genuth NR, Rost HL, Teruel MN, Barna M. Heterogeneous Ribosomes Preferentially Translate Distinct Subpools of mRNAs Genome-wide. Mol Cell. 2017;67(1):71-83 e7. Epub 2017/06/20. doi: 10.1016/j.molcel.2017.05.021. PubMed PMID: 28625553; PMCID: PMC5548184.
135. Landry DM, Hertz MI, Thompson SR. RPS25 is essential for translation initiation by the Dicistroviridae and hepatitis C viral IRESs. Genes Dev. 2009;23(23):2753-64. Epub 2009/12/03. doi: 10.1101/gad.1832209. PubMed PMID: 19952110; PMCID: PMC2788332.
136. Cherry S, Doukas T, Armknecht S, Whelan S, Wang H, Sarnow P, Perrimon N. Genome-wide RNAi screen reveals a specific sensitivity of IRES-containing RNA viruses to host translation inhibition. Genes Dev. 2005;19(4):445-52. Epub 2005/02/17. doi: 10.1101/gad.1267905. PubMed PMID: 15713840; PMCID: PMC548945.

137. Lee AS, Burdeinick-Kerr R, Whelan SP. A ribosome-specialized translation initiation pathway is required for cap-dependent translation of vesicular stomatitis virus mRNAs. Proc Natl Acad Sci U S A. 2013;110(1):324-9. Epub 2012/11/22. doi: 10.1073/pnas.1216454109. PubMed PMID: 23169626; PMCID: PMC3538191.
138. Kondrashov N, Pusic A, Stumpf CR, Shimizu K, Hsieh AC, Ishijima J, Shiroishi T, Barna M. Ribosome-mediated specificity in Hox mRNA translation and vertebrate tissue patterning. Cell. 2011;145(3):383-97. Epub 2011/05/03. doi: 10.1016/j.cell.2011.03.028. PubMed PMID: 21529712; PMCID: PMC4445650.
139. Xue S, Tian S, Fujii K, Kladwang W, Das R, Barna M. RNA regulons in Hox 5' UTRs confer ribosome specificity to gene regulation. Nature. 2015;517(7532):33-8. Epub 2014/11/20. doi: 10.1038/nature14010. PubMed PMID: 25409156; PMCID: PMC4353651.
140. Leppek K, Fujii K, Quade N, Susanto TT, Boehringer D, Lenarcic T, Xue S, Genuth NR, Ban N, Barna M. Gene- and Species-Specific Hox mRNA Translation by Ribosome Expansion Segments. Mol Cell. 2020;80(6):980-95 e13. Epub 2020/11/18. doi: 10.1016/j.molcel.2020.10.023. PubMed PMID: 33202249; PMCID: PMC7769145.
141. Sloan KE, Warda AS, Sharma S, Entian KD, Lafontaine DLJ, Bohnsack MT. Tuning the ribosome: The influence of rRNA modification on eukaryotic ribosome biogenesis and function. RNA Biol. 2017;14(9):1138-52. Epub 2016/12/03. doi: 10.1080/15476286.2016.1259781. PubMed PMID: 27911188; PMCID: PMC5699541.
142. Henras AK, Plisson-Chastang C, Humbert O, Romeo Y, Henry Y. Synthesis, Function, and Heterogeneity of snoRNA-Guided Posttranscriptional Nucleoside Modifications in Eukaryotic Ribosomal RNAs. Enzymes. 2017;41:169-213. Epub 2017/06/12. doi: 10.1016/bs.enz.2017.03.007. PubMed PMID: 28601222.
143. Sauert M, Temmel H, Moll I. Heterogeneity of the translational machinery: Variations on a common theme. Biochimie. 2015;114:39-47. Epub 2014/12/30. doi: 10.1016/j.biochi.2014.12.011. PubMed PMID: 25542647; PMCID: PMC4894553.
144. Genuth NR, Barna M. The Discovery of Ribosome Heterogeneity and Its Implications for Gene Regulation and Organismal Life. Mol Cell. 2018;71(3):364-74. Epub 2018/08/04. doi: 10.1016/j.molcel.2018.07.018. PubMed PMID: 30075139; PMCID: PMC6092941.
145. Tang H, Hornstein E, Stolovich M, Levy G, Livingstone M, Templeton D, Avruch J, Meyuhas O. Amino acid-induced translation of TOP mRNAs is fully dependent on phosphatidylinositol 3-kinase-mediated signaling, is partially inhibited by rapamycin, and is independent of S6K1 and rpS6 phosphorylation. Mol Cell Biol. 2001;21(24):8671-83. Epub 2001/11/20. doi: 10.1128/MCB.21.24.8671-8683.2001. PubMed PMID: 11713299; PMCID: PMC100027.
146. Stolovich M, Tang H, Hornstein E, Levy G, Cohen R, Bae SS, Birnbaum MJ, Meyuhas O. Transduction of growth or mitogenic signals into translational activation of TOP mRNAs is fully reliant on the phosphatidylinositol 3-kinase-mediated pathway but requires neither S6K1 nor rpS6 phosphorylation. Mol Cell Biol. 2002;22(23):8101-13. Epub 2002/11/06. doi: 10.1128/mcb.22.23.8101-8113.2002. PubMed PMID: 12417714; PMCID: PMC134064.
147. Simms CL, Yan LL, Zaher HS. Ribosome Collision Is Critical for Quality Control during No-Go Decay. Mol Cell. 2017;68(2):361-73 e5. Epub 2017/09/26. doi: 10.1016/j.molcel.2017.08.019. PubMed PMID: 28943311; PMCID: PMC5659757.
148. Graille M, Seraphin B. Surveillance pathways rescuing eukaryotic ribosomes lost in translation. Nat Rev Mol Cell Biol. 2012;13(11):727-35. Epub 2012/10/18. doi: 10.1038/nrm3457. PubMed PMID: 23072885.
149. Simms CL, Thomas EN, Zaher HS. Ribosome-based quality control of mRNA and nascent peptides. Wiley Interdiscip Rev RNA. 2017;8(1). Epub 2016/05/20. doi: 10.1002/wrna.1366. PubMed PMID: 27193249; PMCID: PMC5116004.
150. Joazeiro CAP. Ribosomal Stalling During Translation: Providing Substrates for Ribosome-Associated Protein Quality Control. Annu Rev Cell Dev Biol. 2017;33:343-68. Epub 2017/07/19. doi: 10.1146/annurev-cellbio-111315-125249. PubMed PMID: 28715909.
151. Komander D, Rape M. The ubiquitin code. Annu Rev Biochem. 2012;81:203-29. Epub 2012/04/25. doi: 10.1146/annurev-biochem-060310-170328. PubMed PMID: 22524316.

152. Brandman O, Hegde RS. Ribosome-associated protein quality control. Nat Struct Mol Biol. 2016;23(1):7-15. Epub 2016/01/07. doi: 10.1038/nsmb.3147. PubMed PMID: 26733220; PMCID: PMC4853245.
153. Brandman O, Stewart-Ornstein J, Wong D, Larson A, Williams CC, Li GW, Zhou S, King D, Shen PS, Weibezahn J, Dunn JG, Rouskin S, Inada T, Frost A, Weissman JS. A ribosome-bound quality control complex triggers degradation of nascent peptides and signals translation stress. Cell. 2012;151(5):1042-54. Epub 2012/11/28. doi: 10.1016/j.cell.2012.10.044. PubMed PMID: 23178123; PMCID: PMC3534965.
154. Wu CC, Peterson A, Zinshteyn B, Regot S, Green R. Ribosome Collisions Trigger General Stress Responses to Regulate Cell Fate. Cell. 2020;182(2):404-16 e14. Epub 2020/07/02. doi: 10.1016/j.cell.2020.06.006. PubMed PMID: 32610081; PMCID: PMC7384957.
155. Juszkiewicz S, Chandrasekaran V, Lin Z, Kraatz S, Ramakrishnan V, Hegde RS. ZNF598 Is a Quality Control Sensor of Collided Ribosomes. Mol Cell. 2018;72(3):469-81 e7. Epub 2018/10/09. doi: 10.1016/j.molcel.2018.08.037. PubMed PMID: 30293783; PMCID: PMC6224477.
156. Juszkiewicz S, Hegde RS. Initiation of Quality Control during Poly(A) Translation Requires Site-Specific Ribosome Ubiquitination. Mol Cell. 2017;65(4):743-50 e4. Epub 2017/01/10. doi: 10.1016/j.molcel.2016.11.039. PubMed PMID: 28065601; PMCID: PMC5316413.
157. Sundaramoorthy E, Leonard M, Mak R, Liao J, Fulzele A, Bennett EJ. ZNF598 and RACK1 Regulate Mammalian Ribosome-Associated Quality Control Function by Mediating Regulatory 40S Ribosomal Ubiquitylation. Mol Cell. 2017;65(4):751-60 e4. Epub 2017/01/31. doi: 10.1016/j.molcel.2016.12.026. PubMed PMID: 28132843; PMCID: PMC5321136.
158. Garzia A, Jafarnejad SM, Meyer C, Chapat C, Gogakos T, Morozov P, Amiri M, Shapiro M, Molina H, Tuschl T, Sonenberg N. The E3 ubiquitin ligase and RNA-binding protein ZNF598 orchestrates ribosome quality control of premature polyadenylated mRNAs. Nat Commun. 2017;8:16056. Epub 2017/07/08. doi: 10.1038/ncomms16056. PubMed PMID: 28685749; PMCID: PMC5504347.
159. Matsuo Y, Ikeuchi K, Saeki Y, Iwasaki S, Schmidt C, Udagawa T, Sato F, Tsuchiya H, Becker T, Tanaka K, Ingolia NT, Beckmann R, Inada T. Ubiquitination of stalled ribosome triggers ribosome-associated quality control. Nat Commun. 2017;8(1):159. Epub 2017/08/02. doi: 10.1038/s41467-017-00188-1. PubMed PMID: 28757607; PMCID: PMC5534433.
160. Koutmou KS, Schuller AP, Brunelle JL, Radhakrishnan A, Djuranovic S, Green R. Ribosomes slide on lysine-encoding homopolymeric A stretches. Elife. 2015;4:1-18. Epub 2015/02/20. doi: 10.7554/eLife.05534. PubMed PMID: 25695637; PMCID: PMC4363877.
161. Tesina P, Lessen LN, Buschauer R, Cheng J, Wu CC, Berninghausen O, Buskirk AR, Becker T, Beckmann R, Green R. Molecular mechanism of translational stalling by inhibitory codon combinations and poly(A) tracts. EMBO J. 2020;39(3):e103365. Epub 2019/12/21. doi: 10.15252/embj.2019103365. PubMed PMID: 31858614; PMCID: PMC6996574.
162. Ikeuchi K, Inada T. Ribosome-associated Asc1/RACK1 is required for endonucleolytic cleavage induced by stalled ribosome at the 3' end of nonstop mRNA. Sci Rep. 2016;6:28234. Epub 2016/06/18. doi: 10.1038/srep28234. PubMed PMID: 27312062; PMCID: PMC4911565.
163. Xu C, Min J. Structure and function of WD40 domain proteins. Protein Cell. 2011;2(3):202-14. Epub 2011/04/07. doi: 10.1007/s13238-011-1018-1. PubMed PMID: 21468892; PMCID: PMC4875305.
164. Murzin AG. Structural principles for the propeller assembly of beta-sheets: the preference for seven-fold symmetry. Proteins. 1992;14(2):191-201. Epub 1992/10/01. doi: 10.1002/prot.340140206. PubMed PMID: 1409568.
165. Sengupta J, Nilsson J, Gursky R, Spahn CM, Nissen P, Frank J. Identification of the versatile scaffold protein RACK1 on the eukaryotic ribosome by cryo-EM. Nat Struct Mol Biol. 2004;11(10):957-62. Epub 2004/08/31. doi: 10.1038/nsmb822. PubMed PMID: 15334071.
166. Coyle SM, Gilbert WV, Doudna JA. Direct link between RACK1 function and localization at the ribosome in vivo. Mol Cell Biol. 2009;29(6):1626-34. Epub 2008/12/31. doi: 10.1128/MCB.01718-08. PubMed PMID: 19114558; PMCID: PMC2648249.
167. Gandin V, Senft D, Topisirovic I, Ronai ZA. RACK1 Function in Cell Motility and Protein Synthesis. Genes Cancer. 2013;4(9-10):369-77. Epub 2013/12/19. doi: 10.1177/1947601913486348. PubMed PMID: 24349634; PMCID: PMC3863339.

168. Gallo S, Manfrini N. Working hard at the nexus between cell signaling and the ribosomal machinery: An insight into the roles of RACK1 in translational regulation. Translation (Austin). 2015;3(2):e1120382. Epub 2016/01/30. doi: 10.1080/21690731.2015.1120382. PubMed PMID: 26824030; PMCID: PMC4721502.
169. Nielsen MH, Flygaard RK, Jenner LB. Structural analysis of ribosomal RACK1 and its role in translational control. Cell Signal. 2017;35:272-81. Epub 2017/02/06. doi: 10.1016/j.cellsig.2017.01.026. PubMed PMID: 28161490.
170. Gallo S, Ricciardi S, Manfrini N, Pesce E, Oliveto S, Calamita P, Mancino M, Maffioli E, Moro M, Crosti M, Berno V, Bombaci M, Tedeschi G, Biffo S. RACK1 Specifically Regulates Translation through Its Binding to Ribosomes. Mol Cell Biol. 2018;38(23):e00544-18. Epub 2018/09/12. doi: 10.1128/MCB.00230-18. PubMed PMID: 30201806; PMCID: PMC6234289.
171. Dobrikov MI, Dobrikova EY, Gromeier M. Ribosomal RACK1:Protein Kinase C betaII Modulates Intramolecular Interactions between Unstructured Regions of Eukaryotic Initiation Factor 4G (eIF4G) That Control eIF4E and eIF3 Binding. Mol Cell Biol. 2018;38(19):e00306-18. Epub 2018/07/18. doi: 10.1128/MCB.00306-18. PubMed PMID: 30012864; PMCID: PMC6146829.
172. Dobrikov MI, Dobrikova EY, Gromeier M. Ribosomal RACK1:Protein Kinase C betaII Phosphorylates Eukaryotic Initiation Factor 4G1 at S1093 To Modulate Cap-Dependent and -Independent Translation Initiation. Mol Cell Biol. 2018;38(19):e00304-18. Epub 2018/07/18. doi: 10.1128/MCB.00304-18. PubMed PMID: 30012863; PMCID: PMC6146833.
173. Sung MK, Reitsma JM, Sweredoski MJ, Hess S, Deshaies RJ. Ribosomal proteins produced in excess are degraded by the ubiquitin-proteasome system. Mol Biol Cell. 2016;27(17):2642-52. Epub 2016/07/08. doi: 10.1091/mbc.E16-05-0290. PubMed PMID: 27385339; PMCID: PMC5007085.
174. Volta V, Beugnet A, Gallo S, Magri L, Brina D, Pesce E, Calamita P, Sanvito F, Biffo S. RACK1 depletion in a mouse model causes lethality, pigmentation deficits and reduction in protein synthesis efficiency. Cell Mol Life Sci. 2013;70(8):1439-50. Epub 2012/12/06. doi: 10.1007/s00018-012-1215-y. PubMed PMID: 23212600.
175. Thompson MK, Rojas-Duran MF, Gangaramani P, Gilbert WV. The ribosomal protein Asc1/RACK1 is required for efficient translation of short mRNAs. Elife. 2016;5:1-22. Epub 2016/04/28. doi: 10.7554/eLife.11154. PubMed PMID: 27117520; PMCID: PMC4848094.
176. Kim HD, Kong E, Kim Y, Chang JS, Kim J. RACK1 depletion in the ribosome induces selective translation for non-canonical autophagy. Cell Death Dis. 2017;8(5):e2800. Epub 2017/05/19. doi: 10.1038/cddis.2017.204. PubMed PMID: 28518135; PMCID: PMC5520723.
177. Johnson AG, Lapointe CP, Wang J, Corsepius NC, Choi J, Fuchs G, Puglisi JD. RACK1 on and off the ribosome. RNA. 2019;25(7):881-95. Epub 2019/04/27. doi: 10.1261/rna.071217.119. PubMed PMID: 31023766; PMCID: PMC6573788.
178. LaFontaine E, Miller CM, Permaul N, Martin ET, Fuchs G. Ribosomal protein RACK1 enhances translation of poliovirus and other viral IRESs. Virology. 2020;545:53-62. Epub 2020/04/21. doi: 10.1016/j.virol.2020.03.004. PubMed PMID: 32308198; PMCID: PMC7804209.
179. Jha S, Rollins MG, Fuchs G, Procter DJ, Hall EA, Cozzolino K, Sarnow P, Savas JN, Walsh D. Trans-kingdom mimicry underlies ribosome customization by a poxvirus kinase. Nature. 2017;546(7660):651-5. Epub 2017/06/22. doi: 10.1038/nature22814. PubMed PMID: 28636603; PMCID: PMC5526112.
180. Shirokikh NE, Spirin AS. Poly(A) leader of eukaryotic mRNA bypasses the dependence of translation on initiation factors. Proc Natl Acad Sci U S A. 2008;105(31):10738-43. Epub 2008/07/29. doi: 10.1073/pnas.0804940105. PubMed PMID: 18658239; PMCID: PMC2485544.
181. Arthur L, Pavlovic-Djuranovic S, Smith-Koutmou K, Green R, Szczesny P, Djuranovic S. Translational control by lysine-encoding A-rich sequences. Sci Adv. 2015;1(6):e1500154. Epub 2015/09/01. doi: 10.1126/sciadv.1500154. PubMed PMID: 26322332; PMCID: PMC4552401.
182. Guo C, Spinelli M, Liu M, Li QQ, Liang C. A Genome-wide Study of "Non-3UTR" Polyadenylation Sites in Arabidopsis thaliana. Sci Rep. 2016;6:28060. Epub 2016/06/16. doi: 10.1038/srep28060. PubMed PMID: 27301740; PMCID: PMC4908657.

183. Xu G, Greene GH, Yoo H, Liu L, Marques J, Motley J, Dong X. Global translational reprogramming is a fundamental layer of immune regulation in plants. Nature. 2017;545(7655):487-90. Epub 2017/05/18. doi: 10.1038/nature22371. PubMed PMID: 28514447; PMCID: PMC5485861.
184. Sleat DE, Gallie DR, Jefferson RA, Bevan MW, Turner PC, Wilson TM. Characterisation of the 5'-leader sequence of tobacco mosaic virus RNA as a general enhancer of translation in vitro. Gene. 1987;60(2-3):217-25. Epub 1987/01/01. doi: 10.1016/0378-1119(87)90230-7. PubMed PMID: 2832252.
185. Gallie DR, Sleat DE, Watts JW, Turner PC, Wilson TM. The 5'-leader sequence of tobacco mosaic virus RNA enhances the expression of foreign gene transcripts in vitro and in vivo. Nucleic Acids Res. 1987;15(8):3257-73. Epub 1987/04/24. doi: 10.1093/nar/15.8.3257. PubMed PMID: 3575095; PMCID: PMC340728.
186. Gallie DR, Walbot V. Identification of the motifs within the tobacco mosaic virus 5'-leader responsible for enhancing translation. Nucleic Acids Res. 1992;20(17):4631-8. Epub 1992/09/11. doi: 10.1093/nar/20.17.4631. PubMed PMID: 1408765; PMCID: PMC334194.
187. Hinnebusch AG, Ivanov IP, Sonenberg N. Translational control by 5'-untranslated regions of eukaryotic mRNAs. Science. 2016;352(6292):1413-6. Epub 2016/06/18. doi: 10.1126/science.aad9868. PubMed PMID: 27313038; PMCID: PMC7422601.
188. Dinman JD. Pathways to Specialized Ribosomes: The Brussels Lecture. J Mol Biol. 2016;428(10 Pt B):2186-94. Epub 2016/01/15. doi: 10.1016/j.jmb.2015.12.021. PubMed PMID: 26764228; PMCID: PMC4884523.
189. Genuth NR, Barna M. Heterogeneity and specialized functions of translation machinery: from genes to organisms. Nat Rev Genet. 2018;19(7):431-52. Epub 2018/05/05. doi: 10.1038/s41576-018-0008-z. PubMed PMID: 29725087; PMCID: PMC6813789.
190. Kouba T, Rutkai E, Karaskova M, Valasek L. The eIF3c/NIP1 PCI domain interacts with RNA and RACK1/ASC1 and promotes assembly of translation preinitiation complexes. Nucleic Acids Res. 2012;40(6):2683-99. Epub 2011/11/30. doi: 10.1093/nar/gkr1083. PubMed PMID: 22123745; PMCID: PMC3315329.
191. Grosso S, Volta V, Sala LA, Vietri M, Marchisio PC, Ron D, Biffo S. PKCbetaII modulates translation independently from mTOR and through RACK1. Biochem J. 2008;415(1):77-85. Epub 2008/06/19. doi: 10.1042/BJ20080463. PubMed PMID: 18557705.
192. Ceci M, Welshhans K, Ciotti MT, Brandi R, Parisi C, Paoletti F, Pistillo L, Bassell GJ, Cattaneo A. RACK1 is a ribosome scaffold protein for beta-actin mRNA/ZBP1 complex. PLoS One. 2012;7(4):e35034. Epub 2012/04/24. doi: 10.1371/journal.pone.0035034. PubMed PMID: 22523568; PMCID: PMC3327689.
193. Nunez A, Franco A, Madrid M, Soto T, Vicente J, Gacto M, Cansado J. Role for RACK1 orthologue Cpc2 in the modulation of stress response in fission yeast. Mol Biol Cell. 2009;20(18):3996-4009. Epub 2009/07/25. doi: 10.1091/mbc.E09-05-0388. PubMed PMID: 19625445; PMCID: PMC2743619.
194. Nunez A, Franco A, Soto T, Vicente J, Gacto M, Cansado J. Fission yeast receptor of activated C kinase (RACK1) ortholog Cpc2 regulates mitotic commitment through Wee1 kinase. J Biol Chem. 2010;285(53):41366-73. Epub 2010/10/27. doi: 10.1074/jbc.M110.173815. PubMed PMID: 20974849; PMCID: PMC3009862.
195. Rachfall N, Schmitt K, Bandau S, Smolinski N, Ehrenreich A, Valerius O, Braus GH. RACK1/Asc1p, a ribosomal node in cellular signaling. Mol Cell Proteomics. 2013;12(1):87-105. Epub 2012/10/17. doi: 10.1074/mcp.M112.017277. PubMed PMID: 23071099; PMCID: PMC3536911.
196. Romano N, Veronese M, Manfrini N, Zolla L, Ceci M. Ribosomal RACK1 promotes proliferation of neuroblastoma cells independently of global translation upregulation. Cell Signal. 2019;53:102-10. Epub 2018/10/06. doi: 10.1016/j.cellsig.2018.09.020. PubMed PMID: 30287278.
197. Ruan Y, Sun L, Hao Y, Wang L, Xu J, Zhang W, Xie J, Guo L, Zhou L, Yun X, Zhu H, Shen A, Gu J. Ribosomal RACK1 promotes chemoresistance and growth in human hepatocellular carcinoma. J Clin Invest. 2012;122(7):2554-66. Epub 2012/06/02. doi: 10.1172/JCI58488. PubMed PMID: 22653060; PMCID: PMC3386807.

198. Shor B, Calaycay J, Rushbrook J, McLeod M. Cpc2/RACK1 is a ribosome-associated protein that promotes efficient translation in Schizosaccharomyces pombe. J Biol Chem. 2003;278(49):49119-28. Epub 2003/09/16. doi: 10.1074/jbc.M303968200. PubMed PMID: 12972434.
199. Kuroha K, Akamatsu M, Dimitrova L, Ito T, Kato Y, Shirahige K, Inada T. Receptor for activated C kinase 1 stimulates nascent polypeptide-dependent translation arrest. EMBO Rep. 2010;11(12):956-61. doi: 10.1038/embor.2010.169. PubMed PMID: WOS:000284827600016.
200. Letzring DP, Wolf AS, Brule CE, Grayhack EJ. Translation of CGA codon repeats in yeast involves quality control components and ribosomal protein L1. Rna. 2013;19(9):1208-17. Epub 2013/07/05. doi: 10.1261/rna.039446.113. PubMed PMID: 23825054; PMCID: PMC3753928.
201. Sitron CS, Park JH, Brandman O. Asc1, Hel2, and Slh1 couple translation arrest to nascent chain degradation. Rna. 2017;23(5):798-810. Epub 2017/02/23. doi: 10.1261/rna.060897.117. PubMed PMID: 28223409; PMCID: PMC5393187.
202. Wang J, Zhou J, Yang Q, Grayhack EJ. Multi-protein bridging factor 1(Mbf1), Rps3 and Asc1 prevent stalled ribosomes from frameshifting. Elife. 2018;7:e39637. Epub 2018/11/23. doi: 10.7554/eLife.39637. PubMed PMID: 30465652; PMCID: PMC6301793.
203. Wolf AS, Grayhack EJ. Asc1, homolog of human RACK1, prevents frameshifting in yeast by ribosomes stalled at CGA codon repeats. RNA. 2015;21(5):935-45. Epub 2015/03/21. doi: 10.1261/rna.049080.114. PubMed PMID: 25792604; PMCID: PMC4408800.
204. Ullah H, Scappini EL, Moon AF, Williams LV, Armstrong DL, Pedersen LC. Structure of a signal transduction regulator, RACK1, from Arabidopsis thaliana. Protein Sci. 2008;17(10):1771-80. Epub 2008/08/22. doi: 10.1110/ps.035121.108. PubMed PMID: 18715992; PMCID: PMC2548356.
205. Adams DR, Ron D, Kiely PA. RACK1, A multifaceted scaffolding protein: Structure and function. Cell Commun Signal. 2011;9:22. Epub 2011/10/08. doi: 10.1186/1478-811X-9-22. PubMed PMID: 21978545; PMCID: PMC3195729.
206. Chen J-G, Ullah H, Temple B, Liang J, Guo J, Alonso JM, Ecker JR, Jones AM. RACK1 mediates multiple hormone responsiveness and developmental processes in Arabidopsis. Journal of Experimental Botany. 2006;57(11):2697-708. doi: 10.1093/jxb/erl035.
207. McCahill A, Warwicker J, Bolger GB, Houslay MD, Yarwood SJ. The RACK1 scaffold protein: a dynamic cog in cell response mechanisms. Mol Pharmacol. 2002;62(6):1261-73. Epub 2002/11/19. doi: 10.1124/mol.62.6.1261. PubMed PMID: 12435793.
208. DiGiuseppe S, Rollins MG, Bartom ET, Walsh D. ZNF598 Plays Distinct Roles in Interferon-Stimulated Gene Expression and Poxvirus Protein Synthesis. Cell Rep. 2018;23(5):1249-58. Epub 2018/05/03. doi: 10.1016/j.celrep.2018.03.132. PubMed PMID: 29719242; PMCID: PMC5951170.
209. Xia X, MacKay V, Yao X, Wu J, Miura F, Ito T, Morris DR. Translation Initiation: A Regulatory Role for Poly(A) Tracts in Front of the AUG Codon in Saccharomyces cerevisiae. Genetics. 2011;189(2):469-78. doi: 10.1534/genetics.111.132068.
210. Gallie DR, Walbot V, Hershey JW. The ribosomal fraction mediates the translational enhancement associated with the 5'-leader of tobacco mosaic virus. Nucleic Acids Res. 1988;16(17):8675-94. Epub 1988/09/12. doi: 10.1093/nar/16.17.8675. PubMed PMID: 3166519; PMCID: PMC338584.
211. Schwer B, Visca P, Vos JC, Stunnenberg HG. Discontinuous transcription or RNA processing of vaccinia virus late messengers results in a 5' poly(A) leader. Cell. 1987;50(2):163-9. Epub 1987/07/17. doi: 10.1016/0092-8674(87)90212-1. PubMed PMID: 3594569; PMCID: PMC7133236.
212. Steel LF, Jacobson A. Sequence Elements That Affect mRNA Translational Activity in Developing Dictyostelium Cells. Developmental Genetics. 1991;12:98-103.
213. Omosigho NN, Swaminathan K, Plomann M, Müller-Taubenberger A, Noegel AA, Riyahi TY. The Dictyostelium discoideum RACK1 orthologue has roles in growth and development. Cell Communication and Signaling. 2014;12(1):37. doi: 10.1186/1478-811X-12-37.
214. Tremblay BJ-M. universalmotif: Import, Modify, and Export Motifs with R. 2020.
215. McMahon R, Zaborowska I, Walsh D. Noncytotoxic Inhibition of Viral Infection through eIF4F-Independent Suppression of Translation by 4EGi-1. Journal of Virology. 2011;85(2):853-64. Epub 2010/11/12. doi: 10.1128/Jvi.01873-10. PubMed PMID: WOS:000285554300021; PMCID: PMC3019991.

216. Meade N, Furey C, Li H, Verma R, Chai Q, Rollins MG, DiGiuseppe S, Naghavi MH, Walsh D. Poxviruses Evade Cytosolic Sensing through Disruption of an mTORC1-mTORC2 Regulatory Circuit. Cell. 2018;174(5):1143-57 e17. Epub 2018/08/07. doi: 10.1016/j.cell.2018.06.053. PubMed PMID: 30078703; PMCID: PMC6172959.
217. Cox EA, Bennin D, Doan AT, O'Toole T, Huttenlocher A. RACK1 regulates integrin-mediated adhesion, protrusion, and chemotactic cell migration via its Src-binding site. Molecular biology of the cell. 2003;14(2):658-69. doi: 10.1091/mbc.e02-03-0142. PubMed PMID: 12589061.
218. Schmitt K, Smolinski N, Neumann P, Schmaul S, Hofer-Pretz V, Braus GH, Valerius O. Asc1p/RACK1 Connects Ribosomes to Eukaryotic Phosphosignaling. Mol Cell Biol. 2017;37(3):1-23. Epub 2016/11/09. doi: 10.1128/MCB.00279-16. PubMed PMID: 27821475; PMCID: PMC5247610.
219. Ceci M, Gaviraghi C, Gorrini C, Sala LA, Offenhauser N, Marchisio PC, Biffo S. Release of eIF6 (p27(BBP)) from the 60S subunit allows 80S ribosome assembly. Nature. 2003;426(6966):579-84. doi: 10.1038/nature02160. PubMed PMID: WOS:000186944300044.
220. Gerbasi VR, Weaver CM, Hill S, Friedman DB, Link AJ. Yeast Asc1p and mammalian RACK1 are functionally orthologous core 40S ribosomal proteins that repress gene expression. Mol Cell Biol. 2004;24(18):8276-87. Epub 2004/09/02. doi: 10.1128/MCB.24.18.8276-8287.2004. PubMed PMID: 15340087; PMCID: PMC515043.
221. Marqusee S, Robbins VH, Baldwin RL. Unusually Stable Helix Formation in Short Alanine-Based Peptides. Proceedings of the National Academy of Sciences of the United States of America. 1989;86(14):5286-90. doi: DOI 10.1073/pnas.86.14.5286. PubMed PMID: WOS:A1989AG35900015.
222. Giri K, Ghosh U, Bhattacharyya NP, Basak S. Caspase 8 mediated apoptotic cell death induced by β-sheet forming polyalanine peptides. FEBS Letters. 2003;555(2):380-4. doi: https://doi.org/10.1016/S0014-5793(03)01294-8.
223. Brina D, Grosso S, Miluzio A, Biffo S. Translational control by 80S formation and 60S availability: the central role of eIF6, a rate limiting factor in cell cycle progression and tumorigenesis. Cell Cycle. 2011;10(20):3441-6. Epub 2011/10/28. doi: 10.4161/cc.10.20.17796. PubMed PMID: 22031223.
224. Guo J, Wang S, Valerius O, Hall H, Zeng Q, Li JF, Weston DJ, Ellis BE, Chen JG. Involvement of Arabidopsis RACK1 in protein translation and its regulation by abscisic acid. Plant Physiol. 2011;155(1):370-83. Epub 2010/11/26. doi: 10.1104/pp.110.160663. PubMed PMID: 21098678; PMCID: PMC3075769.
225. Sanvito F, Piatti S, Villa A, Bossi M, Lucchini G, Marchisio PC, Biffo S. The beta4 integrin interactor p27(BBP/eIF6) is an essential nuclear matrix protein involved in 60S ribosomal subunit assembly. J Cell Biol. 1999;144(5):823-37. doi: 10.1083/jcb.144.5.823. PubMed PMID: 10085284.
226. Gandin V, Miluzio A, Barbieri AM, Beugnet A, Kiyokawa H, Marchisio PC, Biffo S. Eukaryotic initiation factor 6 is rate-limiting in translation, growth and transformation. Nature. 2008;455(7213):684-8. Epub 2008/09/10. doi: 10.1038/nature07267. PubMed PMID: 18784653.
227. Opitz N, Schmitt K, Hofer-Pretz V, Neumann B, Krebber H, Braus GH, Valerius O. Capturing the Asc1p/Receptor for Activated C Kinase 1 (RACK1) Microenvironment at the Head Region of the 40S Ribosome with Quantitative BioID in Yeast*. Molecular & Cellular Proteomics. 2017;16(12):2199-218. doi: https://doi.org/10.1074/mcp.M116.066654.
228. Wek RC. Role of eIF2α Kinases in Translational Control and Adaptation to Cellular Stress. Cold Spring Harbor perspectives in biology. 2018;10(7):a032870. doi: 10.1101/cshperspect.a032870. PubMed PMID: 29440070.
229. Guo J, Jin Z, Yang X, Li JF, Chen JG. Eukaryotic initiation factor 6, an evolutionarily conserved regulator of ribosome biogenesis and protein translation. Plant Signal Behav. 2011;6(5):766-71. Epub 2011/05/06. doi: 10.4161/psb.6.5.15438. PubMed PMID: 21543889; PMCID: PMC3172860.
230. Inada T, Winstall E, Tarun SZ, Yates JR, Schieltz D, Sachs AB. One-step affinity purification of the yeast ribosome and its associated proteins and mRNAs. Rna. 2002;8(7):948-58. doi: 10.1017/S1355838202026018. PubMed PMID: WOS:000176943100010.
231. Link AJ, Eng J, Schieltz DM, Carmack E, Mize GJ, Morris DR, Garvik BM, Yates JR, 3rd. Direct analysis of protein complexes using mass spectrometry. Nat Biotechnol. 1999;17(7):676-82. Epub 1999/07/15. doi: 10.1038/10890. PubMed PMID: 10404161.

232. Kovtun AA, Shirokilch NE, Gudkov AT, Spirin AS. The leader sequence of tobacco mosaic virus RNA devoid of Watson-Crick secondary structure possesses a cooperatively melted, compact conformation. Biochemical and Biophysical Research Communications. 2007;358(1):368-72. Epub 2007/05/08. doi: 10.1016/j.bbrc.2007.04.152. PubMed PMID: WOS:000246790800060.
233. Higgins R, Gendron JM, Rising L, Mak R, Webb K, Kaiser SE, Zuzow N, Riviere P, Yang B, Fenech E, Tang X, Lindsay SA, Christianson JC, Hampton RY, Wasserman SA, Bennett EJ. The Unfolded Protein Response Triggers Site-Specific Regulatory Ubiquitylation of 40S Ribosomal Proteins. Mol Cell. 2015;59(1):35-49. Epub 2015/06/09. doi: 10.1016/j.molcel.2015.04.026. PubMed PMID: 26051182; PMCID: PMC4491043.
234. Saito K, Horikawa W, Ito K. Inhibiting K63 polyubiquitination abolishes no-go type stalled translation surveillance in Saccharomyces cerevisiae. PLoS Genet. 2015;11(4):e1005197. Epub 2015/04/25. doi: 10.1371/journal.pgen.1005197. PubMed PMID: 25909477; PMCID: PMC4409330.
235. Silva GM, Finley D, Vogel C. K63 polyubiquitination is a new modulator of the oxidative stress response. Nat Struct Mol Biol. 2015;22(2):116-23. Epub 2015/01/27. doi: 10.1038/nsmb.2955. PubMed PMID: 25622294; PMCID: PMC4318705.
236. Sitron CS, Brandman O. Detection and Degradation of Stalled Nascent Chains via Ribosome-Associated Quality Control. Annu Rev Biochem. 2020;89:417-42. Epub 2020/06/23. doi: 10.1146/annurev-biochem-013118-110729. PubMed PMID: 32569528; PMCID: PMC8258965.
237. Chandrasekaran V, Juszkiewicz S, Choi J, Puglisi JD, Brown A, Shao S, Ramakrishnan V, Hegde RS. Mechanism of ribosome stalling during translation of a poly(A) tail. Nat Struct Mol Biol. 2019;26(12):1132-40. Epub 2019/11/27. doi: 10.1038/s41594-019-0331-x. PubMed PMID: 31768042; PMCID: PMC6900289.
238. Zhou Y, Kastritis PL, Dougherty SE, Bouvette J, Hsu AL, Burbaum L, Mosalaganti S, Pfeffer S, Hagen WJH, Forster F, Borgnia MJ, Vogel C, Beck M, Bartesaghi A, Silva GM. Structural impact of K63 ubiquitin on yeast translocating ribosomes under oxidative stress. Proc Natl Acad Sci U S A. 2020;117(36):22157-66. Epub 2020/08/29. doi: 10.1073/pnas.2005301117. PubMed PMID: 32855298; PMCID: PMC7486741.
239. DiGiuseppe S, Rollins MG, Astar H, Khalatyan N, Savas JN, Walsh D. Proteomic and mechanistic dissection of the poxvirus-customized ribosome. J Cell Sci. 2020;134(5):jcs246603. Epub 2020/05/30. doi: 10.1242/jcs.246603. PubMed PMID: 32467327; PMCID: PMC7358139.
240. Rollins MG, Jha S, Bartom ET, Walsh D. RACK1 evolved species-specific multifunctionality in translational control through sequence plasticity within a loop domain. J Cell Sci. 2019;132(12):jcs228908. Epub 2019/05/24. doi: 10.1242/jcs.228908. PubMed PMID: 31118235; PMCID: PMC6602301.
241. Johnson AG, Flynn RA, Lapointe CP, Ooi YS, Zhao ML, Richards CM, Qiao W, Yamada SB, Couthouis J, Gitler AD, Carette JE, Puglisi JD. A memory of eS25 loss drives resistance phenotypes. Nucleic Acids Res. 2020;48(13):7279-97. Epub 2020/05/29. doi: 10.1093/nar/gkaa444. PubMed PMID: 32463448; PMCID: PMC7367175.
242. Cornish PV, Ermolenko DN, Noller HF, Ha T. Spontaneous intersubunit rotation in single ribosomes. Mol Cell. 2008;30(5):578-88. Epub 2008/06/10. doi: 10.1016/j.molcel.2008.05.004. PubMed PMID: 18538656; PMCID: PMC2491453.
243. Wells JN, Buschauer R, Mackens-Kiani T, Best K, Kratzat H, Berninghausen O, Becker T, Gilbert W, Cheng J, Beckmann R. Structure and function of yeast Lso2 and human CCDC124 bound to hibernating ribosomes. PLoS Biol. 2020;18(7):e3000780. Epub 2020/07/21. doi: 10.1371/journal.pbio.3000780. PubMed PMID: 32687489; PMCID: PMC7392345.
244. Brown A, Baird MR, Yip MC, Murray J, Shao S. Structures of translationally inactive mammalian ribosomes. Elife. 2018;7:e40486. Epub 2018/10/26. doi: 10.7554/eLife.40486. PubMed PMID: 30355441; PMCID: PMC6226290.
245. Anger AM, Armache JP, Berninghausen O, Habeck M, Subklewe M, Wilson DN, Beckmann R. Structures of the human and Drosophila 80S ribosome. Nature. 2013;497(7447):80-5. Epub 2013/05/03. doi: 10.1038/nature12104. PubMed PMID: 23636399.
246. Liu B, Qian S-B. Characterizing inactive ribosomes in translational profiling. Translation (Austin, Tex). 2016;4(1):e1138018-e. doi: 10.1080/21690731.2015.1138018. PubMed PMID: 27335722.

247. Wild K, Aleksić M, Lapouge K, Juaire KD, Flemming D, Pfeffer S, Sinning I. MetAP-like Ebp1 occupies the human ribosomal tunnel exit and recruits flexible rRNA expansion segments. Nat Commun. 2020;11(1):776. Epub 2020/02/09. doi: 10.1038/s41467-020-14603-7. PubMed PMID: 32034140; PMCID: PMC7005732.
248. Bhaskar V, Desogus J, Graff-Meyer A, Schenk AD, Cavadini S, Chao JA. Dynamic association of human Ebp1 with the ribosome. RNA (New York, NY). 2021;27(4):411-9. Epub 2021/01/21. doi: 10.1261/rna.077602.120. PubMed PMID: 33479117.
249. Balagopal V, Parker R. Stm1 modulates translation after 80S formation in Saccharomyces cerevisiae. RNA. 2011;17(5):835-42. Epub 2011/04/05. doi: 10.1261/rna.2677311. PubMed PMID: 21460238; PMCID: PMC3078733.
250. Zinoviev A, Hellen CUT, Pestova TV. Multiple mechanisms of reinitiation on bicistronic calicivirus mRNAs. Mol Cell. 2015;57(6):1059-73. Epub 2015/03/22. doi: 10.1016/j.molcel.2015.01.039. PubMed PMID: 25794616; PMCID: PMC4521216.
251. Abaeva IS, Vicens Q, Bochler A, Soufari H, Simonetti A, Pestova TV, Hashem Y, Hellen CUT. The Halastavi arva Virus Intergenic Region IRES Promotes Translation by the Simplest Possible Initiation Mechanism. Cell Rep. 2020;33(10):108476. Epub 2020/12/10. doi: 10.1016/j.celrep.2020.108476. PubMed PMID: 33296660; PMCID: PMC7934607.
252. Hayashi H, Nagai R, Abe T, Wada M, Ito K, Takeuchi-Tomita N. Tight interaction of eEF2 in the presence of Stm1 on ribosome. J Biochem. 2018;163(3):177-85. Epub 2017/10/27. doi: 10.1093/jb/mvx070. PubMed PMID: 29069440.
253. Coppolecchia R, Buser P, Stotz A, Linder P. A new yeast translation initiation factor suppresses a mutation in the eIF-4A RNA helicase. EMBO J. 1993;12(10):4005-11. Epub 1993/10/01. PubMed PMID: 8404866; PMCID: PMC413683.
254. Van Dyke N, Pickering BF, Van Dyke MW. Stm1p alters the ribosome association of eukaryotic elongation factor 3 and affects translation elongation. Nucleic Acids Res. 2009;37(18):6116-25. Epub 2009/08/12. doi: 10.1093/nar/gkp645. PubMed PMID: 19666721; PMCID: PMC2764444.
255. Van Dyke N, Baby J, Van Dyke MW. Stm1p, a ribosome-associated protein, is important for protein synthesis in Saccharomyces cerevisiae under nutritional stress conditions. J Mol Biol. 2006;358(4):1023-31. Epub 2006/04/04. doi: 10.1016/j.jmb.2006.03.018. PubMed PMID: 16580682.
256. Van Dyke N, Chanchorn E, Van Dyke MW. The Saccharomyces cerevisiae protein Stm1p facilitates ribosome preservation during quiescence. Biochem Biophys Res Commun. 2013;430(2):745-50. Epub 2012/12/05. doi: 10.1016/j.bbrc.2012.11.078. PubMed PMID: 23206692.
257. Muto A, Sugihara Y, Shibakawa M, Oshima K, Matsuda T, Nadano D. The mRNA-binding protein Serbp1 as an auxiliary protein associated with mammalian cytoplasmic ribosomes. Cell Biochem Funct. 2018;36(6):312-22. Epub 2018/07/25. doi: 10.1002/cbf.3350. PubMed PMID: 30039520.
258. Iordanov MS, Pribnow D, Magun JL, Dinh TH, Pearson JA, Magun BE. Ultraviolet radiation triggers the ribotoxic stress response in mammalian cells. J Biol Chem. 1998;273(25):15794-803. Epub 1998/06/23. doi: 10.1074/jbc.273.25.15794. PubMed PMID: 9624179.
259. Iordanov MS, Pribnow D, Magun JL, Dinh TH, Pearson JA, Chen SL, Magun BE. Ribotoxic stress response: activation of the stress-activated protein kinase JNK1 by inhibitors of the peptidyl transferase reaction and by sequence-specific RNA damage to the alpha-sarcin/ricin loop in the 28S rRNA. Mol Cell Biol. 1997;17(6):3373-81. Epub 1997/06/01. doi: 10.1128/MCB.17.6.3373. PubMed PMID: 9154836; PMCID: PMC232190.
260. Laskin JD, Heck DE, Laskin DL. The ribotoxic stress response as a potential mechanism for MAP kinase activation in xenobiotic toxicity. Toxicol Sci. 2002;69(2):289-91. Epub 2002/10/16. doi: 10.1093/toxsci/69.2.289. PubMed PMID: 12377976.
261. Shifrin VI, Anderson P. Trichothecene mycotoxins trigger a ribotoxic stress response that activates c-Jun N-terminal kinase and p38 mitogen-activated protein kinase and induces apoptosis. J Biol Chem. 1999;274(20):13985-92. Epub 1999/05/13. doi: 10.1074/jbc.274.20.13985. PubMed PMID: 10318810.
262. Vind AC, Genzor AV, Bekker-Jensen S. Ribosomal stress-surveillance: three pathways is a magic number. Nucleic Acids Res. 2020;48(19):10648-61. Epub 2020/09/18. doi: 10.1093/nar/gkaa757. PubMed PMID: 32941609; PMCID: PMC7641731.

263. Kim TS, Kim HD, Park YJ, Kong E, Yang HW, Jung Y, Kim Y, Kim J. JNK activation induced by ribotoxic stress is initiated from 80S monosomes but not polysomes. BMB Rep. 2019;52(8):502-7. Epub 2019/01/24. doi: 10.5483/BMBRep.2019.52.8.273. PubMed PMID: 30670151; PMCID: PMC6726213.
264. Bogoyevitch MA, Ketterman AJ, Sugden PH. Cellular stresses differentially activate c-Jun N-terminal protein kinases and extracellular signal-regulated protein kinases in cultured ventricular myocytes. J Biol Chem. 1995;270(50):29710-7. Epub 1995/12/15. doi: 10.1074/jbc.270.50.29710. PubMed PMID: 8530360.
265. Hazzalin CA, Cano E, Cuenda A, Barratt MJ, Cohen P, Mahadevan LC. p38/RK is essential for stress-induced nuclear responses: JNK/SAPKs and c-Jun/ATF-2 phosphorylation are insufficient. Curr Biol. 1996;6(8):1028-31. Epub 1996/08/01. doi: 10.1016/s0960-9822(02)00649-8. PubMed PMID: 8805335.
266. Sinha NK, Ordureau A, Best K, Saba JA, Zinshteyn B, Sundaramoorthy E, Fulzele A, Garshott DM, Denk T, Thoms M, Paulo JA, Harper JW, Bennett EJ, Beckmann R, Green R. EDF1 coordinates cellular responses to ribosome collisions. Elife. 2020;9. Epub 2020/08/04. doi: 10.7554/eLife.58828. PubMed PMID: 32744497; PMCID: PMC7486125.
267. Meng Z, Jackson NL, Shcherbakov OD, Choi H, Blume SW. The human IGF1R IRES likely operates through a Shine-Dalgarno-like interaction with the G961 loop (E-site) of the 18S rRNA and is kinetically modulated by a naturally polymorphic polyU loop. J Cell Biochem. 2010;110(2):531-44. Epub 2010/05/01. doi: 10.1002/jcb.22569. PubMed PMID: 20432247; PMCID: PMC2997104.
268. Demeshkina N, Repkova M, Ven'yaminova A, Graifer D, Karpova G. Nucleotides of 18S rRNA surrounding mRNA codons at the human ribosomal A, P, and E sites: a crosslinking study with mRNA analogs carrying an aryl azide group at either the uracil or the guanine residue. Rna. 2000;6(12):1727-36. Epub 2001/01/06. doi: 10.1017/s1355838200000996. PubMed PMID: 11142373; PMCID: PMC1370043.
269. Dao Duc K, Batra SS, Bhattacharya N, Cate JHD, Song YS. Differences in the path to exit the ribosome across the three domains of life. Nucleic Acids Res. 2019;47(8):4198-210. Epub 2019/02/26. doi: 10.1093/nar/gkz106. PubMed PMID: 30805621; PMCID: PMC6486554.
270. Shanmuganathan V, Schiller N, Magoulopoulou A, Cheng J, Braunger K, Cymer F, Berninghausen O, Beatrix B, Kohno K, von Heijne G, Beckmann R. Structural and mutational analysis of the ribosome-arresting human XBP1u. Elife. 2019;8:e46267. Epub 2019/06/28. doi: 10.7554/eLife.46267. PubMed PMID: 31246176; PMCID: PMC6624018.
271. Yanshina DD, Bulygin KN, Malygin AA, Karpova GG. Hydroxylated histidine of human ribosomal protein uL2 is involved in maintaining the local structure of 28S rRNA in the ribosomal peptidyl transferase center. FEBS J. 2015;282(8):1554-66. Epub 2015/02/24. doi: 10.1111/febs.13241. PubMed PMID: 25702831.
272. Eggers DK, Welch WJ, Hansen WJ. Complexes between nascent polypeptides and their molecular chaperones in the cytosol of mammalian cells. Mol Biol Cell. 1997;8(8):1559-73. Epub 1997/08/01. doi: 10.1091/mbc.8.8.1559. PubMed PMID: 9285825; PMCID: PMC276176.
273. Wong W, Bai XC, Brown A, Fernandez IS, Hanssen E, Condron M, Tan YH, Baum J, Scheres SH. Cryo-EM structure of the Plasmodium falciparum 80S ribosome bound to the anti-protozoan drug emetine. Elife. 2014;3:e03080. Epub 2014/06/11. doi: 10.7554/eLife.03080. PubMed PMID: 24913268; PMCID: PMC4086275.
274. Garreau de Loubresse N, Prokhorova I, Holtkamp W, Rodnina MV, Yusupova G, Yusupov M. Structural basis for the inhibition of the eukaryotic ribosome. Nature. 2014;513(7519):517-22. Epub 2014/09/12. doi: 10.1038/nature13737. PubMed PMID: 25209664.
275. Dorokhov YL, Ivanov PA, Komarova TV, Skulachev MV, Atabekov JG. An internal ribosome entry site located upstream of the crucifer-infecting tobamovirus coat protein (CP) gene can be used for CP synthesis in vivo. J Gen Virol. 2006;87(Pt 9):2693-7. Epub 2006/08/09. doi: 10.1099/vir.0.82095-0. PubMed PMID: 16894210.
276. May J, Johnson P, Saleem H, Simon AE. A Sequence-Independent, Unstructured Internal Ribosome Entry Site Is Responsible for Internal Expression of the Coat Protein of Turnip Crinkle

Virus. J Virol. 2017;91(8):e02421-16. Epub 2017/02/10. doi: 10.1128/JVI.02421-16. PubMed PMID: 28179526; PMCID: PMC5375686.

277. Varallyay E, Valoczi A, Agyi A, Burgyan J, Havelda Z. Plant virus-mediated induction of miR168 is associated with repression of ARGONAUTE1 accumulation. EMBO J. 2010;29(20):3507-19. Epub 2010/09/09. doi: 10.1038/emboj.2010.215. PubMed PMID: 20823831; PMCID: PMC2964164.
278. Cencic R, Pelletier J. Hippuristanol - A potent steroid inhibitor of eukaryotic initiation factor 4A. Translation (Austin). 2016;4(1):e1137381. Epub 2016/06/24. doi: 10.1080/21690731.2015.1137381. PubMed PMID: 27335721; PMCID: PMC4909409.
279. Liu T, Nair SJ, Lescarbeau A, Belani J, Peluso S, Conley J, Tillotson B, O'Hearn P, Smith S, Slocum K, West K, Helble J, Douglas M, Bahadoor A, Ali J, McGovern K, Fritz C, Palombella VJ, Wylie A, Castro AC, Tremblay MR. Synthetic silvestrol analogues as potent and selective protein synthesis inhibitors. J Med Chem. 2012;55(20):8859-78. Epub 2012/10/03. doi: 10.1021/jm3011542. PubMed PMID: 23025805.
280. Pestova TV, Kolupaeva VG. The roles of individual eukaryotic translation initiation factors in ribosomal scanning and initiation codon selection. Genes Dev. 2002;16(22):2906-22. Epub 2002/11/19. doi: 10.1101/gad.1020902. PubMed PMID: 12435632; PMCID: PMC187480.
281. Acosta-Reyes F, Neupane R, Frank J, Fernandez IS. The Israeli acute paralysis virus IRES captures host ribosomes by mimicking a ribosomal state with hybrid tRNAs. EMBO J. 2019;38(21):e102226. Epub 2019/10/15. doi: 10.15252/embj.2019102226. PubMed PMID: 31609474; PMCID: PMC6826211.
282. Murray J, Savva CG, Shin BS, Dever TE, Ramakrishnan V, Fernandez IS. Structural characterization of ribosome recruitment and translocation by type IV IRES. Elife. 2016;5:e13567. Epub 2016/05/10. doi: 10.7554/eLife.13567. PubMed PMID: 27159451; PMCID: PMC4861600.
283. Yamamoto H, Collier M, Loerke J, Ismer J, Schmidt A, Hilal T, Sprink T, Yamamoto K, Mielke T, Burger J, Shaikh TR, Dabrowski M, Hildebrand PW, Scheerer P, Spahn CM. Molecular architecture of the ribosome-bound Hepatitis C Virus internal ribosomal entry site RNA. EMBO J. 2015;34(24):3042-58. Epub 2015/11/26. doi: 10.15252/embj.201592469. PubMed PMID: 26604301; PMCID: PMC4687786.
284. Quade N, Boehringer D, Leibundgut M, van den Heuvel J, Ban N. Cryo-EM structure of Hepatitis C virus IRES bound to the human ribosome at 3.9-A resolution. Nat Commun. 2015;6:7646. Epub 2015/07/15. doi: 10.1038/ncomms8646. PubMed PMID: 26155016; PMCID: PMC4510694.
285. Spahn CM, Kieft JS, Grassucci RA, Penczek PA, Zhou K, Doudna JA, Frank J. Hepatitis C virus IRES RNA-induced changes in the conformation of the 40s ribosomal subunit. Science. 2001;291(5510):1959-62. Epub 2001/03/10. doi: 10.1126/science.1058409. PubMed PMID: 11239155.
286. Hinnebusch AG. Structural Insights into the Mechanism of Scanning and Start Codon Recognition in Eukaryotic Translation Initiation. Trends Biochem Sci. 2017;42(8):589-611. Epub 2017/04/27. doi: 10.1016/j.tibs.2017.03.004. PubMed PMID: 28442192.
287. Passmore LA, Schmeing TM, Maag D, Applefield DJ, Acker MG, Algire MA, Lorsch JR, Ramakrishnan V. The eukaryotic translation initiation factors eIF1 and eIF1A induce an open conformation of the 40S ribosome. Mol Cell. 2007;26(1):41-50. Epub 2007/04/17. doi: 10.1016/j.molcel.2007.03.018. PubMed PMID: 17434125.
288. Schluenzen F, Tocilj A, Zarivach R, Harms J, Gluehmann M, Janell D, Bashan A, Bartels H, Agmon I, Franceschi F, Yonath A. Structure of functionally activated small ribosomal subunit at 3.3 angstroms resolution. Cell. 2000;102(5):615-23. Epub 2000/09/28. doi: 10.1016/s0092-8674(00)00084-2. PubMed PMID: 11007480.
289. Lomakin IB, Steitz TA. The initiation of mammalian protein synthesis and mRNA scanning mechanism. Nature. 2013;500(7462):307-11. Epub 2013/07/23. doi: 10.1038/nature12355. PubMed PMID: 23873042; PMCID: PMC3748252.
290. Neupane R, Pisareva VP, Rodriguez CF, Pisarev AV, Fernandez IS. A complex IRES at the 5'-UTR of a viral mRNA assembles a functional 48S complex via an uAUG intermediate. Elife. 2020;9:e54575. Epub 2020/04/15. doi: 10.7554/eLife.54575. PubMed PMID: 32286223; PMCID: PMC7190351.

291. Dorokhov YL, Skulachev MV, Ivanov PA, Zvereva SD, Tjulkina LG, Merits A, Gleba YY, Hohn T, Atabekov JG. Polypurine (A)-rich sequences promote cross-kingdom conservation of internal ribosome entry. Proc Natl Acad Sci U S A. 2002;99(8):5301-6. Epub 2002/04/18. doi: 10.1073/pnas.082107599. PubMed PMID: 11959981; PMCID: PMC122764.
292. Tang TTL, Passmore LA. Recognition of Poly(A) RNA through Its Intrinsic Helical Structure. Cold Spring Harb Symp Quant Biol. 2019;84:21-30. Epub 2020/04/17. doi: 10.1101/sqb.2019.84.039818. PubMed PMID: 32295929; PMCID: PMC7116106.
293. Vopálenský V, Sýkora M, Mašek T, Pospíšek M. Messenger RNAs of Yeast Virus-Like Elements Contain Non-templated 5′ Poly(A) Leaders, and Their Expression Is Independent of eIF4E and Pab1. Frontiers in Microbiology. 2019;10(2366). doi: 10.3389/fmicb.2019.02366.
294. Fukuhara H. Linear DNA plasmids of yeasts. FEMS Microbiology Letters. 1995;131(1):1-9. doi: 10.1111/j.1574-6968.1995.tb07745.x.
295. Sýkora M, Pospíšek M, Novák J, Mrvová S, Krásný L, Vopálenský V. Transcription apparatus of the yeast virus-like elements: Architecture, function, and evolutionary origin. PLoS Pathog. 2018;14(10):e1007377. Epub 2018/10/23. doi: 10.1371/journal.ppat.1007377. PubMed PMID: 30346988; PMCID: PMC6211774.
296. Vopálenský V, Sýkora M, Mělková Z, Mašek T, Pospíšek M. Transcripts of vaccinia virus postreplicative genes do not contain a 5’ methylguanosine cap. bioRxiv. 2020:2020.07.15.204867. doi: 10.1101/2020.07.15.204867.
297. Pavlovic Djuranovic S, Erath J, Andrews RJ, Bayguinov PO, Chung JJ, Chalker DL, Fitzpatrick JA, Moss WN, Szczesny P, Djuranovic S. Plasmodium falciparum translational machinery condones polyadenosine repeats. Elife. 2020;9. Epub 2020/05/30. doi: 10.7554/eLife.57799. PubMed PMID: 32469313; PMCID: PMC7295572.
298. Djuranovic S, Erath J. Association of RACK1 protein with ribosomes in Plasmodium falciparum. bioRxiv. 2021. doi: 10.1101/2021.09.21.461325.
299. Sun M, Li W, Blomqvist K, Das S, Hashem Y, Dvorin JD, Frank J. Dynamical features of the Plasmodium falciparum ribosome during translation. Nucleic Acids Res. 2015;43(21):10515-24. Epub 2015/10/04. doi: 10.1093/nar/gkv991. PubMed PMID: 26432834; PMCID: PMC4666399.